Acceleration of Hardware Testing and Validation Algorithms using Graphics Processing Units

Min Li

Dissertation submitted to the Faculty of the
Virginia Polytechnic Institute and State University
in partial fulfillment of the requirements for the degree of

Doctor of Philosophy
in
Computer Engineering

Michael S. Hsiao, Chair
Sandeep K. Shukla
Patrick Schaumont
Yaling Yang
Weiguo Fan

September 5, 2012
Blacksburg, Virginia

Keywords: Fault simulation, fault diagnosis, design validation, parallel algorithm, general purpose computation on graphics processing unit (GPGPU),
©Copyright 2012, Min Li

Acceleration of Hardware Testing and Validation Algorithms using Graphics Processing Units

Min Li

(ABSTRACT)

With the advances of very large scale integration (VLSI) technology, the feature size has been shrinking steadily together with the increase in the design complexity of logic circuits. As a result, the efforts taken for designing, testing, and debugging digital systems have increased tremendously. Although the electronic design automation (EDA) algorithms have been studied extensively to accelerate such processes, some computational intensive applications still take long execution times. This is especially the case for testing and validation. In order to meet the time-to-market constraints and also to come up with a bug-free design or product, the work presented in this dissertation studies the acceleration of EDA algorithms on Graphics Processing Units (GPUs). This dissertation concentrates on a subset of EDA algorithms related to testing and validation. In particular, within the area of testing, fault simulation, diagnostic simulation and reliability analysis are explored. We also investigated the approaches to parallelize state justification on GPUs, which is one of the most difficult problems in the validation area.

Firstly, we present an efficient parallel fault simulator, FSimGP^2, which exploits the high degree of parallelism supported by a state-of-the-art graphic processing unit (GPU) with the NVIDIA Compute Unified Device Architecture (CUDA). A novel three-dimensional parallel fault simulation technique is proposed to achieve extremely high computation efficiency on the GPU. The experimental results demonstrate a speedup of up to 4$\times$ compared to another GPU-based fault simulator.

Then, another GPU based simulator is used to tackle an even more computation-intensive task, diagnostic fault simulation. The simulator is based on a two-stage framework which exploits high computation efficiency on the GPU. We introduce a fault pair based approach to alleviate the limited memory capacity on GPUs. Also, multi-fault-signature and dynamic load balancing

techniques are introduced for the best usage of computing resources on-board.

With continuously feature size scaling and advent of innovative nano-scale devices, the reliability analysis of the digital systems becomes more important nowadays. However, the computational cost to accurately analyze a large digital system is very high. We proposes an high performance reliability analysis tool on GPUs. To achieve high memory bandwidth on GPUs, two algorithms for simulation scheduling and memory arrangement are proposed. Experimental results demonstrate that the parallel analysis tool is efficient, reliable and scalable.

In the area of design validation, we investigate state justification. By employing the swarm intelligence and the power of parallelism on GPUs, we are able to efficiently find a trace that could help us reach the corner cases during the validation of a digital system.

In summary, the work presented in this dissertation demonstrates that several applications in the area of digital design testing and validation can be successfully rearchitected to achieve maximal performance on GPUs and obtain significant speedups. The proposed algorithms based on GPU parallelism collectively aim to contribute to improving the performance of EDA tools in Computer aided design (CAD) community on GPUs and other many-core platforms.

This work is supported in part by NSF grants 0840936 and 1016675.

To my beloved family

Parents Changlin Li and Xiuqin Tao

Wife Ting Wang

Acknowledgments

First and foremost I thank my advisor Dr. Michael S. Hsiao for his inspiration and support throughout my PhD life. I am so grateful to have opportunities discussing my research works with him and be able to obtain remarkable guidance, high expertise in the digital testing and verification area. Without the help from him, this dissertation would not have been completed or written.

I would like to thank Dr. Sandeep Shukla, Dr. Patrick Schaumont, Dr. Yaling Yang and Dr. Weiguo (Patrick) Fan to serve on my committee and spend precious time on the dissertation review and oral presentation. I would like also to thank all the PROACITVE members, Lei Fang, Weixin Wu, Xuexi Chen and Kelson Gent for their suggestions on my research and dissertation.

I am fortunate to befriend some excellent folks at Virginia Tech. I am especially grateful to my roommates Shiguang Xie, Yu Zhao, Yexin Zheng, Kaigui Bian and Huijun Xiong for having fun and being patient with me. I also thank friends Hua Lin, Hao Wu, Yi Deng, Xu Guo, Zhimin Chen, Shucai Xiao, Guangying Wang for providing a stimulating and fun environment in my five-year campus life. I am grateful to my friends and family who helped me in ways one too many to list.

Last but not the least, I would like to express my deep gratitude to my family members: parents Changlin Li and Xiuqin Tao, and my wife Ting Wang, for their love and constant support, without which I would never make this work possible. I sincerely appreciate all the help.

Min Li

September, 2012

Contents

List of Figures xi

List of Tables xiii

1 Introduction 1

1.1 Problem Scope and Motivation 2

1.1.1 Digital Circuit Testing 2

1.1.2 Digital Design Validation 3

1.1.3 Parallel Computing with Processing Graphics Units 5

1.2 Contributions of the Dissertation 5

1.2.1 Publications 7

1.3 Dissertation Organization 8

2 Background 11

2.1 Graphic Processing Units 11

2.1.1 Hardware Architecture 13

2.1.2 Memory Hierarchy 13

2.1.3 Programming Model 15
2.1.4 Applications 16
2.2 Digital Systems Testing 18
2.2.1 Single Stuck at Fault Model 18
2.2.2 Fault Simulation 19
2.2.3 Reliablity Analysis 21
2.3 Digital Systems Validation 22
2.3.1 State Justification 22
2.3.2 Abstraction Guided Simulation 23
2.3.3 Partition Navigation Tracks 27
3 Parallel Fault Simulator **30**
3.1 Chapter Overview 30
3.2 Introduction 31
3.3 Background 32
3.3.1 Fault Simulation 32
3.3.2 Previous Work 33
3.4 FSimGP^2 Architecture 35
3.4.1 Three-Dimensional Parallel Fault Simulation 35
3.4.2 Framework 37
3.4.3 Data Structure 40
3.4.4 Compact Fault List Generation 41

3.4.5 Static and Dynamic Load Balancing 42
3.4.6 Memory Usage and Scalability 43
3.5 Experimental Results 44
3.5.1 Performance Evaluation 47
3.5.2 Characteristics of FSimGP^2 51
3.6 Chapter Summary 56
4 Parallel Diagnostic Fault Simulator 57
4.1 Chapter Overview 57
4.2 Introduction 58
4.3 Background 59
4.3.1 Diagnostic Fault Simulation 59
4.3.2 Previous Work 60
4.4 Proposed Method 61
4.4.1 Framework 62
4.4.2 Dynamic Load Balancing 65
4.5 Experimental Results 66
4.5.1 Performance Evaluation 68
4.5.2 Characteristics of Diagnostic Fault Simulator 69
4.6 Chapter Summary 72
5 Parallel Reliablity Analysis 74

5.1 Chapter Overview . . . 74

5.2 Introduction . . . 75

5.3 Background . . . 77

5.3.1 Previous Work . . . 77

5.4 Proposed Method . . . 79

5.4.1 Framework . . . 80

5.4.2 Scheduling of Stems . . . 83

5.4.3 Scheduling of Non-stem Gates . . . 87

5.5 Experimental Results . . . 87

5.5.1 Scheduling Evaluation and Memory Performance . . . 89

5.5.2 Accuracy and Performance Evaluation . . . 90

5.6 Chapter Summary . . . 95

6 Parallel Design Validation with a Modified Ant Colony Optimization 97

6.1 Chapter Overview . . . 97

6.2 Introduction . . . 98

6.3 Background . . . 99

6.3.1 Previous Work . . . 99

6.3.2 Ant colony optimization . . . 101

6.3.3 Random Synchronization Avoidance . . . 102

6.4 Proposed Method . . . 103

6.4.1 Modified Ant Colony Optimization . . . 104

6.4.2 GPGPU Ants 105

6.4.3 BMC to traverse narrow paths 106

6.5 Experimental Results 107

6.6 Chapter Summary 108

7 Conclusion **111**

8 Bibliography **114**

List of Figures

1.1 Organization of the dissertation. 9

2.1 The Interface between CPU and GPU. 13

2.2 NVIDIA hardware architecture. 14

2.3 NVIDIA CUDA architecture. 15

2.4 Stuck-at Fault Model. 19

2.5 Miter Circuit for Fault Simulation. 20

2.6 State transition graph 23

2.7 Abstract model and concrete state mapping 25

2.8 Framework of abstraction engine 25

2.9 Preimages of two partition sets 26

2.10 Framework of computing preimage 28

3.1 Fanout region of compact fault. FR: Fanout region; TID: Thread ID. 36

3.2 Three-dimensional fault simulation architecture. 37

3.3 FSimGP^2 framework. 38

3.4 FSimGP^2's execution time w/ and w/o cf-parallelism. 51

3.5 FSimGP^2's execution time with different load schemes. 53

3.6 FSimGP^2's execution time with different parallelism factors. 54

4.1 The framework of GDSim. 63

4.2 Parallel diagnostic simulation architecture. 65

4.3 Comparison with different vector length for b17_1. 70

4.4 Comparison between dynamic and static load balancing. 70

4.5 Execution time with respect to different SIG_LEN. 72

4.6 GDSim's execution time with different parallelism factors. 73

5.1 Fanout Stems and Fanout Free Regions. 79

5.2 The framework of RAG. 81

5.3 RAG's execution time with different GPU configuration. 88

5.4 Comparison among RAG and two observability-based analysis on benchmark b17. 93

5.5 Comparison between Monte Carlo and Observability on benchmark b09 from [24]. 94

6.1 Ant Colony Optimization Branches 102

6.2 Modified Ant Colony Optimization 104

List of Tables

3.1 Comparison with 32K random patterns in [38] . . . 46

3.2 Comparison with tools on the same platform . . . 50

3.3 Runtime in steps . . . 52

3.4 Memory scalability . . . 56

4.1 Comparison with other tools. . . . 67

4.2 Number of faulty pairs with different SIG_LEN. . . . 71

5.1 Circuit Characteristics. . . . 86

5.2 Accuracy of RAG for Different Number of Samples . . . 89

5.3 Comparison with Other Tools. . . . 89

5.4 Comparison With Tools on the Same Platform with Large Circuits . . . 92

5.5 Runtime in Steps . . . 95

6.1 Comparison with other state justification methods . . . 109

Chapter 1

Introduction

According to Moore's law [64], the feature size for manufacturing semiconductors is shrinking while the complexity of the logic design is increasing exponentially. These advances have brought about challenges in ensuring that the products are free of bugs and defects. Various kinds of bugs and defects may exist in digital designs as well as fabricated chips that are hard to detect.

With larger and more complex chips, there is a tremendous need for efficient Electronic Design Automation (EDA) tools that can scale to handle them. However, more recently, the improvement in the performance of general-purpose single-core processors has diminished due to the fact that improvement in operating frequencies has stalled and limited additional gains from further exploits from instruction-level parallelism. Hence, researches are investigating multi-core platforms that could parallelize the algorithms for Computer Aided Design (CAD).

In this dissertation, we concentrate on a specific architecture for parallelizing test and validation algorithms. The architecture chosen is the state-of-the-art many-core system, Graphics Processing Units (GPUs). We have parallelized four algorithms in the testing and validation domains, namely logic fault simulation, diagnostic fault simulation, reliability analysis and state justification with modified Ant Colony Optimization (ACO) on GPUs. Our GPU-based implementations could achieve more than one magnitude speed-up against other parallel and sequential heuristics.

1.1 Problem Scope and Motivation

1.1.1 Digital Circuit Testing

Testing of a digital system is a process in which the system is exercised and its resulting response is analyzed to ascertain whether it behaved correctly [2]. In this dissertation, *testing* refers to *manufacture testing* which is a methodology to screen and identify *physical defects* in Integrated Chips (ICs).

Physical defects include fabrication errors, defects injected, and process variations. The design errors which are directly attributable to human error are not included here. The effects of the physical defects on the operation of the system are represented as logical faults in the context of *fault model*. In the past, the physical defects in integrated circuits have been studied and several fault models are proposed including stuck-at faults, bridging faults, transition faults and path-delay faults [18, 89, 95]. It is widely accepted in both industry and academia that test patterns generated using *single stuck-at fault* (SSF) model can help in detecting several arbitrary defects [95]. Thus, the algorithms proposed in the dissertation assume single stuck-at fault model. Generally, *test patterns*, which are sets of pre-designed stimuli, are applied to the primary inputs (PIs) and pseudo primary inputs (PPIs) of the chip. Then, the corresponding responses, called *test responses* are observed at the primary outputs (POs) and pseudo primary outputs (PPOs). We could conclude that the circuit-under-testing (CUT) is defective if the expected and observed output values are different. In other words, a fault is detected when the response of the faulty-circuit differs from the expected response of the fault-free circuit. The process to compute the response of the CUT in the presence of faults is called *fault simulation*. It is an important procedure to evaluate the quality of the test patterns. Also, fault simulation is an essential part in the Automatic Test Pattern Generation (ATPG). One of the important metrics given by fault simulation is *fault coverage*, which evaluates the effectiveness, or the quality, of a test. It is defined as the ratio between the number of faults detected and the total number of modeled faults in the CUT.

If incorrect behavior is detected, the next goal of a testing experiment is to *diagnose*, or locate,

the cause of the misbehavior. *Fault diagnosis*, a process of locating defects in a defective chip, plays an important role in today's very-large-scale integrated (VLSI) circuits. Finding the cause of the fault could help to improve the yield of the chips. For a circuit-under-diagnosis (CUD) in the presence of modeled faults, the process of evaluating diagnostic capability of the given test patterns is called diagnostic fault simulation. In addition to measuring diagnostic capability, diagnostic simulators can also help to accelerate automated diagnostic pattern generation (ADPG). The diagnostic capability could be evaluated by several measures such as *diagnostic resolution (DR)*, the fraction of fault pairs distinguished, and *diagnostic power (DP)*, the fraction of fully distinguishable faults [17].

Besides checking and locating the defects in a chip, an accurate reliability evaluation is also an essential part with continuous scaling of CMOS technology. Researchers believe that the probability of error due to manufacturing defects, process variation, aging and transient faults will sharply increase due to rapidly diminishing feature sizes and complex fabrication processes [45, 63, 100, 13, 14]. Therefore, *reliability analysis*, a process of evaluating the effects of errors due to both intrinsic noise and external transients will play an important role for nano-scale circuits. However, reliability analysis is computationally complex because of the exponential number of combinations and correlations in possible gate failures, and their propagation and interaction at multiple primary outputs. Hence, it is necessary to have an efficient reliability analysis tool which is accurate, robust and scalable with design size and complexity.

1.1.2 Digital Design Validation

Design validation is the process of ensuring if a given implementation adheres to its specification. In today's design cycle, more than 70% of the resources need to be allocated to validation [25, 85]. However, the complexity of modern chip designs has stretched the ability of the validation techniques and methodologies. Traditional validation techniques use simulators with random test vectors to validate the design. However, the coverage of random generated patterns is usually very low due to the corner cases which are hard to reach. In another side, mathematical models and

analysis are employed for formal verification. It is called ”formal” because these techniques can guarantee that no corner cases will be missed. Usually, formal verification methods are complete because they perform an implicit and complete search on all the possible scenarios. However, formal verification encounters the problem of *state explosion* due to the increasing number of state variables. With the significantly increasing number of state variables, explicitly traversing all the states cannot scale to current industrial size designs.

A key problem in the field is to decide whether a set of target states can be reached from a set of initial states, and if so, to compute a trajectory to demonstrate it. We call this process as *state justification*. The complexity of current designs makes it hard to generate effective vectors for covering corner cases. An example corner case is a hard-to-reach state needed to detect a fault or prove a property. Despite the advances made over the years, *state justification* remains to be one of the hardest tasks in sequential ATPG and design validation.

Deterministic approaches based on branch-and-bound search [70, 40] in sequential ATPGs work well for small circuits, but they quickly become intractable when faced with large designs. Some approaches from formal verification have been proposed such as symbolic/bounded model checking [16, 12]. Essentially formal methods compute the complete reachability information, usually in a depth-first fashion, for the circuit under test. Although these aforementioned methods are capable of analyzing *all* hard-to-reach states in theory, they are not scalable to tackle the complexity of state-of-the-art designs. Simulation-based techniques [16, 35], on the other hand, have advantages in handling large design sizes and avoids backtracking when validating a number of target states. However, they cannot justify some corner cases in complex designs. While simulation-based methods have been widely used for design validation in industry due to its scalability, researchers have been exploring semi-formal techniques which hold potential in reaching hard corner cases at an acceptable cost for complex designs [99, 90, 68, 34, 78]. Among these, the abstraction-guided simulation is one of the most promising techniques which first applies formal methods to abstract the design. Abstraction, in a nutshell, removes certain portions of the design to simplify the model, so that the cost of subsequent analysis can be reduced.

1.1.3 Parallel Computing with Processing Graphics Units

One of the dominant trends in microprocessor architecture in recent years has been continually increasing chip-level parallelism. Modern platforms such as multi-core CPUs with 2 to 4 scalar cores, are offering significant computing power. It is indicated that the trend towards increasing parallelism will continue on towards *many-core* chips that provide far higher degrees of parallelism. One promising platform in the many-core family is the *Graphic Processing units* (GPUs), which are designed to operate in a Single-Instruction-Multiple-Data (SIMD) fashion. Nowadays, GPUs are being actively explored for general purpose computations [33, 60, 74]. The rapid increase in the number and diversity of scientific communities exploring the computational power of GPUs for their data intensive algorithms has arguably had a contribution in encouraging GPU manufacturers to design easily programmable general purpose GPUs (GPGPUs). GPU architectures have been continuously evolving towards higher performance, larger memory sizes, larger memory bandwidths and relatively lower costs. Also, the EDA community is investigating the approaches to accelerate some computationally intensive algorithms on GPUs [38, 21, 39, 20, 47, 54, 56].

1.2 Contributions of the Dissertation

The electronic design automation (EDA) fields collectively use a diverse set of software algorithms and tools, which are required to design complex next generation electronics products. The increase in VLSI design complexity poses a challenge to the EDA community, since single-threaded performance is not scaling effectively due to reasons mentioned above. Parallel hardware presents an opportunity to tackle this dilemma, and opens up new design automation opportunities which yield orders of magnitude faster algorithms. In this dissertation, we investigate a state-of-the-art hardware platform, many-core architecture, especially the streaming processors such as Graphics Processing Units are studied.

We first proposed FSimGP^2, an efficient fault simulator with GPGPU. In this work, a novel notion of compact gate fault is introduced to achieve fault-parallelism on GPUs. In other words, we could

simulate multiple single faults concurrently. Also, pattern and block-parallelism are also exploited by FSimGP^2. Therefore, the proposed three dimensional parallelism could take advantage of the high computational power of GPUs. A novel memory architecture is introduced to improve the memory bandwidth during simulation. As a result, we achieved more than one magnitude speed-up against the state-of-the-art fault simulator on conventional processors and GPUs.

Next, we implemented a high-performance GPU based Diagnostic fault Simulator, called GDSim. To the best of our knowledge, this work is the first that accelerates diagnostic fault simulation on a GPU platform. We introduced a two-stage simulation framework to efficiently utilize the computation power of the GPU without exceeding its memory limitation. First, a fault simulation kernel is launched to determine the detectability of each fault. Then the detected faults are distinguished by the fault pair based diagnostic simulation kernel. Both kernels are parallelized on the GPU architecture. In the simulation kernel, multi-fault-signature (MFS) is proposed to facilitate fault pair list generation. MFSs can be obtained directly from the parallel fault simulator, FSimGP^2, without introducing any computational overhead. By clever selection of the size of the MFS, GDSim is able to reduce the number of fault pairs by 66%. The fault pair based diagnostic simulation kernel exploits both fault pair- and pattern- parallelism, which allows for efficient utilization of memory bandwidth and massive data parallelism on GPUs. Also, dynamic load balancing is introduced to guarantee an even workload onto each processing elements.

Besides fault simulation and diagnosis, we introduced an efficient parallel tool for reliability analysis of logic circuits. It is a fault injection based parallel stochastic simulator implemented on a state-of-the-art GPU. A two-stage simulation framework is proposed to exploit the high computation efficiency of GPUs. We could achieve high memory and instrument bandwidth with novel algorithms for simulation scheduling and memory management. Experimental results demonstrate the accuracy and performance of RAG. A speedup of up to 793$\times$ and 477$\times$ (with average speedup of 353.24$\times$ and 116.04$\times$) is achieved compared to two state-of-the-art CPU-based approaches for reliability analysis.

In the area of design validation, we presented a novel parallel abstraction-guided state justifica-

tion tool using GPUs. A probabilistic state transition model based on Ant Colony Optimization (ACO) [30, 32] is developed to help formulate the state justification problem as a searching scheme of artificial ants. More ants allow us to explore a larger search space, while parallel simulation on GPUs allows us to reduce execution costs. Experimental results demonstrate that our approach is superior in reaching hard-to-reach states in sequential circuit compared to other methods.

It is noted that we applied GPU-oriented performance optimization strategies on all our works to ensure a maximal speedup. Global memory accesses are coalesced to achieve maximum memory bandwidth. The maximum instruction bandwidth is obtained by avoiding branch divergence. Our tools also take advantage of the inherent bit-parallelism of logic operations on computer words.

1.2.1 Publications

The publications regarding this dissertation are listed below:

- [57] Min Li and Michael S. Hsiao, "RAG: An efficient reliability analysis of logic circuits on graphics processing units," in Proceedings of the IEEE Design Automation and Test in Europe Conference, March 2012, pp. 316-319.
- [52] Min Li, Kelson Gent and Michael S. Hsiao, "Utilizing GPGPUs for design validation with a modified ant colony optimization," in Proceedings of the IEEE High Level Design Validation and Test Workshop, November 2011, pp. 128-135.
- [55] Min Li, Michael S. Hsiao, "3-D parallel fault simulation with GPGPU," in IEEE Transactions on Computer-Aided Design of Integrated Circuits and Systems, vol. 30, no. 10, October 2011, pp. 1545-1555.
- [56] Min Li, Michael S. Hsiao, "High-performance diagnostic fault simulation on GPUs,". in Proceedings of the IEEE European Test Symposium, May 2011, pp. 210.
- [54] Min Li, Michael S. Hsiao, "FSimGP^2: an efficient fault simulator with GPGPU," in Proceedings of the IEEE Asian Test Symposium, December 2011, pp. 15-20.

- [53] Min Li, Michael S. Hsiao, "An ant colony optimization technique for abstraction-guided state justification," in Proceedings of the IEEE International Test Conference, November 2009, pp. 1-10.

Other research products that were indirectly related are listed below:

- Min Li, Kelson Gent, and Michael S. Hsiao, "Design validation of RTL circuits using evolutionary swarm intelligence," to appear in Proceedings of the IEEE International Test Conference, November, 2012.
- [58] Min Li, Yexin Zheng, Michael S. Hsiao, and Chao Huang, "Reversible logic synthesis through ant colony optimization," in Proceedings of the IEEE Design Automation and Test in Europe Conference, April 2010, pp. 307-310.

1.3 Dissertation Organization

This dissertation is organized according to the areas illustrated in Fig. 1.1.

1. Chapter 2 introduces the fundamentals of Graphic Processing Units, including its hardware architecture, memory hierarchy, and programming environment. Meanwhile, the fault model used in our work and basic knowledge of fault simulation is also presented.
2. Chapter 3 discusses the implementation of fault simulation on GPUs. The novel three-dimensional parallelism on the GPUs is presented. We demonstrate the improvement achieved by exploiting compact gate and GPU oriented optimization. In addition, a dynamic load balancing technique is introduced for further performance improvement.
3. Chapter 4 presents a two-step framework for the parallel diagnostic fault simulation on GPUs. We demonstrate that the fault pair based fault diagnostic simulation could be efficiently parallelized on GPUs. Also, we propose a novel idea of multiple fault signatures

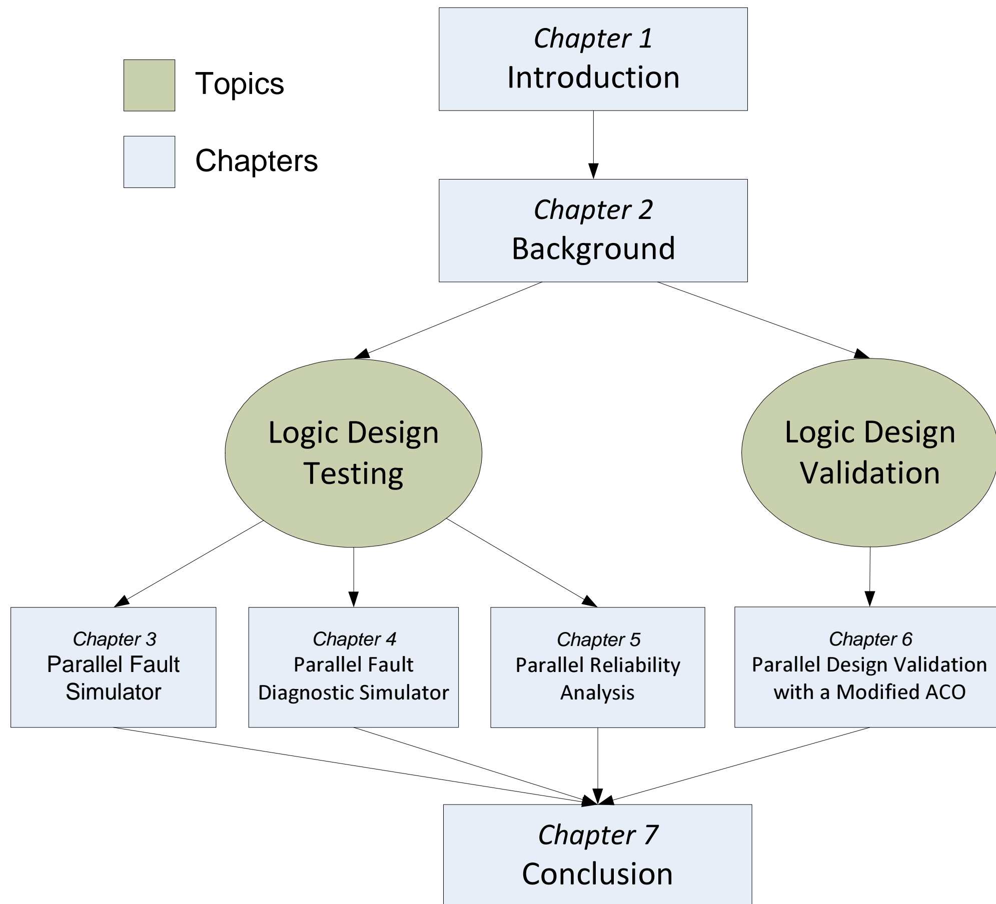

Figure 1.1: Organization of the dissertation.

which help group the single faults into fault pairs while introducing few overhead during parallel fault simulation.

4. Chapter 5 investigates the reliability analysis for logic circuits. One of the most challenging issue when porting this application to GPUs is the memory limitation on-board. Two algorithms for memory compression and simulation scheduling are introduced to improve the memory usage so as to achieve high throughput on GPUs.

5. Chapter 6 explores the swarm intelligence, particularly using ant colony optimization (ACO) to guide the search for target states. We also parallelize ACOs on GPUs and achieve significant speed-up against the applications on CPUs.

6. Chapter 7 concludes the dissertation. It summarizes the initial attempts for accelerating applications in two major EDA areas: digital design testing and Validation using the state-of-the-art many-core system, graphics processing units.

Chapter 2

Background

In this chapter, we present the hardware platform we used in our implementation, which is NVIDIA GeForce 285 GTX device. The hardware architecture, memory hierarchy and programming model will be described in order to provide the background of GPU platform. Also, the concepts related to logic system testing and validation are introduced.

2.1 Graphic Processing Units

Back in 1999, the notion of GPU was defined and popularized by NVIDIA. The unit was designed as a specialized chip to accelerate the building of images for display. As displays became more complex and demanding, the GPU evolved rapidly from a single-core processor to today's many-core architecture which is capable of processing millions of polygons per second. This is because most of the graphical display manipulation tasks such as transform, lighting and rendering, can be performed independently on different regions of the display. In other words, the same instruction can simultaneously operate on multiple independent data. Therefore, GPUs were designed as a parallel system in a Single Instruction Multiple Data (SIMD) fashion.

Recently, GPUs have emerged as an attractive and effective platform for parallel processing, espe-

cially for those data-intensive applications. With enhanced programmability and higher precision arithmetic, this has coined the term "general purpose processing using GPU (GPGPU)." [33, 60, 74, 81]. The popularity of GPGPU stems from the following.

1. Large dedicated graphics memories. Our NVIDIA GTX285 graphic card is equipped with 1 GB DDR3 dedicated graphics memory. With large size of memories, more data could be placed on the GPUs and intuitively higher levels of parallelism could be achieved.

2. High memory bandwidth. The reason that GPU is extremely memory intensive is because that the dedicated graphics memories guaranteed a high memory bandwidth. The interconnect between the memory and the GPU processors supports very high bandwidth of up to 159.0 GB/s. While the conventional CPU is only 16 GB/s, which translates to around 10 times slower.

3. High Computational power. With more than 200 hundred processing units under a highly pipelined and parallel architecture, GTX285 could achieve more than 1000 GFlops in single precision.

4. Availability. GPUs card are available off-the-shelf devices equipped in every desktops and even laptops. And also, it is relatively inexpensive considering its computational power.

Several years ago, the GPU was a fixed-function processor designed for a particular class of applications. Over the past few years, the GPU has evolved into a powerful programmable processor, with application programming interface (APIs). One of the most popular one is the Compute Unified Device Architecture (CUDA) provided by NVIDIA which abstracts away the hardware details and makes the GPUs become accessible for computation like CPUs [72]. Also, CUDA provides developers access to the virtual instruction set the memory in GPUs.

The interaction between the host (CPU) and the device (GPU) in the paradigm of CUDA is shown in Figure 2.1. The right part is the device portion which consists of a many-core GPU and the dedicated memory on-board. GPUs can directly read and write from its own memory. The graphics

controller links with the host and the device. Before the launching of the GPU kernel, users need to copy the processing data from the CPU's memory to the GPU's memory. Once the computation on the GPU is finished, the results are copied back. Also, the CPU interacts with the GPU by sending instruction and fetching signals through the graphics controller.

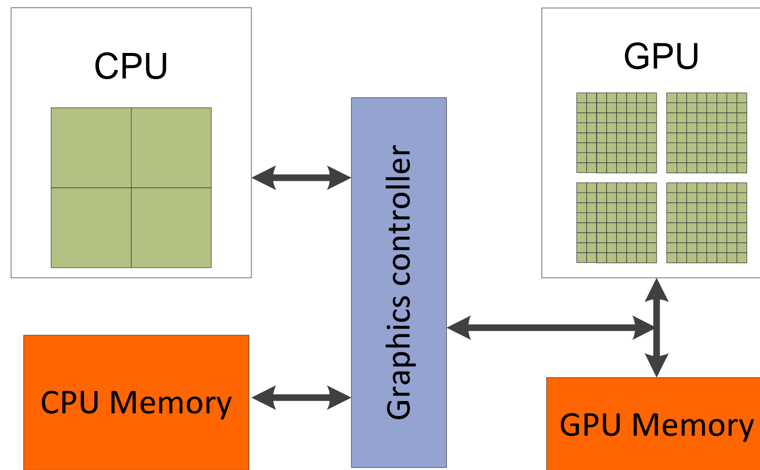

Figure 2.1: The Interface between CPU and GPU.

2.1.1 Hardware Architecture

Figure 2.2 illustrates the architecture of NVIDIA GeForce GTX 285 with 240 streaming-processor (SP) cores evenly distributed over 30 streaming multiprocessors (SMs) in ten independent processing units called texture/processor clusters (TPCs). A SM is a unified graphics and computing multiprocessor with a controller that fetches instructions and schedules them onto eight SPs that the SM contains. Each SP has its own execution hardware clocked at 1.476 GHz. All eight SPs in one SM run a copy of the same program, and in fact, they execute the same instruction synchronously. Two special functional units (SFU) are implemented for mathematical functions.

2.1.2 Memory Hierarchy

The gray boxes in Figure 2.3 illustrate the on-chip memory hierarchy in CUDA architecture:

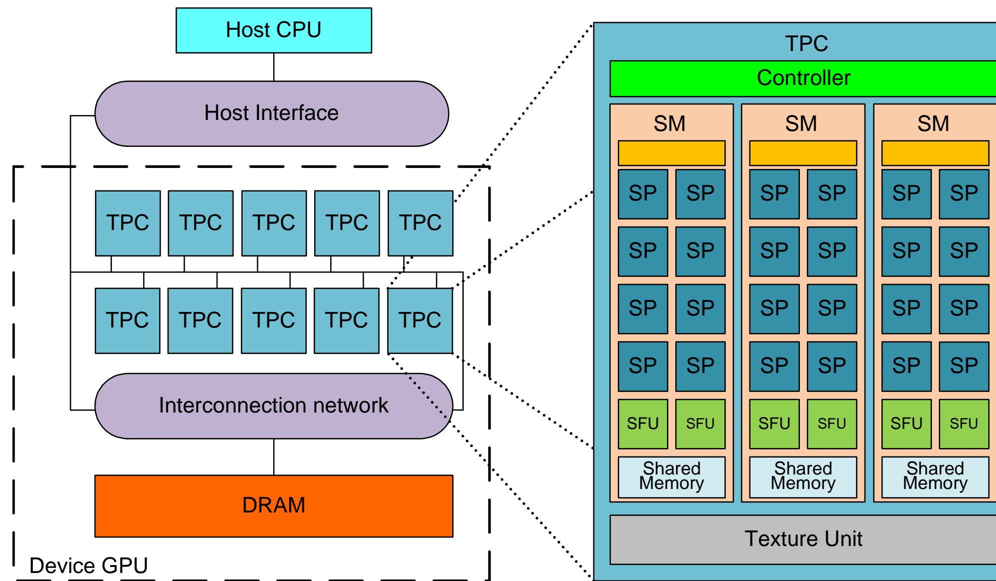

Figure 2.2: NVIDIA hardware architecture.

- *Shared memory* can be read/written from all SPs within the same SM. Every SM is equipped with a 16 KB on-chip share memory organized into 16 banks. Since the shared memory access is provided by a low-latency interconnect network between the SPs and the memory banks, the shared memory is accessible in *one* clock cycle.

- *Global Memory* can be read/written from all SPs on the GPU device. This off-chip memory (or device memory) contains 1 GB of GDDR3 global memory with a latency of 300 to 400 cycles. While the device memory has a long latency, the interconnect between the memory and the GPU processors supports very high bandwidth of up to 159.0 GB/s. To maximize the global memory throughput, it is important to exploit the coalescing mechanism (e.g., spatial locality) such that the accesses to adjacent memory addresses within neighboring SPs could be combined into a single coalesced transaction.

- *Local memory and registers* are used for register spill, stack frame, and addressable temporary variables. The total number of registers is 8 KB on each SM with low latency while accessing local memory is slow because it resides in the device memory.

Figure 2.3: NVIDIA CUDA architecture.

- *Texture memory* is bound to global memory and can provide both cache and some processing capabilities. It is a read-only cached memory shared by all the SPs in a SM. The cache working set per multiprocessor is 8 KB.

2.1.3 Programming Model

NVIDIA provides CUDA as an programing interface to the GPU device. It is based on the C programming language, with extensions to exploit the parallelism of the GPU. As summarized in Figure 2.2, the host CPU executes serial code as a general program and launches *kernels* which are CUDA functions (similar with C functions) executed on the GPU devices. A set of parallel *threads* on GPU runs the same kernel concurrently which follow the SIMT architecture. The programmer organizes these threads into a hierarchy of thread *blocks* and *grids*. The cooperative thread array (CTA), also called a thread block in CUDA terminology, is a batch of threads that can cooperate by efficiently sharing data through some fast shared memory and synchronize their executions to coordinate memory accesses. A block consists of 1 to 512 threads, each of which has a unique thread ID (TID). Figure 2.3 shows a CUDA program executing a series of two parallel kernels,

KernelA and KernelB on a heterogeneous CPU-GPU system. In this figure, KernelA executes on the GPU as a grid of 6 blocks; KernelB executes on the GPU as a grid of two blocks, with 2 threads instantiated per block.

Relevant to the GPU hardware architecture described in Section 2.1.1, one thread block could be allocated to exactly one SM, while one SM executes up to eight blocks concurrently, depending on the demand for resources. When an MP is assigned to execute one or more thread blocks, the controller splits and creates groups of parallel threads called *warps*. CUDA defines the term *warp*, a group of *32* threads which are created, managed, scheduled and executed concurrently on the same SM. Since the threads in a warp have the same instruction execution schedule, such a processor architecture is called single-instruction, multiple-thread (SIMT). It is noted that threads in the same warp can follow different instruction paths which is called *branch divergence*. However, branch divergence can drastically reduce the performance because the warp must serially execute each branch path taken, thereby disabling those threads that are not on the same path. In other words, only the threads that follow the same execution path can be processed in parallel, while the disabled threads must wait until all the threads converge back to the same path. Each warp will synchronize all the threads as they converge back to the same path. Our works achieve full efficiency because all 32 threads of a warp always agree on their execution path throughout the program.

2.1.4 Applications

Recent research shows that the GPU computing density improves faster than the CPU [75]. It has been shown that a massive array of GPU cores could offer an order of magnitude higher raw computation power than the CPU.

Signal and image processing is the initial area that GPU was targeted; FFT computation and matrix manipulation for image rendering. With the advances of GPUs, researchers also investigate the filed of cryptography. Authors in [62] first implement an efficient Advanced Encryption Standard (AES) algorithms using CUDA. The developed solutions run up to 20 times faster than OpenSSL

and in the same range of performance of existing hardware based implementations. Besides the symmetric cryptography, asymmetric cryptography such as RSA and DSA crypto-systems as well as Elliptic Curve Cryptography (ECC) are studied in [92]. Using NVIDIA 8800GTS graphics card, they are able to compute 813 modular exponentiations per second for RSA or DSA-based systems with 1024 bit integers. Moreover, the design for ECC over the prime field even achieves the throughput of 1412 point multiplications per second.

Like many other software communities, the networking area also needs an overhaul of computational power so as to keep pace with the ever increasing networking complexity. It is thus appealing to unleash the computing power of GPU for networking applications [36, 42, 9]. PacketShader, a high-performance software router framework for general packet processing acceleration is proposed in [42]. The authors implemented IPv4 and IPv6 forwarding, OpenFlow switching, and IPsec tunneling to demonstrate the flexibility and performance advantage of PacketShader. Combined with their high-performance packet I/O engine, PacketShader outperforms existing software routers by more than a factor of four, forwarding 64B IPv4 packets at 39 Gbps on a single commodity PC. An immature idea of upgrading NS-2 simulator using GPGPU is proposed in [36]. Although no experimental results are given in the paper, the authors claimed that if they can accelerate the propagation model, the gained speedup could have a significant value for large scale networks. Researches in [9] implemented a similar idea to accelerate a discrete-event parallel network simulator, PRIME SSFNet using GPUs. Basically, GPUs are used to perform ray-tracing at high speeds to facilitate propagation modeling based on geometric optics. On average, the proposed system with four GPUs and a CPU achieves a throughput five times faster than a single GPU.

Data mining algorithms are an integral part of a wide variety of commercial applications such as online searching, shopping and social network systems. Many of these applications analyze large volumes of online data and are highly computation and memory-intensive. As a result, researchers have been actively seeking new techniques and architectures to improve the query execution time. In [37], data is streamed to and from the GPU in real time and the blending and texture mapping functionalities of GPUs are exploited. The experimental results demonstrate a speedup of 2-5 times

over high-end CPU implementations.

The advent of GPGPU also brought new opportunities for speeding up time-consuming electronic design automation (EDA) applications [29, 38, 39, 21, 20, 47, 67]. The authors in [38, 47] are the pioneers who parallelized EDA algorithms on GPUs. They exploited both fault parallelism and pattern parallelism provided by GPUs and implemented an efficient fault simulator. Also, efficient gate level logic simulators are proposed by authors in [21, 20] where the circuits are partitioned into independent portions and processed among blocks in parallel. Besides the gate level simulators, a GPU based System-C simulator is introduced in [67]. The discrete-event simulation is parallelized on the GPU by transforming the model of computation into a model of concurrent threads that synchronize as and when necessary. The GPU-based applications for EDA community are not restricted to simulators. Since the irregular data access patterns are determined by the very nature of VLSI circuits, authors in [29] accelerated sparse matrix manipulations and graph algorithms on GPUs which have widely been used in EDA tools.

2.2 Digital Systems Testing

2.2.1 Single Stuck at Fault Model

Logical faults represent the effect of physical defects on the behavior of the modeled system. Unless explicitly stated, most of the literature in the testing area assumes that at most one fault is present in the system, since multiple faults are generally much easier to detect. This single-fault assumption significantly simplifies the test generation problem. Practically, even when multiple faults are present, the test derived under the single-fault assumption is usually applicable for the detection of multiple faults by composing the individual tests designed for each single fault.

Some well-known fault models are the single stuck-at fault (SSF), bridging fault, and delay fault. In this dissertation, we target the single stuck-at fault model, the simplest but most widely used fault model. The effect of the single stuck-at fault is as if the faulty node is tied to either *VCC*

(s-a-1), or *GND* (s-a-0), shown in Figure 2.4. The advantages of using single stuck-at fault model include:

1. It can detect many different physical defects;
2. It is independent of technology;
3. Experiments have shown that tests that detect SSFs detect many other faults as well;
4. The total number of SSFs in the circuit is linear to the size of the circuit;
5. Many other fault models can be represented as a combination of two or more SSFs.

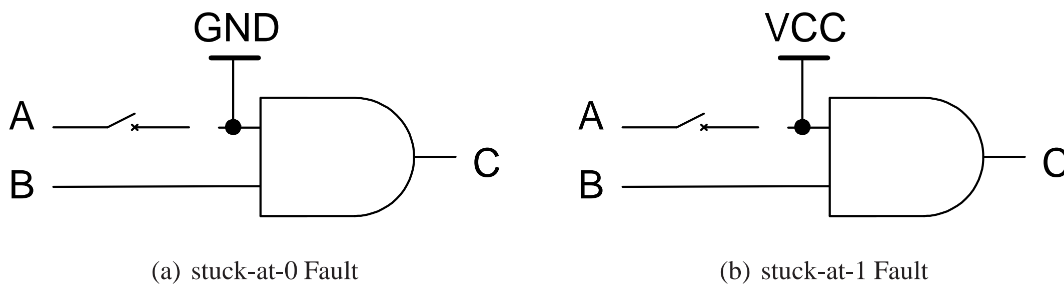

(a) stuck-at-0 Fault (b) stuck-at-1 Fault

Figure 2.4: Stuck-at Fault Model.

2.2.2 Fault Simulation

Fault simulation plays an important role in the testing of logic systems. It is widely used in test generation, fault dictionary construction, and so on. For example, many test generation systems use a fault simulator to evaluate a proposed test *T*, then change T according to the results of the fault simulation until the obtained coverage is considered satisfactory. Therefore, the process of fault simulation will be launched several times which makes it a most time-consuming procedure during the test generation.

The process of fault simulation is illustrated using a miter circuit as shown in Figure 2.5. The miter circuit is built by connecting a fault-free circuit with its copy injected with a single stuck-at

fault in the following manner. The corresponding primary inputs are connected together, and the corresponding primary outputs are connected via XOR gates. Then all XOR gates are connected to an OR gate. As long as at least one value of the outputs is different, the output of the miter circuit will show a logic one which means that the fault is detected by the test pattern *T*. It is noted that during fault simulation, we drop the faults from the fault list that has been detected. This process is called *fault-dropping*.

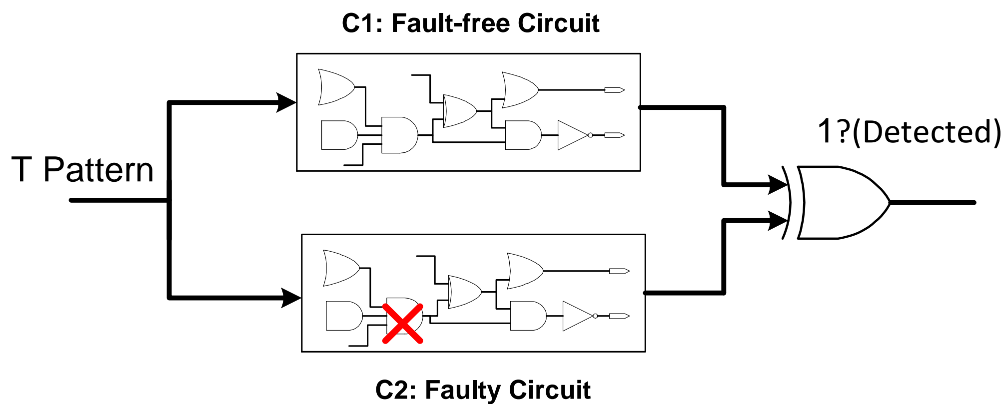

Figure 2.5: Miter Circuit for Fault Simulation.

Parallel-Pattern Single-Fault Propagation (PPSFP) method is widely used for parallel fault simulation on conventional computer architecture which includes two separate concepts, single-fault propagation and parallel-pattern evaluation [97].

First it conducts a parallel fault-free simulation of a group of W vectors which is called parallel-pattern evaluation. The idea is to store the values of a signal in a W-bit memory location. By exploiting the inherent bit parallelism (*32*-bit or *64*-bit), the simulator could evaluate gates by Boolean instructions operating on W-bit operands which generates output values for W vectors in parallel. Then, the remaining undetected faults are serially injected and faulty values are computed in parallel for the same set of vectors. Comparisons between good and faulty values involve W bits. Detected faults are dropped and the above steps are repeated until all vectors are simulated or all faults are detected.

2.2.3 Reliablity Analysis

CMOS scaling has taken us to the nanometer-range feature sizes. In addition, non-conventional nanotechnologies are currently being investigated as potential alternatives to CMOS. Although nano-scale circuits offer low power consumption and high switching speed, they are expected to have higher error rates due to the reduced margins to noise and transients at such small dimensions.

The errors that arise due to temporary deviation or malfunction of nano-devices can be characterized as probabilistic errors, each of which is an intrinsic property of each device. Such errors are hard to detect by regular testing methodologies because they may occur anywhere in the circuit and are not permanent defects. Thus, each device i (logic gate or interconnect) will have a certain probability of error $\tau_i \in [0, 0.5]$, which cause its output to flip symmetrically (from $0 \to 1$ or $1 \to 0$). A common fault model of a circuit with n gates is defined as the failure probability $\vec{\tau} = \{\tau_1, \tau_2, \ldots, \tau_n\}$, where τ_k is the failure probabilities of the kth gate. In our experiments, we assign an universal error rate (failure probability) to all the gates for simplicity. However, RAG is able to consider gates with different error rates.

The reliability of logic circuits could be evaluated by several measures. Suppose we have a logic circuit with m outputs. In [24], the probability of errors for each output i, denoted as δ_i, is employed. Among the m outputs, the maximum probability of error, $max_{i=1}^{m}(\delta_i)$ is used in [86] and authors in [22] utilized the average reliability value, $sum_{i=1}^{m}(1 - \delta_i)/m$. The authors using PTMs [49] proposed *Fidelity*, denoted as F, which is the probability that the entire circuit is functionally correct (all m outputs are fault free). They also employed the average reliability among outputs (R_{avg}) which is also the metric we used in this work.

2.3 Digital Systems Validation

2.3.1 State Justification

The complexity of current designs makes it hard to generate effective vectors for covering corner cases. An example corner case is a hard-to-reach state needed to detect a fault or prove a property. Despite the advances made over the years, state justification remains to be one of the hardest tasks in sequential ATPG and design validation. In this section, we presents background of status justification.

Definition 1. *For a digital circuit with m inputs and n Flip-Flops (FFs), the state space and the primary inputs (PIs) are defined by indexed sets of Boolean variables $V = \{v_1, \ldots, v_n\}$ and $W = \{w_1, \ldots, w_m\}$ respectively, where v_i/w_j denotes for the logic value ($q \in \{0, 1\}$) of the ith Flip-Flop / j^{th} PI.*

Let $V' = \{v'_1, \ldots, v'_n\}$ be the next state variables, then the next state function can be expressed as $V' = \delta(V, W)$. Based on the next state function, a transition relation $T(V, W, V')$ can be constructed such that $T(V, W, V') = 1$ iff $V' = \delta(V, W)$.

For the variables in time frame t, we use $V^t = \{v_1^t, \ldots, v_n^t\}$ and $W^t = \{w_1^t, \ldots, w_n^t\}$. Particularly, the initial state is denoted by V^0 and target state is V^f. Also, a sequence of input vectors $W^i, W^{i+1}, \ldots, W^j$ can be represented as $W^{i \ldots j}$ when $i \leq j$. Similarly for state variables V.

Definition 2. *For a sequential circuit, transitions among states can be illustrated by a directed graph $G(N, E)$, namely the State Transition Graph (STG), with the nodes set $N = \{V^0, V^1 \ldots\}$ and the edge set $E = \{e_{V^i V^j} | V^i, V^j \in V, \exists W \; s.t. \; V^j = \delta(V^i, W)\}$.*

Based on the STG, the process of state justification can be formulated as a process of searching for a directed path from vertex V^0 to V^f in $G(N, E)$. Such a path with length t can be expressed as a sequence of inputs: $W^{0 \ldots t}$ which satisfies the Boolean equation:

$$V^0 \wedge \bigwedge_{i=0}^{t-1} T(V^i, W^i, V^{i+1}) \wedge V^f \tag{2.1}$$

For instance, Figure 2.6 illustrates the STG $G(N, E)$ of a design with 1 primary input, w_1 and 4 FFs. It can be observed that there exist several paths from the initial state A to target state L; one such path is $A \to C \to E \to I \to L$. However, it is infeasible to construct a STG for a complex design. To overcome this, an abstraction engine is used for our purpose.

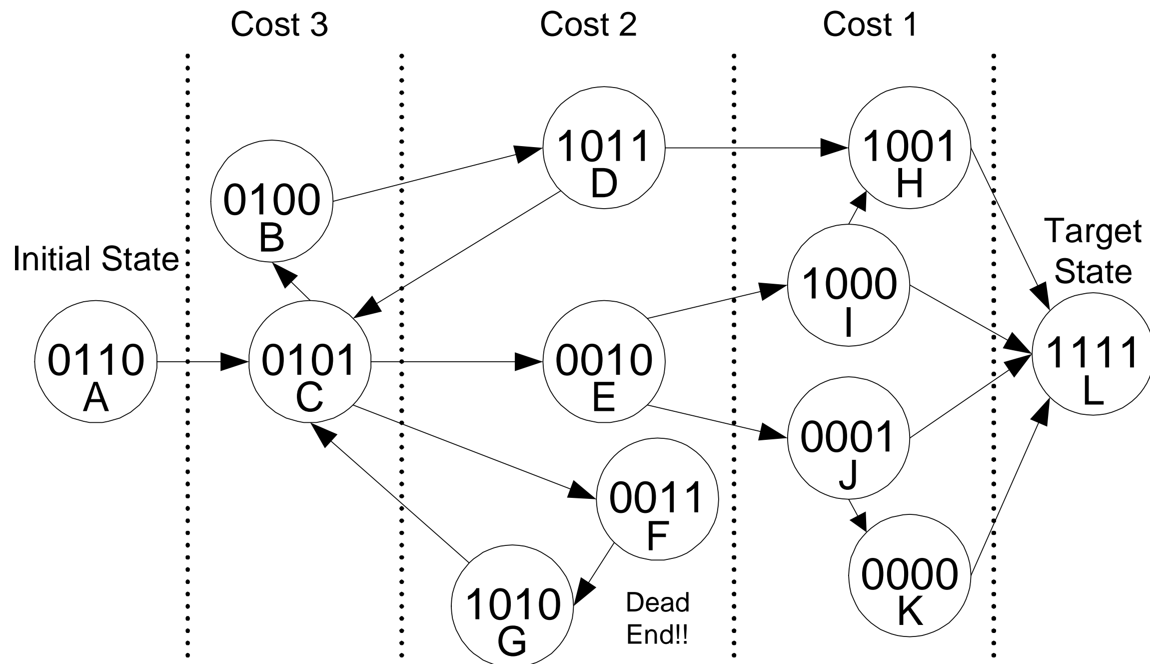

Figure 2.6: State transition graph

2.3.2 Abstraction Guided Simulation

In order to mitigate the computational requirements of formal methods such as [12, 16], which are based on Binary Decision Diagrams (BDDs), deterministic ATPG, and/or Boolean satisfiability, researchers have proposed hybrid techniques that utilize both simulation and formal techniques. These methods have the advantage of greatly reducing the memory and computational requirement of state traversal through the use of simulation, but also are able to justify hard-to-reach corner cases. Early examples, such as [99, 88], utilize enlarged targets, generated from the initial target state and heuristic based sub-graph searches, enabling the system to make the target easier to

reach. However, as circuit complexity grew, these methods became computationally infeasible due to memory explosion in finding an enlarged target, and with the explosion of subgraphs to be checked in local model checking. To handle these limitations, researchers introduced abstraction guided simulation, which utilizes formal techniques to create a simplified model of the behavior of the circuit state variables [28, 78, 90].

The concept of a distance based cost function abstraction was proposed by the authors of [90]. This cost function abstraction interacts closely with the target state allowing for customization of the abstraction for each property to be verified. Additionally, [78] provided a method of abstraction refinement using data-mining to aid a GA-based search engine. However, in both cases, it is still sometimes difficult to guide the search through narrow state paths without the use of a BMC. The authors of [28] propose the method of buckets representing the distance of the states they contain from the abstracted target state. In such a method, after each state has been simulated, the program flips a fair coin to determine if it should continue simulation or backtrack to a different ring. While such an approach avoids some local minima, some states remain hard-to-reach. Finally, [53] proposes the use of ACOs for solving the state justification problem utilizing an abstraction cost function as a heuristic the ACO guides the search and limits the input space based on information discovered during runtime.

Figure 2.7 illustrates how an abstract trace can help guide the generation of the concrete trace. Because the state transition graph for the abstract model is much simpler than the one for the original concrete model, it can be constructed. Every concrete state is mapped into an abstract state via a cost function $Cost()$. During the search, one looks for clues/hints that can help move the current concrete state to the one that maps into the next closer onion ring, until the target is reached.

State Variable Extraction

Our proposed work in Chapter 6 employs state variable extraction scheme which is first introduced in [98] for partitioning the state set. The framework is shown in Figure 2.8. Different from [90]

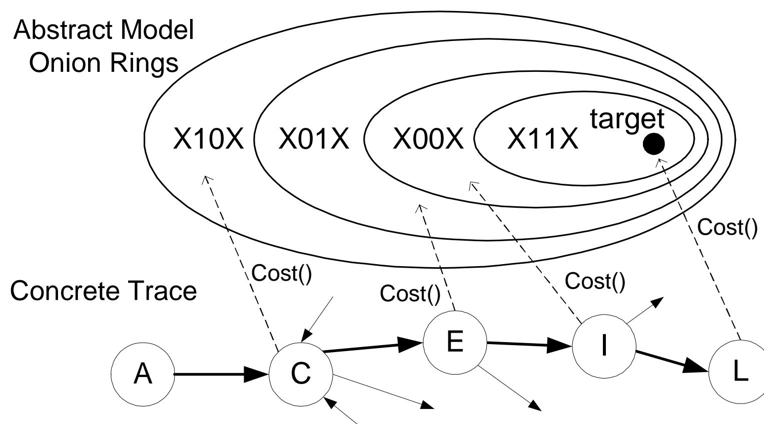

Figure 2.7: Abstract model and concrete state mapping

where the high level description of the design is needed, this technique is only based on the gate level description of the circuit. At first, we perform a random simulation of the circuit using L random vectors (in our work, $L = 10000$) and record the values of each FF. After simulation is finished, correlation among the FFs is extracted. Finally, partitioning is applied based on the characteristic state variables and the state partition set is built.

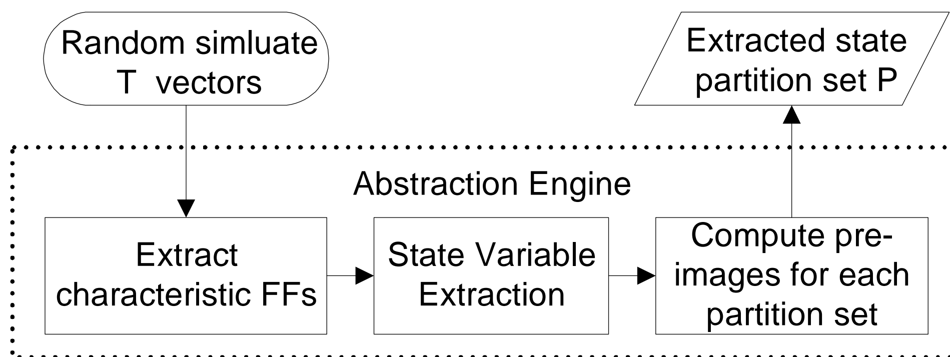

Figure 2.8: Framework of abstraction engine

Definition 3. *The extracted state partition is defined as* $P = \{p_1, p_2, \ldots, p_J\}$, *where the* n *flip-flops are divided into* J *sets.*

The state space V is thus decomposed to $V_{p_1}, V_{p_2}, \ldots, V_{p_J}$. V_{p_i} is defined as an *abstract state* of V in partition set p_i. The state variables excluded in p_i are replaced with *don't care X*. As shown in

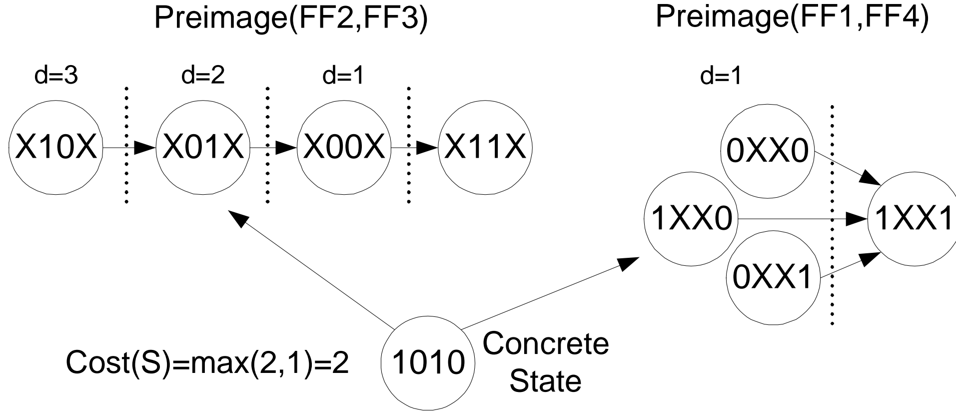

Figure 2.9: Preimages of two partition sets

Figure 2.9, $p_1 = \{v_2, v_3\}$ denotes for a set that includes the second and third FF while the other FFs are set to *X*.

Computing abstract preimages

The *preimage* of a set of state V^f, $S(V^f)$, is the set of states from which the design can transition to V^f in one time frame via the application of a certain vector, W on PIs of the circuit:

$$\forall V \in S(V^f),\ \exists W\ s.t.\ T(V, W, V^f) = 1. \tag{2.2}$$

Computing a preimage to a *fixed point* means iterating the preimage computation until the transitive set of states obtained no longer grows. In our work, we use a SAT engine to compute the abstract preimages for every partition sets to a fix point. Because each partition only consists of eight flip-flops, preimage computation for each partition is fast and effective. As shown in Figure 2.10, the design is modified to a one time-frame unrolled combinational circuit model in which Pseudo-Primary Input (PPI) feeds the FFs in the original circuit and the outputs of the FFs connect to Pseudo-Primary Output (PPO). The PPOs are set to the target states S^f while PPIs are constrained to $\neg S^f$ in order to exclude all the target states in S^f. The inputs to the SAT engine is the target states set, the combinational portion of the design and the constrains to PPIs. After solving the formula, the SAT-solver will give a solution towards the PPIs from which a new state vector V is

assigned. The new state vector is called the 1-step preimage of the states in S^f. For each partition set p_j, we add $V^f_{p_j}$ to set S as well as its complement to PPIs and run the SAT engine again. The procedure is repeated until the instance is unsatisfiable (UNSAT) which means that all possible 1-step preimage solutions of S^f is contained in S. Then, we replace S^f with S and compute the preimages in next time frame. The process is terminated when $S = \emptyset$ which means that all the abstract states are obtained for partition p_j.

The size of each partition set p_i is experimentally limited to a maximum of 8 variables. Thus, the number of distinct abstract states in one group is at most 256 which makes preimage computation very lightweight. At the same time, abstract groups of 8 state variables are demonstrated to be effective for guidance according to our experimental results.

Preimages of two partition sets (FF_2, FF_3) and (FF_1, FF_4) are shown in Figure 2.9.

Definition 4. *The distance of a state V in partition set p_j, $d(V_{p_j})$ is defined as the number of time frames it takes from V_{p_j} to $V^f_{p_j}$.*

Using Figure 2.9 again, the distance between state 1010 and the target is 2 for the partition set $\{p_2, p_3\}$ and 1 for $\{p_1, p_4\}$. By partitioning the state space as in [98], we can find abstract groups that are highly related to the target. Thus, more useful approximate distances can be obtained. For example, the partition set $\{p_2, p_3\}$ is more favorable than $\{p_1, p_4\}$ because the abstract distance in set $\{p_2, p_3\}$ is more accurate when compared to the concrete model.

2.3.3 Partition Navigation Tracks

Partition Navigation Tracks (PNTs) represent the cost function used as our heuristic. A pictorial representation is shown in Fig. 2.7. A PNT is generated for each flip-flop partition utilizing a SAT engine. The SAT engine is fed a set of clauses defining the behavior of the circuit as well as the values of the flip-flops of the partition in the target state. To facilitate the discussion on generating PNTs, the following definitions are needed.

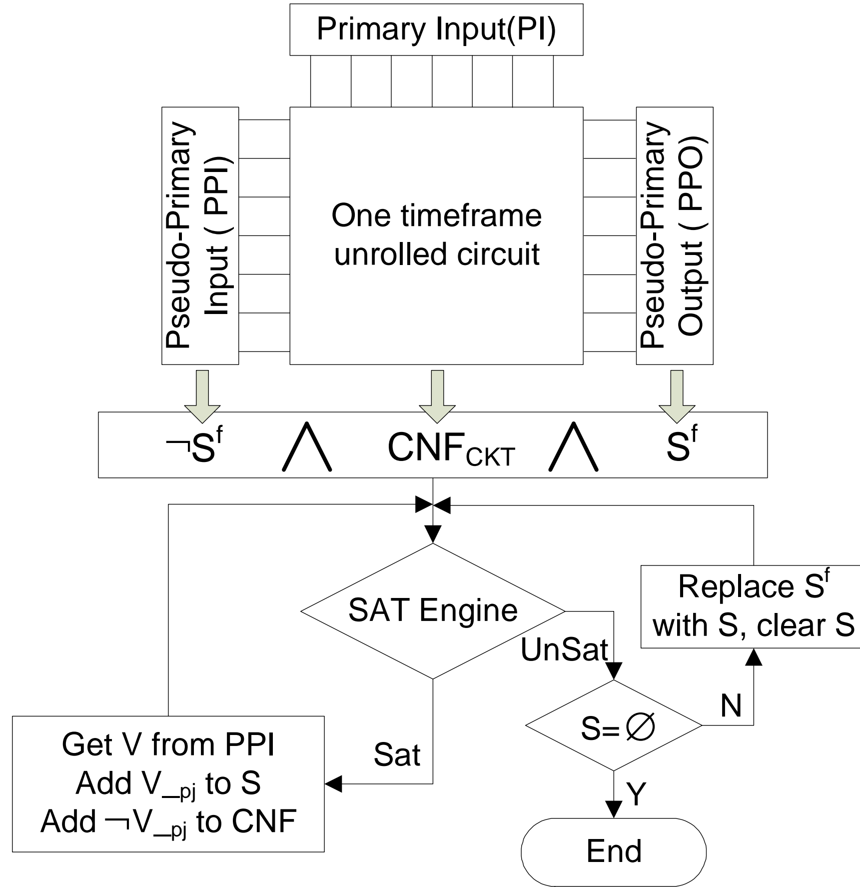

Figure 2.10: Framework of computing preimage

Definition 1: For any circuit with n state variables and m inputs, the state and primary inputs can be represented as sets $V = \{v_1, v_2, ..., v_n\}$ and $W = \{w_1, w_2, ..., w_m\}$ respectively.

Definition 2: A partition is a set of 8 state variables, $P = \{p_1, p_2, ...p_8\}$, such that a one to one mapping exists from each state variable to a partition element $v_k \rightarrow p_i$.

Definition 3: For any state for a set of states, there exists a transition function such that $V' = Next(V, W)$. A partitioned transition function exists as well such that $P' = \{p'_1, p'_2, ..., p'_8\}$, and $P' = Next(P, W)$.

Given a target state T and a partition target T_p, $S(T_p)$ is the set of all partition states that can reach

T_p in one timeframe for some specific input vector W. Formally, $S(T_p)$:

$$\forall P \in S(T_p), \exists W s.t. Next(P, W) = T_p$$

Each subsequent level of the PNT is calculated by applying a state from the previous level as a constraint clause to the SAT engine and finding all possible states that reach that state:

$$\forall P \in S^n(S(T_p)), \exists W s.t. Next(P, W) \in S^{n-1}(T_p)$$

This calculation is continued until a fixed point is reached such that $S^n(T_p) = \emptyset$ or until all 256 possible partition states have been reached.

Due to the small number of flip-flops involved in each partition, this method remains lightweight and helps minimize the amount of initial computation required to create the abstraction. Additionally, 8 flip-flop partitions have been previously shown to be effective in guiding the circuit to the target [78, 53].

Chapter 3

Parallel Fault Simulator

3.1 Chapter Overview

In this chapter, we present an efficient parallel fault simulator, FSimGP^2, that exploits the high degree of parallelism supported by a state-of-the-art graphic processing unit with the NVIDIA Compute Unified Device Architecture. A novel three-dimensional parallel fault simulation technique is proposed to achieve extremely high computation efficiency on the GPU. Global communication is minimized by concentrating as much work as possible on the local device's memory. We present results on a GPU platform from NVIDIA (a GeForce GTX 285 graphics card) that demonstrate a speedup of up to 63$\times$ and 4$\times$ compared to another two GPU-based fault simulators and up to 95$\times$ over a state-of-the-art algorithm on conventional processor architectures.

The rest of the chapter is organized as follows. A brief introduction is given in Section 3.2. In Section 3.3, we review the previous work in the area of GPU-based parallel application for fault simulation. Section 3.4 outlines a high-level process view of the proposed view of FSimGP^2. The experimental results are reported in Section 3.5. Finally Section 3.6 concludes the chapter.

3.2 Introduction

Fault Simulation, a process of simulating the response of a circuit-under-test under a set of testing patterns in the presence of modeled faults, plays an important role to various applications in very-large-scale integration circuit test including Automatic Test Pattern Generation, built-in self-test, testability analysis, etc. In the past several decades, significant efforts have been devoted to accelerate this process [51, 71, 87]. However, with the advances in current VLSI technology, more devices can be placed on a single chip. As a result, there is a need for efficient fault simulators that are able to handle large designs with extremely large test sets. In addition to test-related applications, simulation of a large number of test patterns can also benefit many other applications. Fast (fault) simulators would thus offer tremendous benefit.

In order to alleviate the simulation bottleneck, researchers have proposed several parallel processing approaches by exploiting the power of supercomputers, dedicated hardware accelerates and vector machines. These techniques can be divided into three main classes:

1. *Algorithm Parallelism.* Different tasks such as logic gate evaluation, scheduling and input/output processing are preformed in a pipelined fashion and distributed to dedicated processors. Thus, by functional partitioning of simulation algorithms, the communication and synchronization between processors can be reduced [3, 66, 7, 5].

2. *Model Parallelism.* The gate-level netlist of the CUT is partitioned into several components. Since each sub-circuit can be simulated independently, different elements are computed by several processors in parallel [69, 79, 80, 93].

3. *Data Parallelism.* In fault simulation, either multiple patterns and/or multiple faults can be processed independently on one of the processors [6, 10, 43, 46, 76, 77, 84]. Techniques where sets of input vectors (faults) are simulated in parallel are called *fault-parallel* (*pattern-parallel*). Since there is no data dependence between processors, data parallelism is particularly attractive for our implementation using Graphics Processing Units.

In this chapter, we present a novel three-dimensional parallel fault simulator, called FSimGP^2 - Fault Simulator with GPGPU. The main motivation behind this work is to harness the computational power of modern day GPUs to reduce the total execution time of fault simulation without compromising the output fidelity. Our method exploits block-, fault- and pattern- parallelism together which is capable of efficiently utilizing memory bandwidth and massive data parallelism on the GPU. The overhead of data communication between the host (CPU) and the device (GPU) is minimized by utilizing as much of the individual device's memory as possible. FSimGP^2 also takes advantage of the inherent bit-parallelism of logic operations on computer words. In addition, a clever organization of data structures is developed to exploit the memory hierarchy characteristic of GPUs. The technique is implemented on the NVIDIA GeForce GTX 285 with 30 cores and 8 SIMT execution pipelines per core [59]. Our experimental results demonstrate that the proposed FSimGP^2 achieves more than three times speedup in comparison with recently developed GPU-based fault simulators [47] and [38] as well as a state-of-the-art sequential fault simulation algorithm [51] implemented on conventional processor architecture.

3.3 Background

In this section, we will present the background on parallel fault simulation and previous related work based on the CUDA architecture.

3.3.1 Fault Simulation

A fault simulator computes an output response of a logic circuit for each given input vector under each given fault instance. In this work, our proposed approach targets on full-scan gate-level circuits and assumes the single stuck-at fault model. Our fault simulator is to produce the fault simulation results for a *collapsed* fault list in a circuit under a large set of random vectors. In addition, *fault dropping* is implemented which means that a fault is removed from the fault list as soon as it is detected by any test pattern.

Definition 5. *Let* V *be the total number of test vectors for fault simulation and* N_f *be the number of collapsed faults. The word size,* w*, is defined as the number of bits in the computer word. In our implementation,* w *equals* 32*. The fault/pattern parallelism factors are defined as variables* p *and* t *which denote the number of faults/patterns simulated at a time.*

Recall that parallelism in fault simulation is classified into fault-parallel and pattern-parallel methods. The former simulates p faults for each vector at a time while the latter simulates t patterns simultaneously for one target fault. Parallelism can be furthered on GPUs by extending word-level parallelism onto multiple threads. Hence, we now simulate $p \times w$ faults or $t \times w$ patterns in parallel by simply extending the simulation unit from one CPU word of size w to a vector consisting of p or t words of size w. Such simulation techniques are referred to as *extended* fault- (or pattern-) parallel simulation.

3.3.2 Previous Work

The authors in [38] give the first attempt to implement fault simulation on GPUs. Both fault parallelism and pattern parallelism are employed such that each thread evaluates one gate with different test vectors as well as different injected faults in parallel. The gate evaluation is conducted by a look-up-table (LUT) implemented in the texture memory to exploit the memory bandwidth of GPUs. Although the proposed implementation could achieve 35$\times$ speedup in comparison with a commercial sequential fault simulator, the computation capacity of the GPU has not been fully exploited due to two major factors:

1. *Transmission Overhead* between CPUs and GPUs. Since the netlist of the circuit is not stored on the GPU, the host is responsible for all the scheduling and loading tasks to the device. Therefore, the performance overhead of data transmission between the host and the device becomes a major bottleneck. In our work, we try to minimize such communication overhead by employing a new data structure to store some of the circuit and fault information on the GPU without causing excessive data transmission. *All* the simulation workloads are

processed on the GPU while the CPU is only responsible for providing fundamental data including circuit netlist, fault lists and collecting fault detection results from the GPU.

2. *LUT* implemented in the texture memory exploits the extremely large memory bandwidth of GPUs. However, each thread could only evaluate *2* gates with the LUT at a time. Our method takes advantage of the inherent *bit-parallelism* of logic operations on computer words on GPUs. Thus, a packet word of 32 bits can be simulated concurrently such that each thread could evaluate *32* gates simultaneously.

An efficient fault simulator is proposed in [47], which uses the parallel-pattern single-fault propagation (PPSFP) paradigm. It achieves a considerable speedup of $16\times$ compared to a state-of-the-art fault simulator, FSIM [51]. While PPSFP techniques can prune unnecessary evaluations during simulation, we believe that the overhead of event scheduling and the cost associated with conditional branches within a warp on the GPU may diminish the gain by exploiting such approaches. Moreover, in [47], the circuit topology has a strong impact on the performance because the simulator running on GPU can *only* handle the gates with two inputs. Hence, the speedup may be reduced for circuits having gates with more than two inputs.

The authors in [20, 21] developed a GPU-accelerated logic simulators under the model-parallelism scheme. The circuits are partitioned into several clusters and each of them is assigned to a thread block. Such a model-parallelism algorithm is not applicable for fault simulation because in most cases, only a small percentage of gates in a circuit are required to be simulated for a specific target fault. Consequently, the overhead of unnecessary evaluations on unexcited gates might potentially diminish the gain through computing events in parallel. Our method keeps the fault-free values of all the gates on the GPU's device memory and only simulates the elements in the fanout cone of the faulty gate.

In light of the above discussion, our proposed method introduces a novel three-dimensional parallel fault simulation technique that avoids all those wasteful simulations and thus maximally harnesses the GPU's large memory bandwidth and high computational power. Our method can be applied to any circuit irrespective of its topology. Moreover, a dynamic load balancing algorithm is proposed

based on the atomic function provided by CUDA to distribute the workload evenly across the thread blocks.

3.4 FSimGP^2 Architecture

In this section, we first present our three-dimensional parallel fault simulation algorithm. Then the framework of FSimGP^2 is described, followed by the load balancing and memory scalability techniques.

3.4.1 Three-Dimensional Parallel Fault Simulation

Definition 6. *When injecting a fault f onto the circuit, only the gates in the fanout region (FR) beyond the fault site toward the primary outputs need to be evaluated. We define such set of gates as FR$_f$ and its size as s_f, which is the number of gates in FR$_f$.*

Definition 7. Compact faults set *(CFS) is a set of faults with identical FRs. For simplicity, we call this group of faults a* compact fault*, represented as cf. The total number of compact faults (cfs) in the circuit is denoted as N_{cf}, and the size of the ith CFS is n_i, which is the number of collapsed faults belonging to this CFS.*

Figure 3.1 illustrates a CFS whose faulty gate (location) is g_1. There are five collapsed, non-equivalent faults ($f_1 \sim f_5$) included in this CFS. The position of gate g_1 in the circuit is shown in Figure 3.1. It is clear that all these five faults share the same shaded fanout free region. Thus, we compact these five faults into a compact fault cf which acts as a *virtual single fault* during fault simulation.

In FSimGP^2, for a compact fault cf, each gate in the fanout region of compact fault (FR$_{cf}$) will be fault-simulated with t vectors, processed on t threads, where t is the pattern-parallelism factor defined before. In Figure 3.1, a compact fault cf is injected on gate g_1 and the FR$_{cf}$ is illustrated as

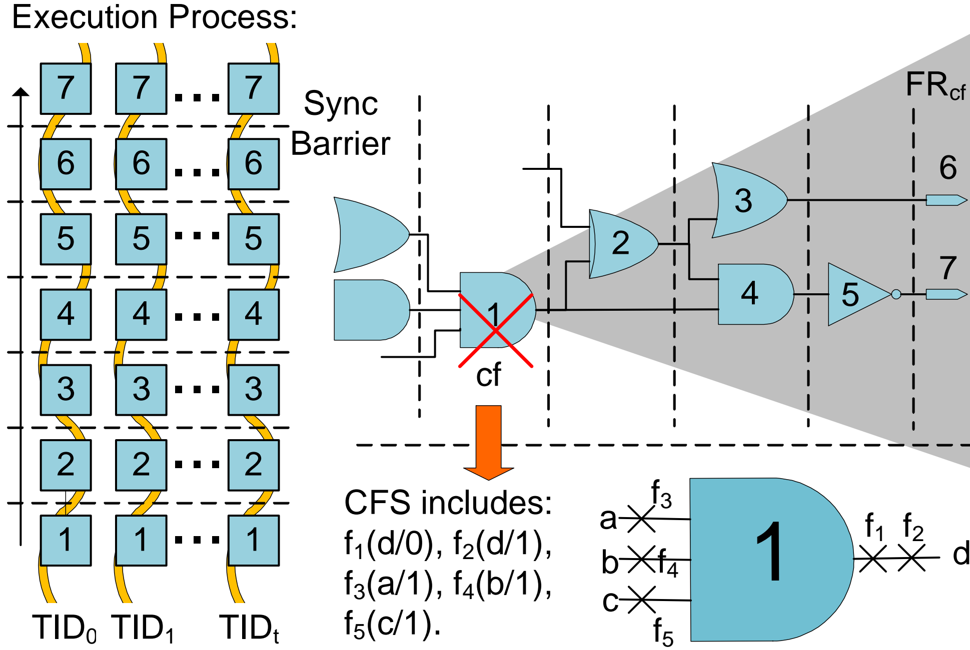

Figure 3.1: Fanout region of compact fault. FR: Fanout region; TID: Thread ID.

the shaded region. During fault simulation, we need not simulate all the faults represented by cf; instead, just one simulation pass is needed since they share the same FR. Note that whenever cf is detected, not all faults represented by this compact fault may be detected because some of them may not be excited by the given vectors. The netlist is levelized a priori and the gates in the FR_{cf} are indexed according to the ascending order of their levels. The left part of Figure 3.1 shows the execution process of a block where t threads indexed from TID_0 to TID_t are launched. All the threads evaluate the same gates in FR_{cf} concurrently followed by a synchronization barrier. Thus, all the gates in the fanout region of compact fault cf, FR_{cf}, are evaluated in a forward levelized fashion.

It is noted that some PPSFP techniques [51] can further prune unnecessary evaluations of gates in FR_{cf}. However, we argue that the overhead of event scheduling and the cost associated with conditional branches within a warp on the GPU may diminish the gain by exploiting such approaches. Moreover, the overhead can be alleviated by simulating compact faults (defined below) in parallel.

Definition 8. *FSimGP^2 employs a novel approach called* cf-parallelism*, wherein different faults*

in the same compact fault set, CFS could be simulated in parallel. Also, multiple compact faults could be assigned to different thread blocks and processed concurrently on the GPU. We defined such technique as block-parallelism *and factor* k *as the block-parallelism factor which represents the number of blocks (cfs) simulated at a time.*

To utilize memory bandwidth and massive data parallelism in an efficient way, FSimGP^2 exploits *block-*, *cf-* and *pattern-parallelism* together. Namely, we simulate multiple compact faults (which represent many single faults) over multiple patterns at a time. We call this technique *three-dimensional parallel fault simulation* illustrated in Figure 3.2. All the collapsed faults with a total number of N_f in the circuit are grouped into compact faults with a total number of N_{cf}. All these N_{cf} compact faults are evenly distributed onto k thread blocks running concurrently on the GPU. For example, $block_1$ is assigned with cf_i (including n_i single faults). Each block allocates t threads simulating t test vectors for one compact fault in parallel. All the compact faults assigned for one block are processed in serial.

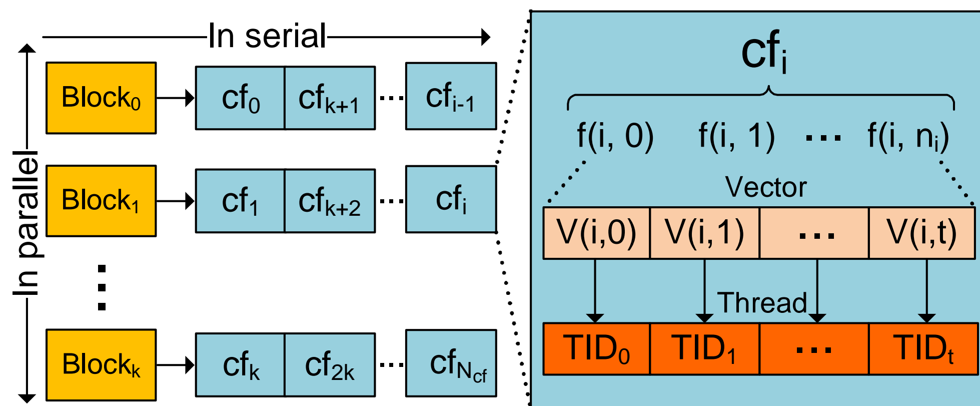

Figure 3.2: Three-dimensional fault simulation architecture.

3.4.2 Framework

The high-level flow of FSimGP^2 is shown in Figure 3.3. At the beginning, the CPU reads in the circuit netlist and generates its collapsed fault list. The original faults will be grouped to form

compact fault sets (CFSs) and for each compact fault, its fanout region, FR_{cf}, is computed by a breadth-first search from the faulty gate location in a forward levelized manner. Compact faults will be partitioned into k blocks according to our static load balancing approach. The initial data transferred from the CPU to the GPU include the circuit netlist, compact fault list with corresponding fanout region (FR_{cf}) and random generated test vectors. Also, some other data structures are claimed on GPU which are t_{val} and f_{val}, two arrays of unsigned integers for storing fault-free and faulty values, respectively. The det is an array of Boolean values for indicating the detection status of faults.

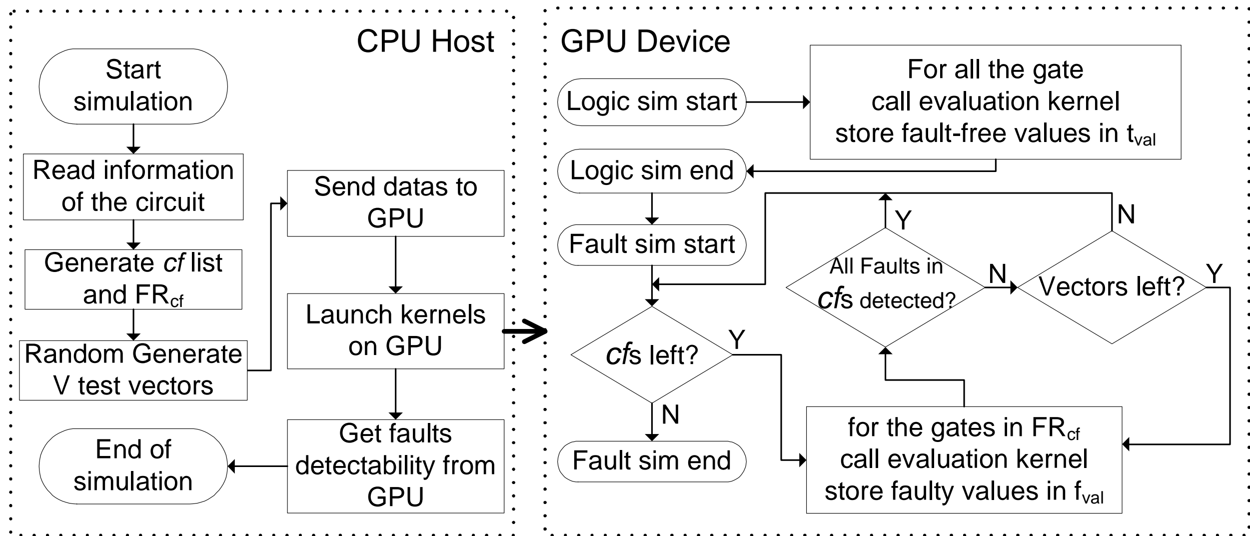

Figure 3.3: FSimGP^2 framework.

Then, the GPU will take over the main work load of fault simulation. First, a logic (fault-free) simulation will be performed for all the test vectors in parallel. The fault-free values are stored in t_{val} array. Next, the three-dimensional parallel fault simulation kernel is launched onto the GPU. For each block, one compact fault set (CFS) will be evaluated by t threads with t different test vectors. As an example, the pseudo-code of the kernel which simulates the faults in a CFS is provided in Algorithm 1. Parameters t_{val} and f_{val}, respectively, are pointers to the global memory of GPU where the fault-free (true) and faulty values of the internal signals are stored. A new data type $gate$ is defined to store the information of the circuit netlist including the gate type and the

list of gate inputs. All the gates to be evaluated for the compact fault are stored in an array on the GPU's global memory pointed by fr. A gate label *flag* also stored on the global memory indicates whether a gate is in the FR$_{cf}$ or not. The detection flags for *all* the single faults are stored in the det array and transmitted back to the CPU after simulation. At line 1, TID is obtained from the built-in CUDA variable $threadIdx.x$. We do not inject faults on the faulty gate as traditional fault simulation because different single faults are compacted into the same compact fault (cf). Here, we just *complement* the fault-free values of the faulty gate for all t vectors and store them in the f_{val} array at line 2. It is noted that the value for a gate i is indexed at a location $(TID+i\times t)$ in the value array. After each gate in the FR is evaluated (line 5), line 6 sets the $flag$ to true indicating that the gate is in the FR of the cf. Then, we go back to the faulty site and evaluate whether the faults are excited (line 9). For a single fault f in the CFS that is excited $(val \oplus t_{val}[tid + fr[0] \times t])$ and the faulty value is propagated to one of the primary outputs in the FR $(f_{val}[tid+k\times t] \oplus t_{val}[tid+k\times t])$, we set its detection flag to true indicating that the fault f has been detected by the thread (line 11). After all the threads have finished simulation, a parallel reduction kernel is launched to determine if the fault is detected by any of the t vectors. If *all* the collapsed faults in the current cf are detected, the next compact fault will be processed in the block. Otherwise, another t test vectors will be simulated until all the V test vectors have been simulated for the current cf. If a single fault is not detected by any vector, we say that the fault is not detected and set its detection flag to false. In the above discussion, we use an efficient implementation of parallel reduction [11] provided in CUDA software development kit (SDK) [72].

As illustrated at line 5 of Algorithm 1, depending on the $fr[j]$'s gate type and the input list available at $gate$ data structure, the $eval$ kernel will launch a separate kernel to evaluate the faulty value of the gate. For example, the gate evaluation kernel for fault simulation of a two-input OR gate is given as a pseudo-code shown in Algorithm 2. The index of the gate under evaluation and its inputs is indicated by arguments id, $in0$ and $in1$. The parameter *flag* that has been set at line 6 in Algorithm 1 determines whether the values of the gate's inputs are fault-free or faulty. Every gate type in our library is implemented with a similar evaluation kernel. By exploiting the sync barrier function provided in CUDA, all the 32 threads in a warp are guaranteed to simulate the same gate

Algorithm 1 cf_sim_kernel – simulation kernel for a cf

Input: $uint *t_{val},\ uint *f_{val},\ bool *flag,\ bool *det,\ gate *fr,\ fault* cf$

1: $tid = threadIdx.x$; { get thread index}
2: $f_{val}[tid + fr[0]\times t] = \neg t_{val}[tid + fr[0]\times t]$;
3: $flag[fr[0]] = 1$; { set gate label for the faulty gate}
4: **for all** gates j in FR except the first faulty gate **do**
5: $\quad eval(t_{val},\ f_{val},\ fr[j],\ flag)$;
6: $\quad flag[fr[j]] = 1$; { set gate label}
7: **end for**
8: **for all** faults j in cf **do**
9: $\quad uint\ val = inject_eval(t_{val},\ cf[j],\ fr[0])$;
10: $\quad$ **for all** primary outputs k in fr **do**
11: $\quad\quad det[tid + cf[j]\times t] \mid= (f_{val}[tid + k\times t]\oplus t_{val}[tid + k\times t])\ \&\ (val\oplus t_{val}[tid + fr[0]\times t])$;
12: $\quad$ **end for**
13: **end for**

but for different vectors. Since the same kernel will be launched among the threads in a warp, no branch divergence will occur in FSimGP^2.

Algorithm 2 $eval_kernel$ – evaluation kernel of OR2 gate

Input: $uint *t_{val},\ uint *f_{val},\ bool *flag,\ int\ id, int\ in0,\ int\ in1$

1: $tid = threadIdx.x$; { get thread index}
2: $val_in0 = t_{val}[tid + in0 \times t]\ \&\ (1 - flag[in0]) + f_{val}[tid + in0 \times t]\ \&\ flag[in0]$;
3: $val_in1 = t_{val}[tid + in1 \times t]\ \&\ (1 - flag[in1]) + f_{val}[tid + in1 \times t]\ \&\ flag[in1]$;
4: $f_{val}[tid + id \times t] = val_in0 \mid val_in1$;

3.4.3 Data Structure

For the compact fault set, CFS, a novel data structure is employed as following:

```
typedef struct {
        unsigned int pos;
        unsigned int faults;
} compact_fault_set;
```

The first 4 bits of unsigned integer pos are encoded as an decimal number which represents the number of single faults contained in the set (n). The left 28 bits are the index of the faulty gate. The

unsigned integer $faults$ is composed of 8 single faults. Each fault is denoted by a 4-bit encoding where the first bit is the type of the stuck-at fault and the left three bits represent the index of the faulty line of the gate. For example, we assume that the compact fault set (CFS) denoted in Figure 3.1 is on a three input AND gate with an index number 2588. Such compact fault set can be represented by our structure with $pos = 0xA1C5$, $fault = 0x75310$. The number of single faults in the CFS is 5 ($0xA1C5\&0x0F = 5$) faults on gate number 2588 ($0xA1C5 >> 4 = 2588$). The first fault f_1, a $sa-0$ fault on gate line 0 is represented by a four bit set, 0000. Also, fault f_5 with encoding 0111 is an $sa-1$ fault at line 3. This data type is expandable when the number of single faults is greater than 8 or the index of the gate is exceed the 28 bits encoding.

The netlist of the circuit is an sorted array of logic gates with respect to the their levels. Each logic gate is represented by a bit stream where the first four bits are encoded as an decimal number denoted as the gate type. Also, it can be extended if the number of gate types exceed 16. The following bits are divided into K integers representing the indexes of its fanins. K is decided by the maximum number of fanins of logic gates in the circuit. Therefore, our data structure is compatible with any circuit with arbitrary type of logic gates.

3.4.4 Compact Fault List Generation

As mentioned in Section 3.4.1, *cf-parallelism* could alleviated the overhead of unnecessary evaluations of gates in FR$_{cf}$. In order to increase the cf-parallelism factor, a greedy algorithm in Algorithm 3 is introduced to group as many as single faults into one CFS. At first, FSimGP^2 sorts the gates in an descending order with respect to the number of *uncollapsed* faults and save them in a queue. The program adds the gate on the top of the queue to the compact fault and update the queue to remove the faults that are equivalent to those that have been added. It stops until there are no gates left in the gate_list.

Algorithm 3 Compact Fault List Generation

Input: $gate_list$, f_list

Output: cf_list

1: Sort $gate_list$ by the number of *uncollapsed* faults on it
2: $cf_list = \emptyset$;
3: **while** $|gate_list| \neq 0$ **do**
4: $cf_list \leftarrow$ gate on the top of the $gate_list$
5: **for all** single faults in $f_list_{gate_list[0]}$ **do**
6: update $gate_list$ to remove its equivalent faults
7: remove the gates with no faults in $gate_list$s
8: **end for**
9: **end while**

3.4.5 Static and Dynamic Load Balancing

Although all the compact faults are evenly distributed to each block, our experiments show that the number of cfs is not an accurate estimation of the work load. We found that even if an equal number of cfs were allocated among all the blocks, the variation in the work load (measured as the amount of time spent) could be substantial. Hence, we first propose a static work load balancing technique which takes the number of gates s_{cf} in the fanout region of the compact faults as an estimation of the work load. Since all the gates in the FR will be simulated, for two different cfs with the same size of FR, the computational complexity should be the same for t test vectors. Therefore, we sort the compact faults according to the size of their fanout regions and distributes them evenly to the k blocks.

However, we found that the variation in the work load could still be substantial because the hard-to-detect faults may be undetected by *all* the V vectors while the others are detect by the first t vectors. In such cases, one block will run several rounds to simulate all the vectors while another block finishes at the first attempt. Therefore, FSimGP^2 employs a novel dynamic load balancing strategy by which the workloads are distributed dynamically to the blocks. A global fault counter cnt is allocated in global memory and accessed by all the blocks on-board. Once a block finishes the current workloads, an atomic function (atomicAdd) provided by CUDA is called to increase the value of cnt by a dynamically tuned parameter L. All the faults with indexes between cnt and

$cnt + L$ will be distributed to the blocks for simulation. The operation is atomic in the sense that it is guaranteed to be performed without interference from other blocks.

Initially, all the blocks will be assigned I compact faults to simulate. Once a block finishes the simulation of its assigned faults, it will claim another L cfs and atomically add L to cnt. A small L may diminish the performance because the atomic writing is an expensive operation on GPU. Also, a big L may cause an unbalanced work loading if the assigned L FPs are all hard-to-diagnose. Therefore, we propose a dynamic load balancing strategy where the assignment of L is dynamically tuned according to the number of remaining cfs to be simulated. We set a threshold before which a large L is selected to avoid too many expensive atomic operations, and we set L to be 1 for the cases where few cfs remain so that any workload imbalance is minimized during the final stages of the simulation. Our experimental results show that with such a dynamic load balancing algorithm, FSimGP^2 achieves nearly $2\times$ speed-up against the static load balancing and $4\times$ against the case without load balancing.

3.4.6 Memory Usage and Scalability

Since optimized data access is very important to GPU performance, shared memory is used to store the det array which indicates the detection status of faults and the $gate$ data which represents part of the gates in FR$_{cf}$. For each block, the det array only holds t flag entries so that it can fully fit into the 16 KB shared memory. Only part of the $gate$ information is stored to prevent memory overflow. With such a setup, the low-latency accesses to shared memory is exploited to accelerate the frequent read/write operations on these two arrays. All the other data stored on the global memory of the GPU are accessed under a fully coalesced mechanism because all the threads in a warp always access the same relative addresses on the GPU. For example, the t_{val} of a gate is stored in a linear array of size V corresponding to the number of vectors. Thus, when 32 threads in a warp evaluate the gate, 32 consecutive entries in t_{val} are coalescedly accessed.

Although our graphic card is equipped with 1 GB device memory, for extremely large circuits,

such amount of memory may still be insufficient for FSimGP^2. Experimental results show that the storage requirements are mainly occupied by the fault-free and faulty values of internal gates over all V test vectors whose memory consumptions are calculated by: $Mem(t_{val}) = V \times G \div w$, $Mem(f_{val}) = k \times t \times s_{fr}$, where V denotes for the number of vectors, w is the word size and G is the total number of gates, k and t are the block and pattern- parallelism factors, and s_{fr} represents the common fanout region size for all the compact faults. Ideally s_{fr} equals to $max(s_{cf})$ which is the maximum fanout region size for all cfs. It is noted that s_{cf} represents the number of gates in the fanout region of compact fault cf. Next, two cases of memory shortage are analyzed, and we give a solution for each case:

1. *Case 1.* $Mem(f_{val})$ consumes too much memory due to $max(s_{cf})$. In such case, we set a fanout region bound S instead of using $max(s_{cf})$ and divide the faults into two groups. The faults in group 1 with an s_{cf} smaller than S will be simulated by original strategy. For those in group 2 with larger FRs, we set a lower pattern parallelism factor t_2 so that one block can simulate the target cf with fewer threads and thus results in less memory usage. It is noted that such a solution will not influence the performance when the number of faults in group 2 is few. Otherwise, case 2 should be taken.

2. *Case 2.* $Mem(t_{val})$ uses up too much memory, leaving insufficient memory for $Mem(f_{val})$. In this case, the set of V vectors is divided into P partitions, and thus the simulation is divided into several passes between the host and the device. Moreover, we could also decrease either the block- or pattern- parallelism factor (k/t) to further shrink $Mem(f_{val})$. Although the parallelism factors are reduced, our results still demonstrate a huge speedup for both cases.

3.5 Experimental Results

We evaluated FSimGP^2's performance on a set of large ISCAS89 [15] and ITC99 [27] benchmark designs which are available from [44]. Our fault simulation platform consists of a workstation

with Intel Xeon 3 GHz CPU, 2 Gb memory and one NVIDIA GeForce GTX 285 graphic card as introduced in Section 2.1.1. We fault simulated 10 sets of 32,768 randomly generated vectors for all circuits. Ten runs were performed to obtain an average run time because the runtime may be slightly affected due to the different set of random patterns used in the experiments. To evaluate the correctness of FSimGP^2, the fault simulation results were verified with an open-sourced sequential fault simulator, FSIM [51]. The number of blocks (k) launched was set to 240 with 64 threads (t) running on each block. As discussed in Section 3.5.2, these parameters are determined according to the characteristics of the GPU and CUDA architecture for FSimGP^2 to achieve the best performance. First, we compared the performance of FSimGP^2 to those obtained in another GPU-based fault simulator and a commercial tool from [38]. Next, we compared FSimGP^2 to a recently proposed GPU-based simulator [47], a sequential event-based PPSFP algorithm implemented in [51] and a sequential (non-parallel) version of FSimGP^2 to determine the speedup of FSimGP^2. As noted from [47], the FSIM implemented in [51] achieves better performance compared to the simulators in [38].

Table 3.1: Comparison with 32K random patterns in [38]

Bench	# Gate	# Faults			Runtimes (in seconds)			Speedup	
		Total	Compact	Undetected	Comm. tool	[38]	FSimGP^2	Comm. tool	[38]
s5378	3042	4603	2130	52	31.95	1.961	0.058	548.150	33.644
s9234	5866	6927	3252	878	26.74	2.043	0.072	372.138	28.432
s13207	8772	9815	4376	317	52.59	0.656	0.103	509.672	6.358
s15850	11067	11725	6399	852	34.03	0.420	0.131	258.988	3.196
s35932	18148	39094	14612	3984	455.38	5.434	0.122	3738.813	44.615
s38584	20995	36303	15540	1687	265.59	7.883	0.158	1680.588	49.882
s38417	23949	31180	14589	1496	296.36	8.234	0.166	1780.496	49.469
b03	190	394	161	0	5.53	0.271	0.043	127.817	6.264
b08	204	452	177	0	4.48	0.229	0.043	103.138	5.272
b09	198	405	158	0	4.9	0.277	0.044	112.378	6.353
b10	223	517	225	0	4.02	0.340	0.053	76.223	6.447
b13	415	852	375	26	9.98	0.322	0.044	224.613	7.247
b17	33741	76625	38236	17164	712.97	19.028	1.402	508.541	13.572
b17_1	41080	88098	44556	24801	736.67	17.866	0.831	886.374	21.497
b21	21061	46154	23948	4726	153.33	46.583	0.739	207.385	63.005
b22	30686	67536	35872	5283	252.04	60.485	0.946	266.565	63.971
Avg								**712.617**	**25.576**

3.5.1 Performance Evaluation

Table 3.1 compared FSimGP^2 with a commercial tool reported from [38] and a GPU-based fault simulator also from [38]. Column 1 lists the name of the benchmark. Benchmarks with $*$ are those with scalability applied (eg., partitioning the test set). The number of gates (N_G) and the number of collapsed faults (N_f) are listed in columns 2 and 3, respectively. Column 4 lists the number of compact faults (N_{cf}) that groups the gates sharing the same fanout region. We find that N_{cf} is approximately equal to half of N_f. Thus the estimated cf-parallelism factor is around 2 which means that the cf-parallelism technique alone could make FSimGP^2 approximately two times faster. This estimation of speedup from cf-parallelism is demonstrated in Section 3.5.2. Column 5 gives the number of undetected faults after applying 32K random vectors. It is noted that some of those faults may not be undetectable, just that they were not detected by any of the vectors in the test set. Columns 6 and 7 list the execution time reported in [38]. The former one is a commercial state-of-the-art fault simulation tool running on a 1.5 GHz UltraSPARC-IV+ processor with 1.6 GB of RAM while the latter tool is implemented on NVIDIA GeForce GTX 8800 which has 128 processing cores clocked at 1350 MHz. The on-chip memory contains 768 MB global memory with 86.4 GB/s bandwidth. We note that our experimental platform is slightly more advanced than the one used in [38]. The time obtained from FSimGP^2 is listed under column 8 which includes all the GPU computation time, the communication overhead between the host and the device and the GPU data initialization run on the CPU. The speedups obtained by FSimGP^2 against the sequential commercial tool and GPU-based fault simulator are listed under columns 9 and 10, respectively. For example, consider circuit s38584, which has more than 20K gates and 36K collapsed faults. With cf-parallelism, these faults are grouped into only 16K compact faults. 1687 of the original collapsed faults were not detected by the 32K vectors. The commercial fault simulation tool reported from [38] took 265.59 seconds, while the the GPU-based tool proposed in [38] took 7.883 seconds. Next, our FSimGP^2 took only 0.158 seconds. This is 1680$\times$ speedup over the commercial tool and 49$\times$ speedup over the GPU-based fault simulator in [38].

An average speed-up of 25.57$\times$ is achieved compared to the GPU-based tool [38]. If we consider

the difference brought about by the new NVIDIA platform, we can conservatively estimate that at least a $10\times$ speed-up is still achieved. It is noted that the benchmarks used in [38] were optimized before-hand while our circuits are obtained directly from the benchmark website without any modifications. Therefore, we believe that the lowest speedup reported for benchmark s15850 is due to the different netlists used. For example, the s15850 circuit used in [38] had only 984 gates while ours has 11067 gates.

To further examine the speedup of FSimGP^2, we implemented a sequential version of FSimGP^2 called FSimGP$^2_{seq}$. In addition, we compared the results with another non-parallel simulator, FSIM [51] and a state-of-the-art GPU based simulator proposed in [47]. The results are reported in Table 3.2. The first five columns are the same as in Table 3.1. Next, the execution time and the speedup of FSimGP^2 over FSimGP$^2_{seq}$ are reported in columns 6 and 10, respectively. Likewise, the results for FSIM [51] and [47] are given in columns 7-8 and 11-12. Both sequential tools are executed on the same workstation which is also used by FSimGP^2. It is noted that the results from [47] are also based on the same platform as ours. We cannot compare all the result against with [47] because some industrial benchmarks in [47] are not openly available. Using the circuit b17_1 as an example, [47] took 3.89 seconds to complete while FSimGP$^2_{seq}$ and FSIM [51] took 539.018 and 79.283 seconds, respectively. Our FSimGP^2 took 0.831 seconds. This is about $4\times$ speedup over [47] and $95\times$, $648\times$ speedup over the sequential version of FSimGP^2 and FSIM, respectively. Note that FSIM was able to complete the simulation in a much shorter time than the commercial tool reported in Table 3.1. Such a difference could be due to the platform difference between them.

For circuit s13207, FSimGP^2 has the smallest speedup against the other tools. This is because the percentage of undetected faults (317 out of 9815) is so low that the number of computations needed for fault simulation is reduced greatly. In other words, most faults in s13207 were easy to be detected. This could also explain the highest speedup gained for circuit b17_1 since there are more than 25% undetected faults and thus the simulation requires more computational efforts.

In Table 3.3, the break up of runtime for various steps during simulation is reported in seconds. The total runtime is listed in column 2 ($Total$). The cost of GPU data initialization process is

listed in column 3 ($Init.$). Since most of the time taken in this process is to allocate memory space on the GPU, the runtime is similar among the benchmarks. The simulation kernel to compute the fault-free value is listed in column 3 ($Sim.$). Column 4 (Fsim.) denotes the runtime for fault simulation kernel which takes most of the runtime for some large benchmarks. The transmission overhead between the CPU and the GPU is presented in column 5 ($Tran.$). As illustrated in 3.4.2, the communication costs only includes the circuit data and test vectors sent from CPU and the faults detection results from GPU. Therefore, the overhead is relatively small comparing with the total runtime. It is noted that the total runtime might be larger than the sum of the four steps' runtime due to the overhead of timing function in use.

Table 3.2: Comparison with tools on the same platform

Bench	# Gate	# Faults			Runtimes (in seconds)				Speedup		
		Total	Compact	Undetected	FSimGP^2_{seq}	FSIM [51]	[47]	FSimGP^2	FSimGP^2_{seq}	FSIM [51]	[47]
s9234	5866	6927	3392	878	3.230	1.383	NA	0.072	44.958	19.247	NA
s13207	8772	9815	4392	317	4.994	0.883	NA	0.103	48.396	8.558	NA
s15850	11067	11725	6484	852	18.278	2.600	NA	0.131	139.106	19.788	NA
s35932	18148	39094	15181	3984	21.067	6.917	NA	0.122	172.968	56.791	NA
s38584	20995	36303	16049	1687	13.310	5.550	NA	0.158	84.222	35.119	NA
s38417	23949	31180	15428	1496	26.064	6.783	NA	0.166	156.586	40.751	NA
b17	33741	76625	41041	17164	540.528	70.850	4.95	1.402	385.543	50.535	3.531
b17_1	41080	88098	46519	24801	539.018	79.283	3.89	0.831	648.556	95.395	4.681
b18*	117963	264267	152329	56313	3698.640	373.100	18.35	6.929	533.805	53.848	2.648
b20*	20716	45459	25406	4085	227.257	18.267	2.65	0.736	308.594	24.805	3.598
b20_1	14933	33255	18097	2873	92.332	8.800	NA	0.445	207.602	19.786	NA
b21*	21061	46154	25609	4773	248.237	18.900	2.65	0.739	335.751	25.563	3.584
b21_1	14932	32948	17802	2818	111.766	8.867	NA	0.457	244.391	19.389	NA
b22*	30686	67536	38061	5221	337.491	30.050	3.40	0.946	356.941	31.782	3.596
b22_1	22507	49945	27487	4169	155.408	15.500	NA	0.593	262.285	26.160	NA
Avg									**261.980**	**35.168**	**3.606**

Benchmarks with $*$ are those with scalability approach applied.

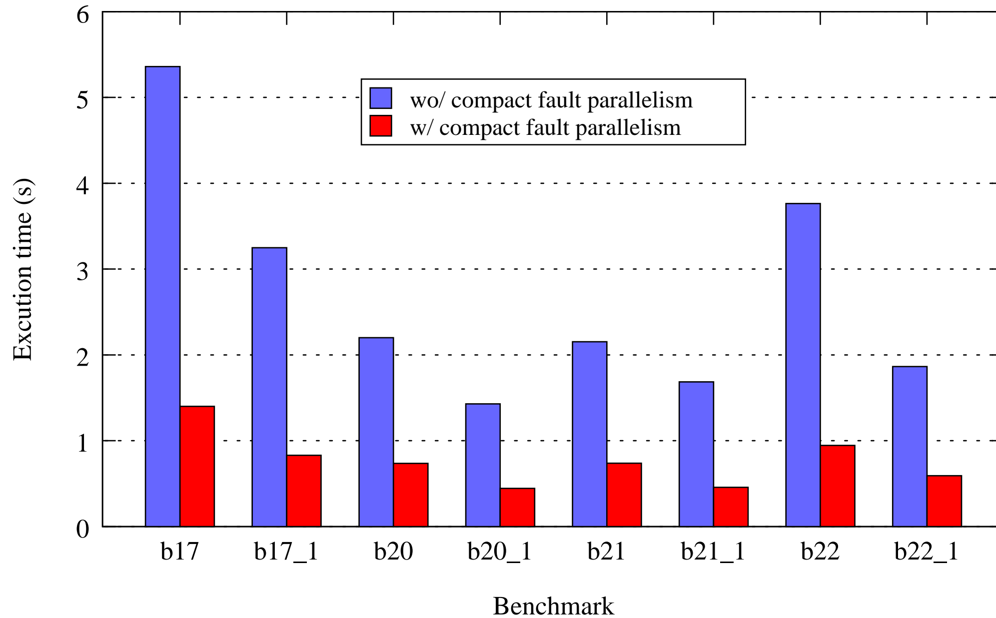

Figure 3.4: FSimGP^2's execution time w/ and w/o cf-parallelism.

3.5.2 Characteristics of FSimGP^2

In this section, we will explore and analyze three characteristics of FSimGP^2. It is noted that we only select the benchmarks with similar computational costs so that they can be fit into the same bar-chart. Other benchmarks also show similar characteristics.

Compact fault parallelism

As shown in Table 3.1, the number of the compact faults is roughly half of the collapsed faults. Figure 3.4 shows that with cf-parallelism, FSimGP^2 could achieve more than $3\times$ speedup against the one without exploiting compact fault parallelism. As a part of future research, we intend to investigate a new method to generate the fault list so that more collapsed faults could be mapped to one gate. Therefore, the cf-parallelism factor could be larger and FSimGP^2 could achieve more speedup.

Table 3.3: Runtime in steps

Bench	Runtimes (in seconds)				
	Total	Init.	Sim.	Fsim.	Tran.
s9234	0.072	0.046	0.011	0.013	0.002
s13207	0.103	0.045	0.018	0.037	0.003
s15850	0.131	0.045	0.021	0.061	0.004
s35932	0.122	0.045	0.037	0.032	0.006
s38584	0.158	0.045	0.043	0.062	0.007
s38417	0.166	0.046	0.048	0.064	0.008
b17	1.402	0.046	0.067	1.266	0.022
b17_1	0.831	0.046	0.081	0.686	0.017
b18	6.929	0.064	0.460	6.330	0.071
b20	0.736	0.045	0.041	0.636	0.013
b20_1	0.445	0.046	0.029	0.360	0.009
b21	0.739	0.046	0.041	0.638	0.013
b21_1	0.457	0.046	0.029	0.373	0.009
b22	0.946	0.046	0.060	0.819	0.019
b22_1	0.593	0.046	0.044	0.488	0.013

Static and Dynamic load balancing

Load balancing can be critical in parallel computing. We compare the FSimGP^2 against two versions, the static one in which fault pairs are evenly distributed and assigned to different blocks before simulation and the unbalanced one in which compact faults are randomly distributed to different blocks. In all cases, the number of cfs assigned in each block are equal. As mentioned in Section 3.4.5, large number of L and I are set as 10 to avoid frequent atomic operations. FSimGP^2 changes L to 1 when less than $2\times k$ CFs are left to distinguish. Figure 3.5 shows that the one with dynamic balancing is nearly $2\times$ faster than the static version. Also, the tool without load balancing is at least three times slower than the original FSimGP^2. Sometimes the speedup could be greater. The consistent speedup achieved for all circuits demonstrates the value brought by dynamic load balancing.

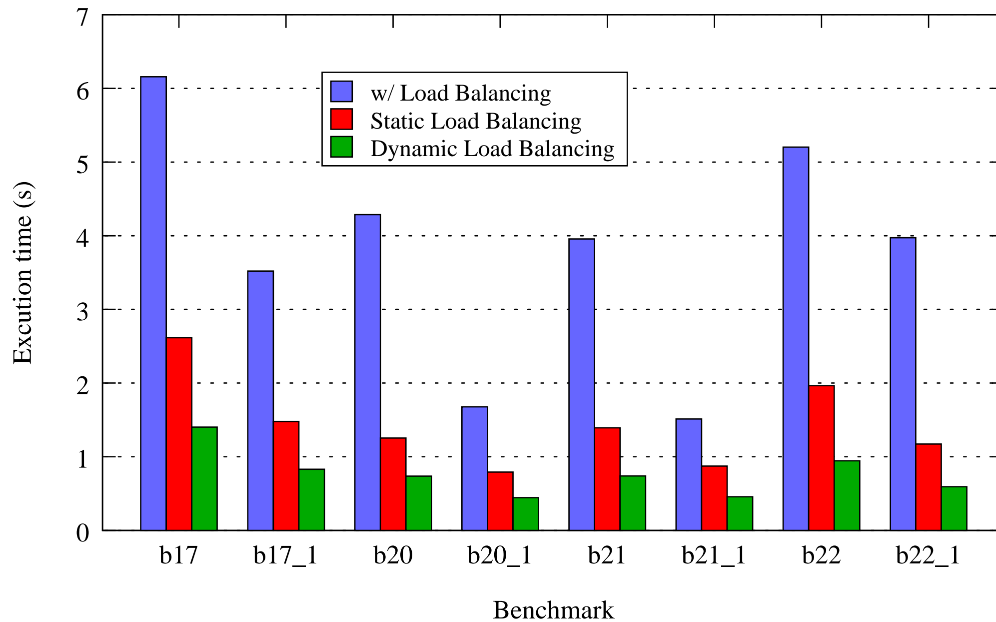

Figure 3.5: FSimGP^2's execution time with different load schemes.

Parallelism factor

We observed that the performance of FSimGP^2 could be influenced by changing the pattern-parallelism factor t, the number of threads in each block and the block-parallelism factor k, the number of blocks allocated on GPU. Figure 3.6 compares three scenarios with different assignments to these factors. The execution time in scenario 1 ($s1$) is twice as much as that in $s2$. This is because our GPU card is equipped with 30 streaming multiprocessors (SMs) and each SM can be mapped with more than one block. By assigning two blocks to each SM in $s2$, CUDA could interleave their execution and mask most of the time spent while waiting for data from device memory, thus reducing the execution time by more than 50% across the benchmarks. Finally, the configuration of $s3$ achieves the best performance in our experiments. For each compact fault, since only 64 test vectors are applied at a time, those easy-to-detect faults are more likely to be detected by the first 64 vectors. Compared with $s2$ in which 256 threads are simulated, $s3$ saves the resources for those 192 threads which could now be applied for the other faults. In other words, more threads in one block may not necessarily be better. Since 32 threads of a *warp* is running concurrently under

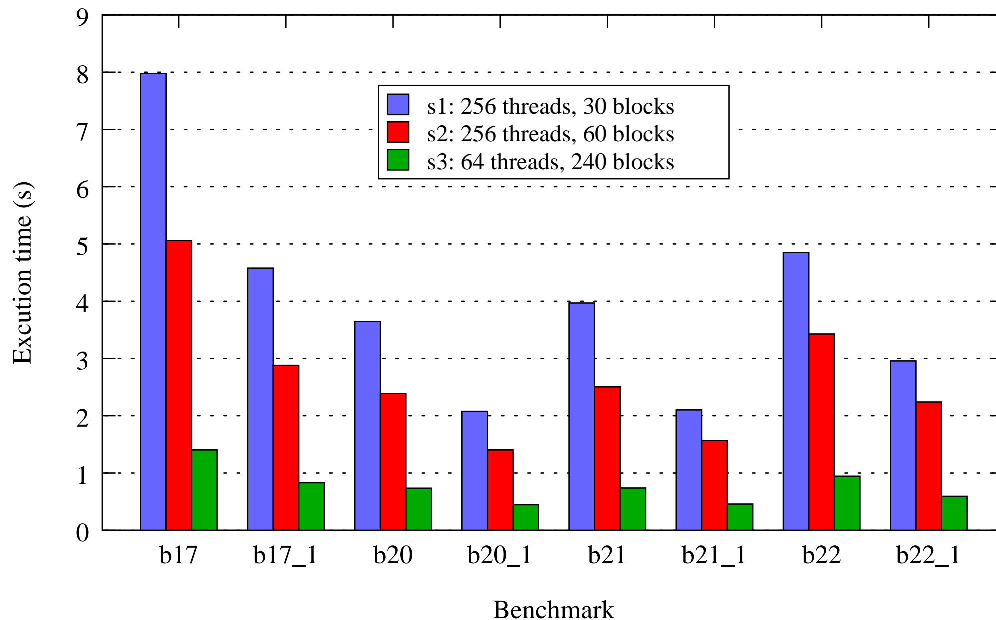

Figure 3.6: FSimGP^2's execution time with different parallelism factors.

SIMT architecture, t should be a multiple of 32 for maximal benefit. We did not reduce the number of threads to 32 because most of the easy-to-detect faults would still need more than the first 32 vectors to be detected.

Scalability

With the memory scalability approach described in Section 3.4.6, FSimGP^2 is capable of simulating large circuits that need more memory than is available. In this experiment, we conservatively set the total available device memory as 950 MB to leave some storage for CUDA needs, GPU device drivers, and desktop display. Table 3.4 shows the benchmarks with scalability applied. Column 2 lists the original memory usage before scalability. The common size of fanout region for all the compacted faults is given in column 3 and 4. Column 3 lists the size before scalability applied which is the maximum fanout region (FR) size while the S shown in column 4 is the bound calculated by FSimGP^2 to reduce the total memory usage to total memory. According to S, the compacted faults are partitioned into two groups, the one with a fanout region smaller than S listed

in column 5, and the one with bigger s_{cf} listed in column 6.

As an example, the memory usage of benchmark b_22 before scaling is 1.38 GB which exceeds 950 MB. After we set the fanout region bound S to be 11841 instead of the original $max(s_{cf})$ of 18936, the total memory consumption reduced to 949 MB which can fit into total memory. Also, only 48 compacted faults have a large fanout region and need to be simulated by fewer threads ($t_2 = 32$) concurrently. Another benchmark b_18 falls into case 2 as discussed in Section 3.4.6 with an original memory usage of 1.9 GB. We partitioned the input vectors into two ($P = 2$) parts, reduced the cf-parallelism factor k to 120 (original k is 240) and set the FR bound S to be 12180 ($max(s_{cf})$ is 17033). Consequently, the total memory usage is reduced to 949 MB.

We note that that the performance should be affected by the scalability approach. However, in both two cases, FSimGP^2 achieves 31.782× and 53.848× speedup over FSIM [1]. We investigated the impact of scalability approach case by case. In case 1, although the pattern parallelism factor t is reduced from 64 to 32, the performance was not affected much as long as all the threads within one warp ran together. Moreover, the number of faults with a large size of fanout region, s_{cf} is limited. For example, only 48 compacted faults in benchmark b_22 need to be simulated with a small t instead of the original 35872 faults.

Case 2 introduces the communication overhead between the host and the device among several passes of simulation. However, our experimental results show that for benchmark b_18, the overhead between the simulation of two partitioned inputs is only 0.01154 seconds which is relatively small compared with the simulation process. Table 3.3 shows that for all circuits, the total transmission cost is small.

We estimated that the $1\ GB$ device memory is insufficient to store large size of fanout region (s_{cf}) with more than one million gates. The reason is that the circuit netlist, true and faulty logic values have to be stored on-board to achieve high bandwidth throughput. However, it is noted that with the recently announced Tesla GPU server s2070 [73] housing up to 24 GB GDDR5 device memory, we can simulate even larger benchmark before we need to apply the scalability methods. Moreover, as a future work, the simulation based on stem region in [47] may help to further reduce

the memory requirement.

Table 3.4: Memory scalability

bench	Mem (MB)	s_{FR}		# cfs	
		$max(s_{cf})$	S	small	large
b18*	1920	17033	12180	152323	6
b20	960	13180	13003	25496	10
b21	984	13529	12960	25653	16
b22	1385	18936	11841	38013	48

Col. 2 - the original memory consumption before scalability.

Col. 5/6 - # cfs whose fanout size is smaller/larger than S.

*In b18, we also partition the test set and tune parallelism factors.

3.6 Chapter Summary

In this chapter, we have proposed FSimGP^2, an efficient parallel fault simulator with GPGPU. FSimGP^2 achieves high algorithmic efficiency by exploiting the parallel computation power of GPUs with a novel three-dimensional parallelism technique. *Pattern-parallelism* harnesses the bandwidth throughput of GPUs where thousands of threads are executing simultaneously. With the novel concept of compact fault set (CFS), *cf-parallelism* helps to achieve a speedup of 3$\times$. *Block-parallelism* enables the concurrent simulation of different compact faults among blocks which utilizes the high computational power of the many-core system. The proposed dynamic load balancing approach also results in an efficient utilization of the available SMs. Experimental results showed that FSimGP^2 could achieve an average of 25.576$\times$ and 3.606$\times$ speedup when compared with two previous GPU-based fault simulators. Moreover, FSimGP^2 is also 35.168$\times$ faster, on average, than a state-of-the-art sequential fault simulator, with a maximal speedup of more than 95$\times$.

Chapter 4

Parallel Diagnostic Fault Simulator

4.1 Chapter Overview

In this chapter, we present an efficient diagnostic fault simulator based on a state-of-the-art graphic processing unit. Diagnostic fault simulation plays an important role to identify and locate the causes of circuit failures. However, today's complex VLSI circuits pose ever higher computational demand for such simulators. Our GPU based diagnostic fault simulator (GDSim) is based on a novel two-stage simulation framework which exploits high computation efficiency on the GPU. The fault pair based simulation is proposed to overcome the limited capacity of GPU memory as well as achieve a substantial fine-grained parallelism. Multi-fault-signature and dynamic load balancing techniques are introduced for the best usage of computing resources on-board. Experimental results demonstrate a speedup of up to 121$\times$ (with average speedup of 38.43$\times$) compared to a state-of-the-art CPU-based diagnostic fault simulator.

The rest of the chapter is organized as follows. A brief introduction is given in Section 4.2. In Section 4.3, we review the previous work related with diagnostic fault simulation. Section 4.4 outlines a high-level process view of the proposed method, with a detail description of some critical approaches. The experimental results are reported in Section 4.5. Finally Section 4.6 concludes

the chapter.

4.2 Introduction

Fault diagnosis, a process of locating defects in a defective chip, plays an important role in today's very-large-scale integrated (VLSI) circuits. The manufacturing defects are becoming more subtle due to rapidly diminishing feature sizes and complex fabrication processes. To improve yield, such defects could be identified and located using fault diagnosis followed by rectification with visual inspection or electron-beam probing. For a circuit-under-diagnosis (CUD) in the presence of modeled faults, the process of evaluating diagnostic capability of the given N test patterns is called diagnostic fault simulation. In addition to measuring diagnostic capability, diagnostic simulators can also help to accelerate automated diagnostic pattern generation (ADPG).

In the past, significant efforts have been devoted to accelerate this process [19, 23, 82]. While fault simulation could already be expensive on industry-sized circuits, diagnostic fault simulation can often cost one to two orders of magnitude higher. Furthermore, the computational requirements increase significantly with the increasing size of the circuit (hence increasing number of fault pairs). Therefore, there is a need for efficient diagnostic fault simulators that are able to handle large designs with extremely large test sets.

In this chapter, we present a fine-grained GPU-based diagnostic fault simulator (GDSim). The main motivation is to harness the computational power of GPUs to reduce the total execution time without compromising the output fidelity. Experimental results show that GDSim achieves one to two orders of magnitude speedup in comparison with a state-of-the-art CPU-based diagnostic fault simulator and a sequential version of the GPU-based implementation. We summarize our contributions as follows.

- To the best of our knowledge, this work is the first that accelerates diagnostic fault simulation on a GPU platform.

- We introduce a two-stage simulation framework to efficiently utilize the computation power of the GPU without exceeding its memory limitation. First, a fault simulation kernel (k_{sim}) is launched to determine the detectability of each fault. Then the detected faults are distinguished by the fault pair based diagnostic simulation kernel (k_{diag}). Both kernels are parallelized on the GPU architecture.

- In the k_{sim} kernel, *multi-fault-signature* (MFS) is proposed to facilitate fault pair list generation. MFSs can be obtained directly from the parallel fault simulation without introducing any computational overhead on GPUs. By clever selection of the size of the MFS (SIG_LEN), GDSim is able to reduce the number of fault pairs by 66%.

- The fault pair based diagnostic simulation kernel, k_{dist}, exploits both fault pair- and pattern-parallelism, which allows for efficient utilization of memory bandwidth and massive data parallelism on GPUs.

- In k_{dist}, dynamic load balancing is introduced to guarantee an even workload onto each processing elements.

- We applied GPU-oriented performance optimization strategies on GDSim to ensure a maximal speedup. Global memory accesses are coalesced to achieve maximum memory bandwidth. The maximum instruction bandwidth is obtained by avoiding branch divergence. GDSim also takes advantage of the inherent bit-parallelism of logic operations on computer words.

4.3 Background

4.3.1 Diagnostic Fault Simulation

A diagnostic fault simulator computes the diagnostic capability of the given test vectors. Our proposed approach targets on full-scan gate-level circuits and assumes the single stuck-at fault model.

Given a large set of random vectors, our GDSim is to obtain and record all the indistinguishable fault pairs from a collapsed fault list.

The diagnostic capability could be evaluated by several measures such as *diagnostic resolution (DR)*, the fraction of fault pairs distinguished [17], and *diagnostic power (DP)*, the fraction of fully distinguishable faults [17]. Here, two faults f and g in a combinational circuit are said to be *distinguishable* if, for at least one input vector, the responses of corresponding circuits are different on at least one primary output (PO). To provide a more accurate diagnostic information, the authors in [50] have proposed a third measure, *Equivalence Class (EC)* which identifies sets of equivalent faults under given test patterns for a circuit. Since *all* the indistinguishable fault pairs are recorded by our GPU-based simulator, EC could be computed in linear time. Also, the measures, DP and DR, can be computed from the sizes of indistinguishable classes in EC. Therefore, GDSim is capable of providing all the above diagnostic measures.

4.3.2 Previous Work

In [19], an algorithm called "multiway list splitting" for computing EC (of stuck-at faults) is presented. Initially the EC is a class including all the faults. For each test vector, all the faults are simulated and their corresponding outputs are recorded. Hence, the faults with the same output vectors are grouped into the same set which divides the original EC into several smaller subsets. The EC is obtained when all the vectors have been simulated. The authors in [23] proposed a distributed approach to get the indistinguishable fault list (IFL) that stores the faults which are indistinguishable from each fault. All the machines run a similar fault simulator to maintain the IFL. Although significant speedups are achieved for both methods mentioned above, they are not applicable to the CUDA architecture due to the expensive global synchronization between blocks as well as the infeasible operations of dynamic list. Finally, since thousands of test vectors are simulated concurrently on GPUs, the storage of the corresponding output vectors for a large number of faults within the same set will cause memory explosion on the GPU. To overcome this, our GDSim targets at fault pairs where each thread block simulates and compares *only* two faults concurrently.

The fault pairs are generated based on indistinguishable fault sets obtained from the initial parallel fault simulation on the GPU (k_{sim}). Such a strategy takes advantage of the GPU's large memory bandwidth and high computational power while avoids the memory limitation on-board.

A fault table generation on GPUs is proposed in [39] which may be used for fault diagnosis. The fault simulation algorithm based on the parallel-pattern single-fault propagation (PPSFP) is mapped to the CUDA architecture. Although the fault table could be used to differentiate faults, it is unnecessary to simulate *all* the test vectors because the complete fault table is an overkill to evaluate diagnostic measures such as EC. Moreover, only those vectors that detect the faults are recorded in [39]. Such information without the exact corresponding output vectors is insufficient to fully distinguish two faults.

4.4 Proposed Method

In this section, we first present some definitions, followed by the two-stage framework of the proposed diagnostic fault simulator and the dynamic load balancing technique.

Definition 9. *The gate on which a set of faults are located is defined as* faulty gate *(FG). For the group of faults on the same gate, only the gates in the fanout region (FR) beyond FG need to be evaluated during fault simulation. The set of gates in the fanout region is termed as* FR_{FG}.

Definition 10. *The* fault signature *(FSIG) for a fault* f *is defined as a pair* $fsig_f(v,p)$*, where the faults are excited by the* v^{th} *vector and its faulty value is propagated to the* p^{th} *PO of the circuit.*

Since the faulty value may be propagated to several POs of the circuit and detected by multiple vectors, we define a *multiple-fault-signature* set for a fault f as $MFS_f(k)$ which records the *first* k FSIGs. The FSIGs detected by the same vector but at different POs are sorted by p, the indices of POs.

Definition 11. *Two faults* $f1$ *and* $f2$ *with the same size of MFS:* $MFS_{f1}(k)$, $MFS_{f2}(k)$*, are distinguished if at least one of the corresponding FSIGs differ.*

Assume that the ith FSIG, fsig$_{f1}$(v1,p1) and fsig$_{f2}$(v2,p2), differ while the first $i-1$ components of the MFSs are the same. Case 1, $v1 \neq v2$. Without loss of generality, assuming $v1 < v2$, we know that $f1$ is detected by vector $v1$ while $f2$ is not. Thus the fault pair could be distinguished by $v1$. Case 2, $v1 = v2, p1 \neq p2$. Assume $p1 < p2$ without loss of generality. Because all the first $i-1$ FSIGs are the same for both faults and they are sorted with respect to the PO indices, $f2$ cannot be detected at PO $p1$ by vector $v1$. Hence, these two faults are distinguishable by $v1$ at PO $p1$.

4.4.1 Framework

The high-level flow of GDSim is shown in Figure 4.1. At the beginning, the CPU reads in the circuit netlist and generates its collapsed fault list. The list of faults will be grouped with respect to their locations. For the faults on the same gate, its fanout region (FR$_{FG}$) is processed by a breadth-first search from the faulty gate location in a forward levelized manner. Then, the test vectors and all the *fundamental data*, including circuit netlist, fault list with corresponding FR_{FG}, and input vectors, will be transferred to the GPU. A GPU-based fault simulator k_{sim} is launched as Kernel 1 on the GPU. It is an extended version of the simulator implemented from [54] with MFSs recorded which will be used to sort the fault list by Kernel 2. The sorted fault list will be transferred back to the host and the CPU will generate the list of fault pairs for further analysis. After the GPU receives the fault pairs to be simulated, the third kernel k_{diag} is launched. We run the given test vectors on each fault pair until the two faults are distinguished. If no pattern is able to distinguish a fault pair, it is also recorded. Finally, the information of the complete list of indistinguishable fault pairs can be used to obtain diagnostic measures such as EC and/or provide a set potential fault locations.

Faulty Gate based Parallel Fault Simulation (k_{sim})

For a faulty gate fg, each gate in FR$_{fg}$ will be fault-simulated with t vectors, processed on t threads in one block. To inject the fault, we just *complement* the fault-free value of the faulty gate for all

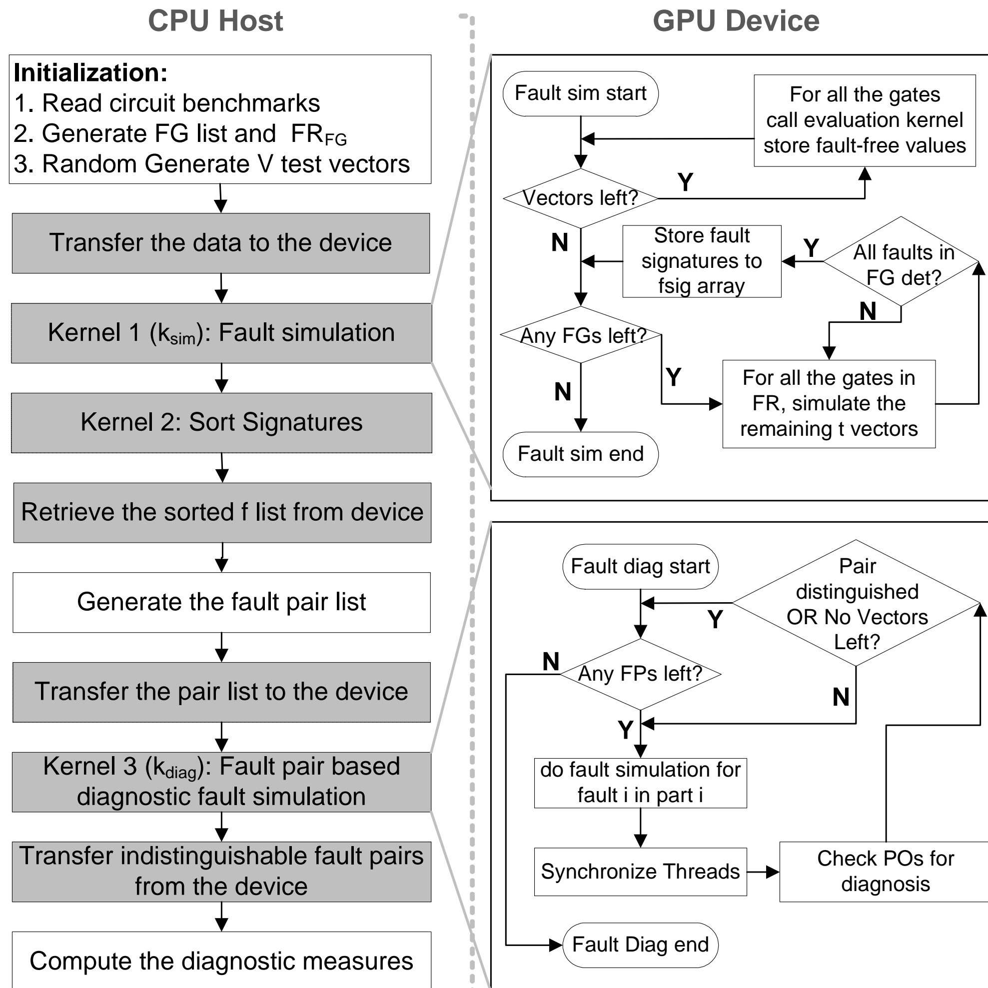

Figure 4.1: The framework of GDSim.

t vectors and store them in the f_{val} array in the global memory. After the simulation of all the gates in FR$_{fg}$, the simulator will check whether each collapsed fault on the FG is excited by the corresponding set of vectors. If the fault is excited and at least one faulty value of the outputs f_{val} is different from the fault-free values (obtained from the previous parallel fault-free simulation and saved in the global memory), the fault is considered as detected and its signature is recorded in $fsig$ array. If *all* the collapsed faults in the current fg are detected, the next faulty gate will be processed in the block. Otherwise, another t vectors will be simulated until all the given test vectors have been simulated for the fg.

Given the above discussion, our approach simulates a set of faults on the same FG under t vectors concurrently. The simulator records detection information as the multi-fault signatures. We set an upper bound of the MFS size as SIG_LEN so that the signatures of fault f_i includes at most SIG_LEN FSIGs. Such MFS mechanisms will not cause any overhead in our implementation because we are simulating only for the faults yet to be detected in fg. However, it is not the case in single fault based simulation because more simulations have to be performed to get multiple signatures for a single fault.

After simulating all the FGs, the simulator will call Kernel 2 which is a parallel radix sort program provided in CUDA software development kit (SDK) [72] to sort the fault list.

Fault pair based Parallel Diagnostic Fault Simulation (k_{diag})

To utilize memory bandwidth and massive data parallelism in an efficient way, our diagnostic fault simulator exploits both *fault pair-* and *pattern-parallelism*. Namely, we simulate multiple fault pairs over multiple test patterns at a time. As illustrated in Figure 4.2, the N_{fp} fault pairs (FPs) are distributed onto k thread blocks running concurrently on the GPU. Each block allocates t threads simulating $t/2$ test vectors for one fault pair in parallel: $t/2$ threads process fault f_1 and the other $t/2$ threads process the other fault f_2 of the pair. For example, $block_1$ in the figure is assigned with fp_i, which includes two single faults, f_1 and f_2. The first half of the threads deal with f_1 while f_2 is simulated by the rest of the threads. Since 32 threads within a warp are running together, the branch divergence is prevented as long as $t/2$ is a multiple of 32. All the fault pairs *dynamically* assigned for one block are processed sequentially.

As we mentioned before, the fault set based simulation in [19] is not applicable here because of the memory limitation on GPUs. Since a certain fault set may contain more than one hundred faults and we are simulating thousands of vectors concurrently on the GPU, the storage of all those faulty signatures on GPUs for comparison can become very large. However, by distinguishing fault pairs separately, the storage of signatures is no longer needed, and we only need to compute the faulty value of POs from f_{val} array. Also, our experiments show that the number of fault pairs to be

distinguished is small when the MFS (as opposed to a single FSIG) is employed.

All the threads within a block are synchronized by exploiting the sync barrier function provided in CUDA. Then, for each group of $t/2$ test vectors, another kernel will be launched on the first $t/2$ threads to check the output responses for the two faults. If one of the threads detects a differences on a certain output, a local distinguishable flag is set. Once all the threads have finished, a parallel reduction kernel is launched to determine if the fault pair is distinguished by any of the $t/2$ vectors. If it fails, another $t/2$ vectors will be launched until all the test vectors are simulated for this pair. At the end, GDSim will record the indices of those fault pairs which were not distinguished and send it back to the CPU.

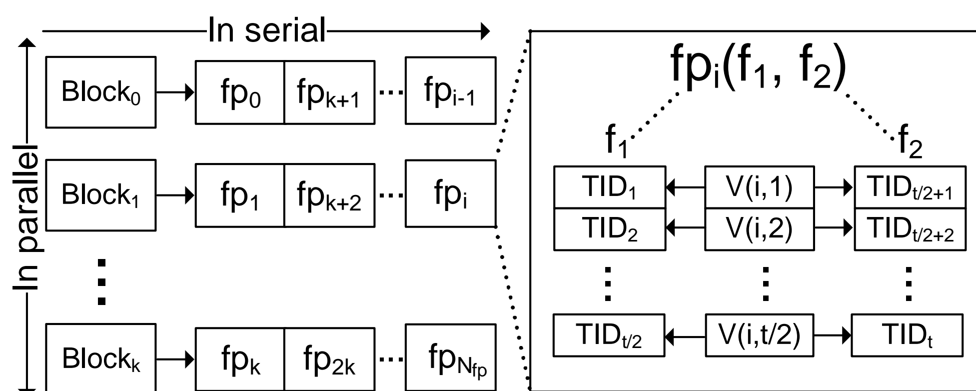

Figure 4.2: Parallel diagnostic simulation architecture.

4.4.2 Dynamic Load Balancing

Since global synchronization among blocks is expensive under the CUDA architecture, a static load balancing strategy seems promising where all the fault pairs are evenly distributed to each block. However, we found that even if an equal number of FPs were allocated among all the blocks, the variation in the work load could be substantial, since the work load for a given fault pairs is hard to estimate (each pair may require a different number of test vectors before they are distinguished). Thus, we propose a novel dynamic load balancing strategy instead. GDSim exploits the atomic function provided by CUDA to maintain a global fault pair counter cnt. Initially, all

the blocks are assigned I fault pairs to distinguish. Once a block finishes the simulation of its assigned FPs, it will claim another L FPs and atomically add L to cnt. A small L may diminish the performance because the atomic writing is an expensive operation on GPU. Also, a big L may cause an unbalanced work loading if the assigned L FPs are all hard-to-diagnose. Therefore, we propose a dynamic load balancing strategy where L is dynamically tuned according to the number of remaining fps to be simulated. We initially set a large L_b to avoid too many expensive atomic operations, and later reduce L to 1 for when few FPs remain so that any workload imbalance is minimized during the final stages of the simulation.

4.5 Experimental Results

We evaluated our diagnostic fault simulator's performance on a set of large ISCAS89 [15] and ITC99 [27] benchmarks. The experimental platform consists of a workstation with Intel Xeon 3 GHz CPU, 2 GB memory and one NVidia GeForce GTX 285 graphic card as introduced in Section 2.1.1. We randomly generated 10 sets of 32,768 test vectors and applied them to all the circuits for diagnostic fault simulation. Ten runs were performed to obtain an average run time. To evaluate the correctness of our simulator, the results were verified with an efficient CPU-based diagnostic fault simulator [19]. The number of blocks (k) launched was set to 120 with 128 threads (t) running on each block. As discussed in Section 4.5.2, these parameters are determined according to the characteristics of the GPU and CUDA architecture for GDSim to achieve the best performance.

Table 4.1: Comparison with other tools.

Circuit	# Gates	# Faults			# Pairs			Run time (seconds)			Speedup	
		Total	FG	Undet.	Total	Dist.	Indist.	GDSim$_{seq}$	MLS [19]	GDSim	Seq	MLS [19]
s9234	6094	6927	3746	905	3748	2254	1494	13.892	6.302	0.234	59.260	26.885
s13207	9441	9815	4638	354	5068	2942	2126	16.132	7.440	0.297	54.405	25.091
s15850	11067	11725	5725	842	6426	3546	2880	42.527	12.671	0.943	45.116	13.442
s35932	19876	39094	13746	3985	19023	6130	12893	146.002	61.343	0.507	288.096	121.043
s38584	22447	36303	16895	1714	9479	6661	2818	38.855	21.549	0.500	77.774	43.133
s38417	25585	31180	14584	1597	15789	10878	4911	177.288	34.876	0.981	180.701	35.547
b15	9371	21988	10273	3419	13425	9240	4185	339.677	81.120	5.355	63.427	15.147
b15_1	13547	28999	14550	8535	12900	5881	7019	205.051	90.371	2.564	79.980	35.249
b17	33741	76625	38236	16162	41455	22384	19071	1398.910	570.040	15.644	89.422	36.438
b17_1	41080	88098	46519	25294	43418	18940	24478	1040.370	442.387	9.980	104.245	44.327
b20_1	14933	33255	18097	2803	10753	7368	3385	167.268	84.851	3.032	55.166	27.984
b21_1	14932	32948	17802	2773	10138	6787	3351	171.103	97.978	2.775	61.669	35.313
b22_1	22507	49945	25544	4148	15840	11119	4721	308.817	159.194	3.985	77.490	39.946
Avg											**95.135**	**38.427**

4.5.1 Performance Evaluation

Table 4.1 compares our GPU-based diagnostic fault simulator (GDSim) with its own sequential (non-parallel) version (GDSim$_{seq}$) and a ”multi-way list splitting” (MLS) algorithm proposed from [19]. Both of these two methods are implemented and tested on the same platform as GDSim. In Table 4.1, Column 1 lists the benchmarks. The number of gates and the number of collapsed faults are listed in columns 2 and 3, respectively. Column 4 lists the number of faulty gates (N_{FG}); recall that each FG denotes a group of faults on the same gate. Columns 5 and 6 give the number of undetected faults and the number of fault pairs, respectively. These fault pairs will be sent to GPU for further pair-based diagnostic fault simulation. It is noted that the pairs consisting of two undetected faults are not included because all those are already identified as indistinguishable by the test set. The size of MFS (SIG_LEN) is limited to *3* in our experiment. SIG_LEN are experimentally determined and will be discussed in Section 4.5.2. After pair-based simulation, the number of obtained distinguishable (indistinguishable) pairs by the total 32K testing vectors are presented in Column 7 (8). Columns 9 and 10 list the execution time in seconds for GDSim$_{seq}$ and MLS [19], respectively. The time obtained from our parallel simulator GDSim is listed under column 11 which includes the GPU computation time, the communication overhead between the host and the device and the pre-processing tasks run on the CPU. The speedups obtained by GDSim against these two tools are listed under columns 12 to 13.

Consider circuit s35932, which has more than 20K gates and 39K collapsed faults. With multi-signatures fault simulation, only 19023 fault pairs need to be simulated, among which 6130 pairs were distinguished and 12893 pairs indistinguishable by the 32K random vectors. GDSim$_{seq}$ took 146 seconds to complete, while MLS proposed in [19] took 61 seconds on the CPU of the setup. Our GDSim on GPU took only 0.51 seconds. This is $288\times$, $121\times$ speedup over these tools, respectively.

We note that GDSim has the smallest speedup for s15850. This is because of the low percentage of indistinguishable faults pairs (2880 out of 6426). Therefore, the number of computations needed for sequential diagnosis simulation is reduced greatly. In other words, the distinguishability of

most pairs in s15850 were easy to be determined. This could also explain the highest speedup gained for circuit s35932 since there are nearly 70% indistinguishable fault pairs and thus the simulation requires more computational resources.

To further examine the performance of GDSim, we applied test vectors generated by a well-known automatic test pattern generator, ATOM [40]. Figure 4.3 shows the execution time between GDSim and MLS [19] with different sizes of test sets applied for circuit b17_1. A speedup of 23.13 is achieved when applied 4783 test vectors which are all generated by ATOM. After appending random vectors to get a total of 32768 test vectors, GDSim is $46.86\times$ faster. More speedup is achieved by GDSim with larger test sets because of the increasing computational effort required especially for those indistinguishable pairs. It is also noted that both tools take longer execution time than those listed in Table 4.1. This is because the high-quality ATPG vectors detect more faults which increase the total number of fault pairs that need to be distinguished.

4.5.2 Characteristics of Diagnostic Fault Simulator

In this section, we will explore and analyze three characteristics of GDSim.

Dynamic load balancing

We compared our GDSim against its static version in which fault pairs are evenly distributed and assigned to different blocks before simulation. In both cases, the configurations of CUDA and fault pair candidates are identical. L_b and I are set as 10 to avoid frequent atomic operations. GDSim changes L to 1 when less than $2\times k$ FPs are left to distinguish. Figure 4.4 shows that the one without dynamic load balancing is at least four times slower than the original GDSim. For benchmark s15850, it was 6.15 secs without dynamic load balancing, $6\times$ slower than with dynamic load balancing.

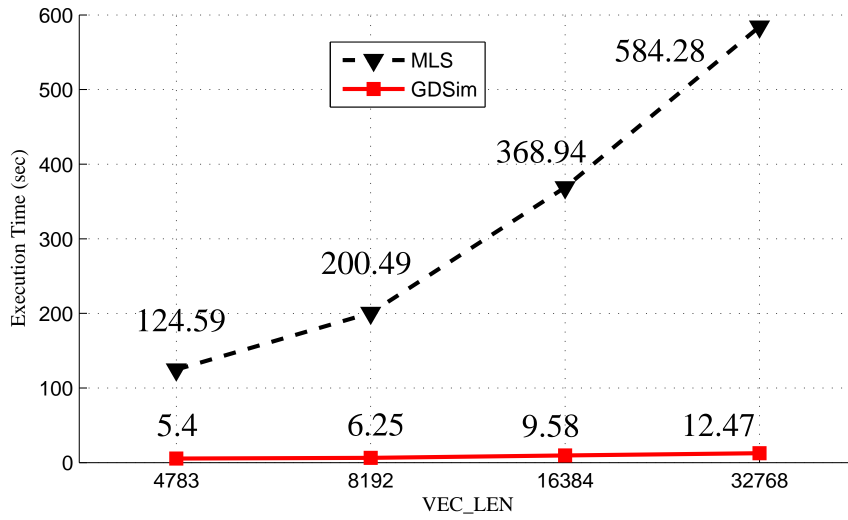

Fig. 4.3: Comparison with different vector length for b17_1.

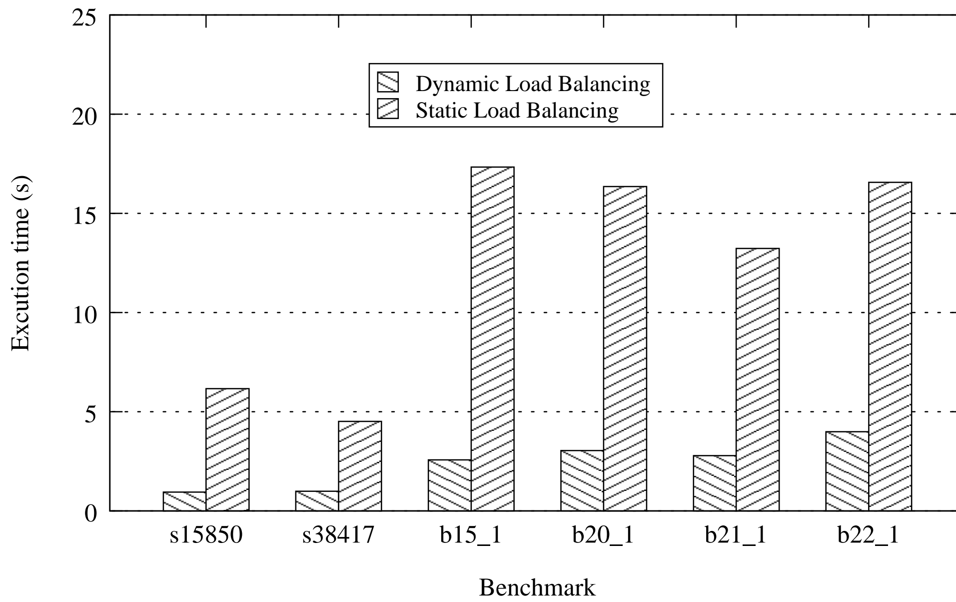

Fig. 4.4: Comparison between dynamic and static load balancing.

Multi-signature

Table 4.2 show that recording different size of MFSs can have an effect on the number of fault pairs that we need to simulate. Column 2 to 7 list the number of pairs with respect to different values of SIG_LEN. By increasing SIG_LEN from 1 to 2, we observe that the number of pairs reduces by roughly 66%. By continuing to increase the SIG_LEN beyond 3, the reduction in the number of fault pairs also slows which may diminish the performance due to the overhead of storage/comparison between larger signatures. Figure 4.5 shows the execution time in terms of SIG_LEN. The top graph is for the sequential version of GDSim while the bottom graph for the original tool. As mentioned in 4.4.1, for GDSim$_{seq}$, increasing SIG_LEN could not help due to the expensive computing overhead to obtain MFSs. However, this is not the case of GDSim.

Table 4.2: Number of faulty pairs with different SIG_LEN.

Bench	# faulty pairs with different SIG_LEN					
	1	2	**3**	4	5	6
s9234	11829	5199	3748	3242	3032	2931
s13207	13753	6415	5068	4710	4550	4437
s15850	15106	7541	6426	5930	5564	5353
s35932	46270	21617	19023	17717	17391	17246
s38584	22896	11816	9479	8510	7889	7516
s38417	44988	19976	15789	13442	12241	11614
b15	46400	18390	13425	11199	10143	9379
b15_1	39004	16614	12900	11676	11180	10892
b17	146354	55838	41455	35771	33524	31959
b17_1	119748	53484	43418	40211	38592	37789
b20_1	66907	18671	10753	8341	7278	6741
b21_1	64496	17920	10138	7675	6849	6363
b22_1	95300	26984	15840	12075	10635	9854

Parallelism factor

We observed that the performance of our GDSim could be influenced by changing the pattern-parallelism factor t, the number of threads in each block and the fault pair-parallelism factor k, the

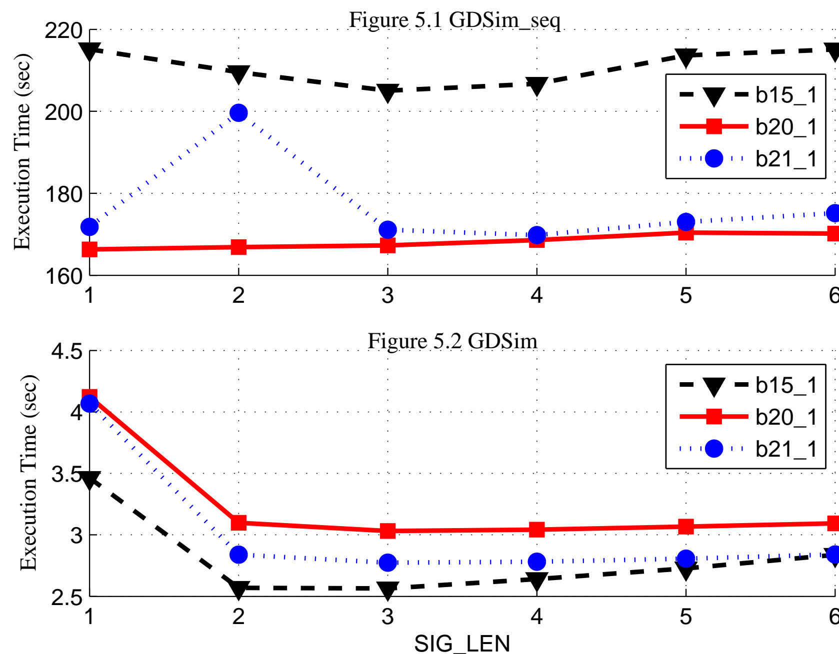

Fig. 4.5: Execution time with respect to different SIG_LEN.

number of blocks allocated on GPU. Figure 4.6 compares four scenarios with different assignments to these factors and shows that the configuration of $s3$ achieves the best performance. When 128 test vectors are applied at a time, those easy-to-diagnose pairs are more likely to be distinguished by the first 64 vectors. Compared with $s2$ in which 256 threads are simulated, $s3$ saves the resources for those 64 threads which could now be applied for the other pairs. In other words, more threads in one block may not necessarily be better. Also, with only 32 threads launched in each block and 16 vectors being simulated at a time, the performance is diminished greatly because the warp of 32 threads are divided into two parts for each fault, and they follow different branches.

4.6 Chapter Summary

In this chapter, We have proposed a high-performance parallel diagnostic fault simulator based on GPUs. Our simulator achieves high algorithmic efficiency by exploiting the parallel computation

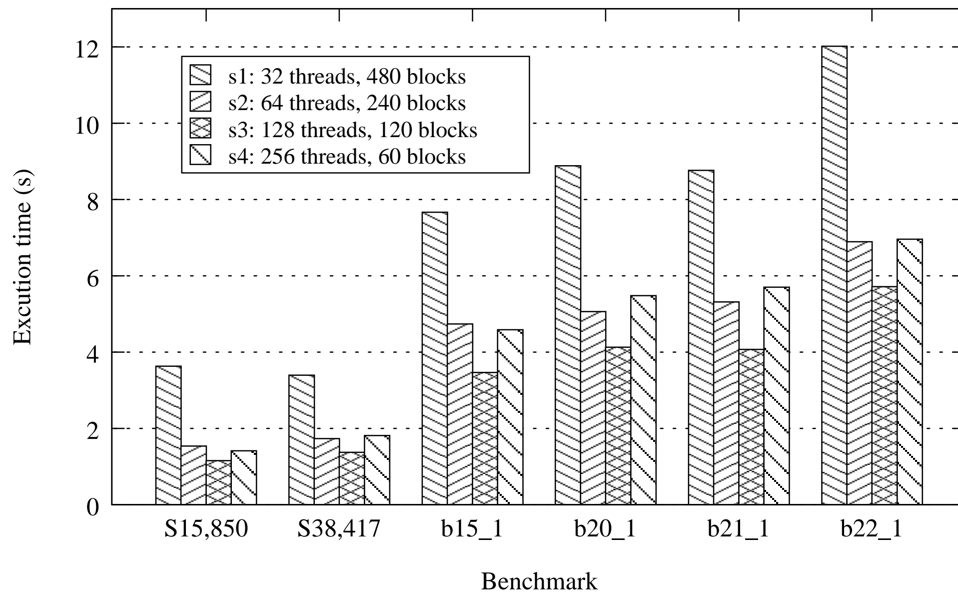

Fig. 4.6: GDSim's execution time with different parallelism factors.

power of GPUs with a novel FG-based and FP-based parallelism. The proposed dynamic load balancing and multi-fault-signature approaches also result in an efficient utilization of the available computational resources. Experimental results showed that GDSim could achieve an average of 38× speedup when compared with a state-of-the-art sequential fault diagnostic simulator. Moreover, GDSim is also 95× faster than its sequential implementation based on conventional processor architectures.

Chapter 5

Parallel Reliablity Analysis

5.1 Chapter Overview

In this chapter, we present a parallel reliability analysis tool of logic circuits on GPUs. In nano-scale technologies, the reliability of logic circuits is emerging as an important concern due to the reduced margins to both intrinsic and extrinsic noise. The computational complexity of reliability analysis increases exponentially with the size of a circuit, making the previous analytical approaches intractable for large circuits. RAG, an efficient parallel Reliability Analysis tool based is a fault injection based parallel stochastic simulator implemented on a state-of-the-art GPU. A two-stage simulation framework is proposed to exploit the high computation efficiency of GPUs. RAG also achieves high memory and instruction bandwidth by optimizing the parallel execution on GPUs. With a novel memory management, RAG could accurately analyze the reliability of large circuits without sacrificing computational occupancy on GPUs. Experimental results demonstrate the accuracy and performance of RAG. A speedup of up to 793$\times$ and 477$\times$ (with average speedup of 353.24$\times$ and 116.04$\times$) is achieved compared to two state-of-the-art CPU-based approaches for reliability analysis.

The remainder of this chapter is organized as follows. A brief introduction is given in Section 5.2.

Section 5.3 presents a background in reliability analysis including metrics and related works. Section 5.4 outlines a high-level process view of the proposed method, with a detail description of some critical approaches. The experimental results are reported in Section 5.5. Finally Section 5.6 summarizes the chapter.

5.2 Introduction

Reliability analysis, a process of evaluating the effects of errors due to both intrinsic noise and external transients at individual transistors, gates, or logic blocks on the outputs of the logic circuit, will play an important role for both today's and tomorrow's nano-scale circuits. The probability of error due to manufacturing defects, process variation, aging and transient faults is believed to sharply increase due to rapidly diminishing feature sizes and complex fabrication processes [45, 63, 100, 13, 14]. Moreover, the non-deterministic characteristics of novel devices such as carbon nanotubes, silicon nanowires and molecular electronics make the circuit more vulnerable to these effects. This necessitates an efficient reliability analysis tool which is accurate, robust and scalable with design size and complexity.

Due to the exponential number of input combinations and the difficulty to model gate failures, the reliability analysis of logic circuits is computationally complex. Exact analysis methods, using probabilistic transfer matrices (PTMs) [48, 49] and probabilistic decision diagrams (PDDs) [1], can provide accurate reliability evaluation. Several analysis heuristics, on the other hand, have been proposed to generate a highly accurate reliability estimation, such as probabilistic gate models (PGMs) [24, 94, 41], Bayesian networks [86] and Markov random fields [8]. However, they all suffer from the problem of exponential complexity and are therefore practically infeasible for even mid-size circuits (with more than ten thousand gates). A simulation scheme based on stochastic computational models (SCMs) is proposed in [22]. Although the approach advances in the linear computational complexity and high accuracy, it requires significant runtimes for large benchmark circuits to get an accurate estimation.

In this chapter, we present RAG, an efficient Reliability Analysis tool on GPUs. RAG is a fault-injection based parallel stochastic simulator for logic circuits. The main motivation is to harness the computational power of GPUs to obtain a highly accurate reliability evaluation of logic circuits within short runtimes. Experimental results show that RAG achieves one to two orders of magnitude speedup in comparison with the CPU-based analysis tools. We summarize our contributions as follows.

- To the best of our knowledge, this is the first work that accelerates the reliability analysis of logic circuits on a GPU platform.
- We introduce a two-stage hierarchical simulation framework to efficiently utilize the computation power of the GPU without exceeding its memory limitation. All the fanout stems in the circuit will be scheduled and processed in order. Within the fanout free region (FFR) of each stem, all the logic gates are also arranged and simulated in sequence. Highly parallel execution is achieved by launching thousands of active threads which evaluate the same logic gate but with different vectors.
- We formulated the device memory assignment for fanout stems as a scheduling problem and propose a greedy heuristic to reduce the memory requirement for GPU based simulation. Therefore, more threads could be launched on the GPU to achieve full occupancy. Also, the overhead of data communication between the host (CPU) and the device (GPU) is minimized by re-using the individual device's memory.
- RAG maximizes the memory bandwidth by using the low-latency shared memory for storing the values of gates within the FFR of each stem. A post-order tree traversal algorithm is employed to tackle the problem of limited share memory resources.
- A novel data structure for storing circuit netlist is developed to exploit the memory hierarchy of GPUs.
- We applied GPU-oriented performance optimization strategies to ensure a maximal speedup. Global memory accesses are coalesced to achieve optimal memory bandwidth. A high in-

struction bandwidth is obtained by avoiding branch divergence. RAG also takes advantage of the inherent bit-parallelism of logic operations on computer words. The execution configuration of each kernel launch is determined for efficiently mapping the algorithm on the GPU.

5.3 Background

Based on fault injection and stochastic simulations illustrated in 2.2.3, RAG is capable of providing all the above metrics from N random simulated samples. Suppose, a number of N random generated vectors are simulated and the fault free and faulty logic values for the m outputs are recorded as $O_i(j)$ and $O_i^e(j)$, respectively, where i is the index of the outputs and j is the index of the vectors. Since a single sample is simulated by one random input vector, this work use the terms *sample* and *vector* interchangeably.

Then, the probability of error for each output i, can be calculated as:

$$\delta_i = \frac{\epsilon_i}{N} = \frac{\sum_{j=1}^{N} O_i(j) \oplus O_i^e(j)}{N}, \tag{5.1}$$

where ϵ_i is the number of faulty samples on output i.

Similarly, the average reliability among all outputs (R_{avg}) is represent as:

$$R_{avg} = \frac{\sum_{i=1}^{m} (1 - \delta_i)}{m}. \tag{5.2}$$

5.3.1 Previous Work

The authors in [48] employ probability transfer matrices (PTMs) to capture non-deterministic behavior in logic circuits. Since the occurrence probability of *every* input-output vector pair for each level in the circuit has to be recorded, PTMs are not applicable for large benchmarks due to the massive matrix storage and manipulation overhead. Although PTMs are extended to a reliability

estimation using input vector sampling in [49], our results show that RAG is more efficient and can handle even bigger circuits with the same accuracy.

Three more scalable algorithms are proposed in [24] for reliability analysis, but for large circuits, accuracy is achieved by constraining on error conditions which is the number of simultaneous gate failures in the circuits (e.g., maximum-k gate failure can co-occur at any given time). In the experiment results, the largest simultaneous gate failures is set to 3. Also, to get an accurate estimation of reliability, high correlation coefficients in signal probability computation have to be used to handle the reconvergent fan-out. However, the algorithms do not scale well for mid-size benchmarks.

In [22], a traditional approach to reliability analysis is proposed that employs fault injection and simulation in a Monte Carlo framework. Although the algorithm is scalable, *only* 1000 samples are simulated with a relatively high execution overhead. Our experimental results show that a large sample size is required for logic circuits to obtain an accurate reliability analysis. The simulation overhead is caused by adding exclusive-or gates for every logic device which makes the circuits size two-times larger. Also, the random bit sequence generation during Monte Carlo simulation requires a significant amount of runtime.

In RAG, we parallelized the Monte Carlo based simulation and implemented it on GPUs. No exclusive-or gates are needed to add into the circuits. A two-stage hierarchical simulation framework is proposed to efficiently utilize the computation power of GPUs. Memory usage is optimized to achieve full computational occupancy and high memory bandwidth on GPUs. Also, the process of random number generation (RNG) is parallelized to minimize the overhead. By simulating millions of samples on thousands of threads running simultaneously on the GPU, RAG could achieve a high accuracy of reliability evaluation for industry size benchmarks within a short runtime.

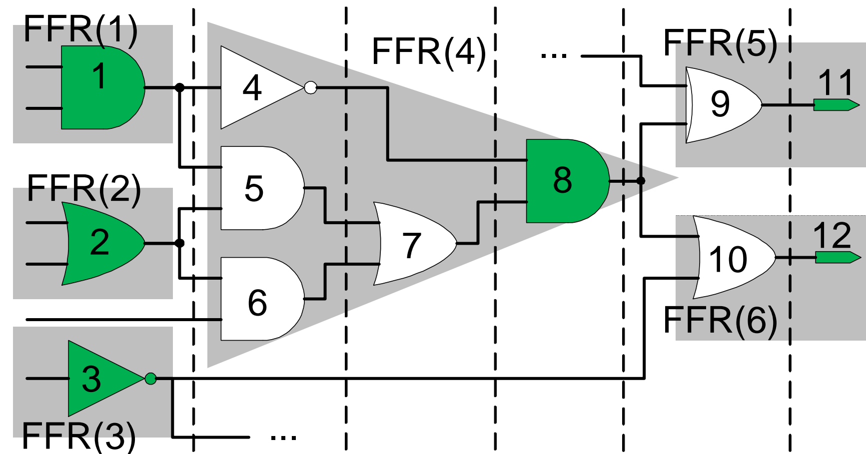

Figure 5.1: Fanout Stems and Fanout Free Regions.

5.4 Proposed Method

In this section, we first present some definitions, followed by the two-stage framework of the proposed reliability analysis tool. Finally, we will analyze the memory assignment and scheduling problem.

Definition 12. *The fanout* stems *in the combinational circuit are defined as those gates with more than one immediate successor gates. Also, primary outputs (POs) are considered as stems in this work. When all these stems are removed, the circuit would be partitioned into independent* fanout-free regions (FFRs). *We denote a FFR region whose output is stem s as $FFR(s)$. All these remained gates are defined as* non-stem gates *in this chapter.*

Figure 5.1 illustrates a sub-circuit with 12 logic gates (including POs). The netlist is levelized a priori and the gates are indexed according to the ascending order of their levels. The circuit could be partitioned into six fanout free regions (shaded in gray) corresponding with 6 stems (in green).

5.4.1 Framework

The high-level flow of RAG is shown in Figure 5.2, where the white boxes denote the CPU workload, and the shaded boxes are the GPU workload. At the beginning, the CPU reads in the circuit netlist and generates the list of stems with the corresponding fanout free regions. A post-order tree traversal algorithm is employed to the arrange the simulation sequence of gates (non-stem gates) within each of the FFRs. Because we only need to store the stems' values, the memory for the FFRs can be shared, thus saving much space. After that, we formulate another scheduling for the simulation of stem as an optimization problem whose objective is to minimize the memory storage of logic values needed. In other words, we need not allocate memory to store the values for all stems. Rather, storage of a stem's value can be reused whenever *all* its successors (child stems) have been evaluated. A greedy approach is employed in this scheduling algorithm to help RAG further reduce the memory usage so as to achieve a high bandwidth and full occupancy during simulation. Then, the scheduled circuit netlist represented as a bit stream is transferred to the GPU. A GPU-based stochastic simulator k_{sim} is launched as Kernel 1 on the GPU. Thousands of threads could be launched with each simulating a total p random vectors. To avoid branch divergence, each thread within the same warp evaluates the same logic gate simultaneously but with different vectors. At the end of simulating each vector, the number of errors arrived at each output will be recorded in vector $\vec{\epsilon}$ on global memory. Since each thread maintains its own error vectors, a parallel reduction kernel k_{red} is launched to compute the total number of errors for each outputs and transfer the summed up $\vec{\epsilon}$ back to the CPU. The parallel reduction kernel is a modified version of the one provided in CUDA software development kit (SDK) [72]. Finally, RAG will compute the average error probability for each output, δ and the R_{avg} to give a comprehensive reliability analysis of the logic circuits.

Circuit Netlist with a bit stream

The netlist of the circuit is an array of logic gates. Their sequences are decided according to a two-stage pre-processed scheduling. The stems are sorted according to a greedy algorithm and the

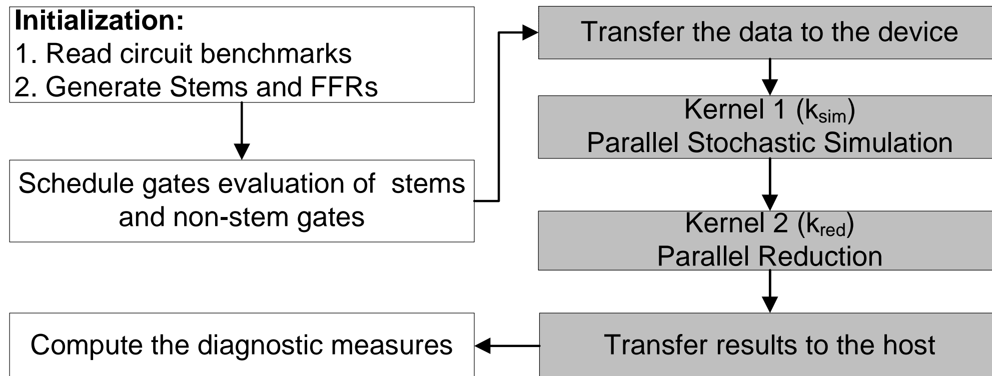

Figure 5.2: The framework of RAG.

gates within each stem are scheduled by a tree traversal algorithm. Similar with what we proposed in Section 3.4.3, Each logic gate is represented by a bit string where the first 32 bits ($uint\ g$) indicate the gate storage location on the GPU. It is noted that the first bit of g represents whether the gate is a stem or not. As mentioned before, the logic values of the stems are stored in the global memory while those of the non-stem gates are stored in the shared memory. The following 16 bits denotes the type of the gate ($short\ type$). The number of inputs are denoted as the next 16 bits ($short\ in_n$) and the following bits are divided into in_n integers representing the storage location of all its fanins. Since the bit string ($int * \ netlist$) is stored in the texture memory, each thread will fetch one entry of the stream. Therefore, the information of the netlist is cached to maximize the memory bandwidth.

Fault Injection based Stochastic Simulation (k_{sim})

Algorithm 4 illustrates the implementation of kernel k_{sim} in detail. A total t threads are launched on the GPU. Each thread will be assigned p vectors and thus runs p iterations to simulate all of them. It is noted that in our actual implementation, each thread is simulating /emphtwo vectors at a time to optimize the memory usage. For each iteration, the scheduled stems and gates within the corresponding FFRs will be processed in sequence. The reading of gate information is optimized by texture cache in Line 5. Although branches exist for different gate types, no branch divergence

Algorithm 4 k_{sim} – stochastic simulation kernel

Input: $uint *v,\ uint *v^e,\ uint *\ netlist,\ float *\ \tau\ ,\ int\ t$

Output: $int *\epsilon$

1: int g, short type, int in$_c$, int* in, int e;
2: $tid = threadId()$; { get global thread index}
3: **for all** vectors $i \in p$ **do**
4:    **for all** gate j in netlist **do**
5:       $texture_fetch(g, type, in_n, in, netlist, j)$;
6:       **if** gate type is PI **then**
7:          $v[tid + g \times t] = v^e[tid + g \times t] = RNG()$;
8:          continue;
9:       **end if**
10:       **if** gate type is PO **then**
11:          $e = bit_count(v[tid + g \times t] \oplus v^e[tid + g \times t])$;
12:          $\epsilon[tid + g_{po} \times t] = \epsilon[tid + g_{po} \times t] + e$;
13:          continue;
14:       **end if**
15:       $eval(v,\ v^e,\ g,\ type,\ in_n,\ in,\ netlist,\ j)$;
16:       $uint\ fault = generate_fault(\tau)$;
17:       $v^e[tid + g \times t] = v^e[tid + g \times t] \oplus fault$;
18:    **end for**
19: **end for**

is introduced because all the threads within one warp are simulating the same gate simultaneously. Therefore, it is guaranteed that all the threads within the same warp will be running on the same branches but simulating different vectors. In line 15, we call the function $eval$ to evaluate both the faulty and fault-free model of the circuit and recorded the value at location g in vectors $\vec{v}$ and $\vec{v^e}$, respectively. In Line 16, the faults are generated by the a parallel random number generator (the same used in Line 7) according to the error rate vector ($\vec{\tau}$). The implemented GPU based RNG is similar with the one proposed in [96]. Faults are injected in Line 17 by flipping the logic values. Since 32 vectors are simulated on every thread concurrently, errors on each output are counted in Line 11 and added to the vector $\vec{\epsilon}$ in Line 12. At the end of simulation of each vector, the number of errors on each output will be recorded in vector $\vec{\epsilon}$ on the global memory.

Memory Requirement versus Performance

A typical requirement for good performance on CUDA is that the application should use a large number of threads. Also, the accuracy of the reliability analysis by stochastic simulation depends on a large number of samples. By simulating millions of samples with thousands threads running concurrently, RAG could achieve a high performance and accuracy. However, the number of threads that could be allocated on GPUs are limited by not only the intrinsic constraints of the CUDA architecture, but also the total memory limitation (M_t). According to our experiments, the storage for logic values, $\vec{v}$ and $\vec{v_e}$ dominates the memory usage. If the total number of threads launched on GPUs is t, the memory requirement would be $M_v = V \times 4 \times t$ (each threads simulate 2 vectors at a time), where V is the size of the space to store $\vec{v}$ and $\vec{v_e}$. Therefore, in order to achieve high performance and accuracy with the limited memory, we propose a method to reduce V.

5.4.2 Scheduling of Stems

Definition 13. *For a circuit with n stems, represented as $\vec{s} = \{s_1, s_2, \ldots, s_n\}$, we define their corresponding simulation slots as $\vec{a} = \{a_1, a_2, \ldots, a_n\}$, and their storage location on $\vec{v}$ and $\vec{v_e}$ as*

$\vec{g} = \{g_1, g_2, \ldots, g_n\}$.

First, we show that the ordering of stems can result in different memory footprints. For example, in Figure 5.1, if all six stems $\{s_1, \ldots, s_6\}$ are simulated in a levelized manner, we have $\vec{a}_1 = \{1, 2, 3, 4, 5, 6\}$. As noted before, the storage of a stem will be released once all its child stems are processed. Therefore, we have $\vec{g}_1 = \{1, 2, 3, 1, 2, 1\},\ V = 3$. When we simulating s_4, all its fanin stems f_1 and f_2 will be free. Therefore, the storage location 1 and 2 could be released and reused for the following stems. However, if we change the processing sequence to $\vec{a}_2 = \{1, 2, 4, 3, 6, 5\}$, we have the storage locations of the stems as $\vec{g}_2 = \{1, 2, 1, 2, 2, 1\},\ V = 2$, in which we only need 2 storage spaces for simulating these six stems instead of 3. Therefore, a different ordering might result in a different storage requirement.

Algorithm 5 greedy algorithm for stems scheduling

Input: $int **in,\ int **out$

Output: $int *a$

```
1:  int *free, int* in_left, int* out_left;
2:  int cnt=0; { the slot count}
3:  initialization();
4:  for all stem s do
5:      if (|in_i| = 0)  s_i→ready; { no fanin stem}
6:  end for
7:  while ready≠∅ do
8:      s = ready.pop_back(); { greedily pick the stem}
9:      a[s] = cnt++; { set slot a, add s to the queue}
10:     for all j∈in[s] do
11:         update(free[out[j]]); { update key }
12:     end for
13:     for all j∈out[s] do
14:         if (in_left[j]-- == 0)  s_j→ready;
15:     end for
16: end while
```

We formulate the stem-scheduling problem as an optimization problem shown in Equation 5.3. The objective is to minimize the maximum distance between any two immediately linked stems so as to minimize the memory usage. Each stem i should be processed before its successor stems in $\vec{out}_i$ to maintain the correctness of the simulation. Also, two stems cannot be assigned to the same

processing slot because each thread is simulating one stem at a time.

$$\begin{aligned}
&\textbf{minimize}: && max_d \\
&\textbf{subject to}: && \\
&\forall i{\in}\{1...n\},\ \ j{\in}\vec{out}_i, && a_i < a_j \\
&\forall i{\in}\{1...n\},\ \ j{\in}\vec{out}_i, && a_j - a_i < max_d \\
&\forall i,j{\in}\{1...n\},\ \ i{\neq}j, && a_i \neq a_j
\end{aligned} \tag{5.3}$$

We note that the computational complexity for solving this ILP formulation is $\mathcal{NP}$-hard. To demonstrate the high cost of an exact solution, we employed a commercial CPLEX Optimizer to solve the problem. Even for the small benchmark (c880), the solver is not able to give us a solution in one hour. Since our main target is to achieve the full occupancy of GPUs within the memory bound, an exact optimum may not be necessary. Hence, we propose a greedy algorithm shown in Algorithm 5 to schedule the stems and reduce the storage requirement. In the algorithm, a sorted list, $ready$ is maintained which includes all the stems that are ready to be processed. In other words, the timing slots of all their ancestor stems have already been determined. The list $ready$ is kept sorted in terms of the key, $free$. For each stem s, $free[s]$ represents the number of storage spaces that could be released after s being added to the simulation queue. As it is greedy, each iteration will pick the stem with the highest $free$ value from $ready$ and add it to the simulation queue (set its a in Line 9). The input of the algorithm is the ancestor and successor stem lists of each stem, denoted as in and out, respectively. The array in_left and out_left represent the number of ancestor and successor stems that have not been added into the simulation queue.

By applying the algorithm, our experimental results in Table 5.1 show that the space requirement is reduced by approximately $3\times$ against the one without stem-scheduling.

Table 5.1: Circuit Characteristics.

Circuit	# Gates	#in	#out	S_{FFR}		S_{stem}		Mem_s (KB)		Mem_t (MB)		
				Orig.	Opt.	Orig.	Opt.	Orig.	Opt.	Comp.	Orig.	Opt.
c880	469	60	26	17	6	165	63	17	6	58	20	8
c7552	3827	207	108	20	6	1538	343	20	6	474	181	43
s35932*	19876	1763	2048	15	4	7375	1538	15	4	2506	913	240
s38584	22447	1464	1730	106	9	5761	2391	109	9	2812	717	329
s38417*	25585	1664	1742	48	8	7350	2001	49	8	3198	901	284
b15_C	9371	485	519	34	9	2872	981	35	9	1168	347	129
b17_C*	33741	1452	1512	120	12	9695	3444	123	12	4193	1164	444
b18_C*	117963	3357	3365	188	12	34431	5605	193	12	14601	4072	751
b20_C	20716	522	512	161	11	5157	1684	165	11	2562	610	210
b21_C	21061	522	512	161	11	5125	1571	165	11	2604	606	197
b22_C*	30686	767	757	166	12	7667	2465	170	12	3795	907	308

5.4.3 Scheduling of Non-stem Gates

As suggested in 2.1, read/write on the shared memory has the advantage of low latency compared with global memory. Therefore, storing the logic value of non-stem gates in the shared memory would help reduce the read/write overhead. Since the gates in each FFR are simulated independently, shared memory can be re-used for each FFR which makes it ideal for storing the values of these gates. However, because only 16 KB share memory is available on each SM, we need to reduce the maximum memory usage among the FFRs.

We also take FFR(4) in Figure 5.1 as an example with the same notation used in Section 5.4.2. The original order $\vec{a}_1 = \{4, 5, 6, 7, 8\}$ results in the assignment, $\vec{g}_1 = \{1, 2, 3, 2, 1\}$, $V = 3$. However, if the gates are simulated by another order $\vec{a}_2 = \{5, 6, 7, 4, 8\}$, the storage would be $\vec{g}_2 = \{1, 2, 1, 2, 1\}$, $V = 2$, which is one space less than the original one. Therefore, for each stem s, we employ an approach based on the post-order tree traverse to determine the gate simulation order within the FFR. Effectively, we consider the gates in FFR(s) as a tree. At the pre-processing stage, for each node, its child nodes are sorted in terms of their number of child nodes. The node with more child nodes are preferable to be simulated earlier so that more memory spaces could be free. After that, another post-order tree traverse is processed to determine the gate simulation order. By applying the algorithm, our experimental results shows that the space requirement for simulating the FFRs can be reduced by more than $10\times$ against the one without scheduling. More importantly, the reduced memory requirement allows the storage of non-stem gates to fit into the 16KB shared memory without going through the global memory when simulating the gates in each FFR.

5.5 Experimental Results

We evaluated RAG's performance on a set of large ISCAS89 [15] and ITC99 [27] benchmark circuits which are available from [44]. Our fault simulation platform consists of a workstation with Intel Quad-core i7 3.33 GHz CPU, 2 GB memory and one NVIDIA GeForce GTX 285 graphics

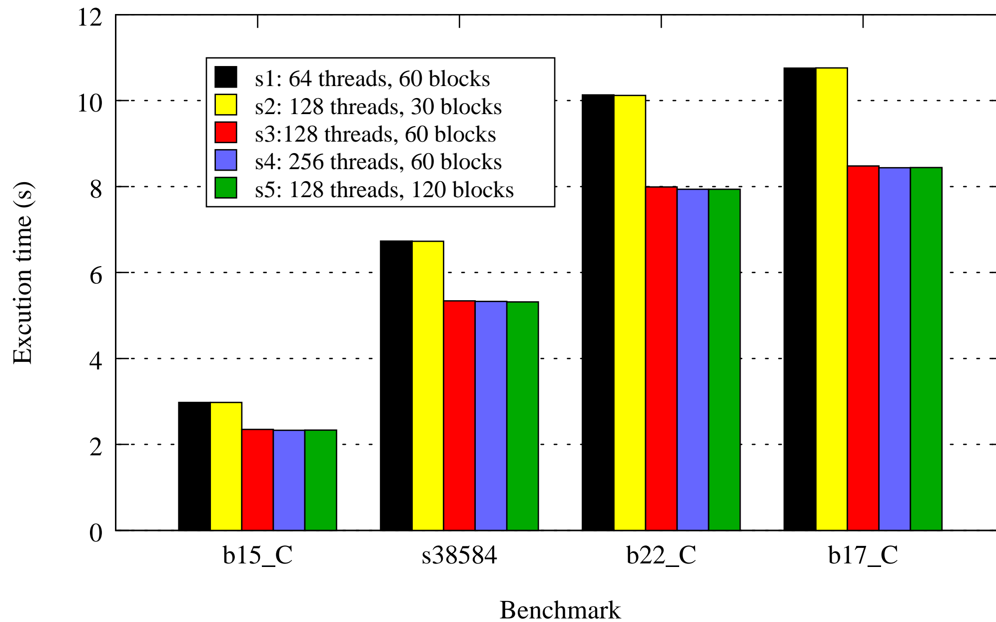

Figure 5.3: RAG's execution time with different GPU configuration.

card as introduced in Section 2.1.1. It is noted that the actual available global memory are limited to around 900 MB because the rest are reserved for CUDA programs and GPU device drivers. The number of blocks launched was set to 60 with 128 threads running on each block (with a total of 7680 threads). Such execution configuration are set according to the characteristics of the GPU and CUDA architecture. By assigning two blocks to each SM and four warps per block, CUDA could interleave their execution and effectively mask most of the time spent while waiting for data from device memory. The results illustrated in Figure 5.3 show that our configuration could achieve full occupancy on the GPU.

To achieve an accurate reliability evaluation, the number of samples to be simulated are determined experimentally. Table 5.2 shows the accuracy of the simulation as the sample size for the simulation is increased from 32 to 2.4 million random patterns. It is noted that both the CPU implementation and RAG employed 32-bit parallelism. The percentage error for each sample size is reported with respect to the result for 24 million random patterns. Because the maximum error for the largest circuit, b18_C, is only 0.52% with 2.4 million random patterns, RAG have used this sample size of 2.4M for all the simulations in this work. Given a total 7680 threads, RAG assigns 320 samples to

each thread. With employing 32-bit parallelism and simulating 2 samples per iteration, each thread will be running 5 iterations on the GPU.

Table 5.2: Accuracy of RAG for Different Number of Samples

Circuit	# Gates	Maximum error over all outputs (%)*				
		32	2k	24k	240k	2.4M
c17	13	49.83	2.11	0.83	0.69	0.14
c880	469	151.46	18.94	5.23	2.62	0.52
c7552	3827	212.01	20.76	7.89	2.81	0.79
s38584	22447	229.12	22.35	6.42	1.84	0.59
b17_C	33741	105.80	20.09	6.42	2.48	0.47
b18_C	1117963	151.46	18.94	5.23	2.62	0.52

*The error is w.r.t. the error produced with 24M samples.

Table 5.3: Comparison with Other Tools.

Circuit	Avg. Reliability			Runtimes (in seconds)			Speedup	
	PTM [49]	RAG	err(%)	PTM [49]	[24]	RAG	PTM [49]	[24]
c499	0.779	0.7787	0.04	18.70	14.70	0.10	192.52	151.34
c880	0.680	0.6802	0.03	30.00	NA	0.15	204.10	NA
c1908	0.627	0.6308	0.60	220.70	30.00	0.28	793.96	107.92
c2670	0.872	0.8727	0.08	72.70	1.10	0.28	258.53	3.91
c3540	0.564	0.5661	0.37	330.94	234.00	0.49	675.16	477.39
c5315	0.697	0.7033	0.91	233.62	NA	0.67	348.41	NA
avg			**0.29**				**353.24**	**116.04**

5.5.1 Scheduling Evaluation and Memory Performance

The characteristics of the circuits and the storage requirements for stems and FFRs are illustrated in Table 5.1. Benchmarks with $*$ are unable to be simulated before applying our proposed scheduling algorithms because the available 900 MB device memory is not enough for storing all the data. For each circuit listed in the first column, the number of logic gates, inputs and outputs are listed in Columns 2, 3 and 4, respectively. Columns 5 and 6 report the original and optimized storage

usage for the gates within FFRs in terms of the number of elements. The original and optimized storage requirements for the stems are reported in Columns 7 and 8, respectively. The actual shared memory usage for storing these FFRs (Columns 5 and 6) (Mem_s) per SMs are listed in Columns 9 and 10 in KB. The original storage usage is the maximum size of FFRs in the circuit before applying our proposed algorithm. It is noted that the storage of the original stems is the total number of stems in the circuit. The total global memory usage (Mem_t) for the GPU are listed in Columns 11 through 13 including the storage of circuit netlist, error counters for each output and the logic values of stems. Column 11 (Comp.) listed the memory usage without the proposed two-stage simulation where all the signal values are stored. For example, consider circuit b18_C with more than one million gates. Without our scheduling algorithms, RAG cannot simulate the circuit due to its large size. However, after applying the proposed scheduling algorithm, the size for storing the value of stems reduced to 5605 (751 MB), which is less than one-sixth of the original value, 34431 (4072 MB). Also, the storage for FFRs reduced from 188 (193 KB) to 12 (12KB) which makes it fit to the shared memory.

5.5.2 Accuracy and Performance Evaluation

First, we compared RAG with two state-of-the-art reliability analysis tools with the results reported in Table 5.3. An exact approach with sampling based on PTMs [49] and the non-exact Observability-based method [24] were used in our comparison. The failure rate used for each gate was 0.1. Note that the benchmarks used in the previous work only targeted ISCAS85 circuits [15], which are notably smaller than the additional ones we use in this work. Nevertheless, we ran RAG on these circuits as well for comparison. Columns 2 and 5 list the average reliability and runtimes for PTMs which are referred from Table III in [49]. As an comparison, both the reliability and run time for the proposed RAG are listed in Columns 3 and 7, respectively. Since the authors in [24] did not provide the results for reliability evaluation, we only list its runtimes in Column 6. Column 4 shows that the reliability analysis using RAG is highly accurate compared with the PTMs approach. Only an average percentage error of 0.29% is introduced. Moreover, RAG could achieve

an average speedup of $353.24\times$ and $116.04\times$ comparing with these two tools.

To further examine the performance of RAG on large circuits, we implemented two stochastic simulators based on fault injection with 32 bit-parallelism. One is event driven based simulator (Sim$_{event}$) and the other is a compiled random logic simulator (Sim$_{comp.}$) which is a sequential version of RAG (all the gates are evaluated). Their results are listed in Table 5.4. We note that the sequential simulators are faster than PTMs [49] and [24] because the tools are bit-parallelized and implemented on a more advanced platform. We evaluated 11 large circuits with three different failure rate, 0.005, 0.05, and 0.10. We note that error rates less than 0.005 were not included, since we assume a high error probability in nano circuits, as previous authors had [48, 49, 1, 24, 94, 41, 86, 8, 22]. The average reliability among outputs are listed in Column 2, 3 and 4 in terms of different error rates. Since RAG and Sim$_{comp.}$ evaluate all the gates for each simulation run, the runtimes will be the same under any error rate. Therefore, we only list their runtimes for an error rate of 0.05 in Column 8 and 9. However, since Sim$_{event}$ only processes the gates whose logic values are changed, different error rate will affect different runtimes. Columns 5, 6 and 7 show the runtime for different error rate, τ. It is noted that Sim$_{event}$ is much faster than Sim$_{comp.}$ when $\tau = 0.005$. However, when τ increases to 0.05 or larger, Sim$_{comp.}$ becomes better since the overhead of event scheduling begin to take a toll on the even-driven simulator. Therefore, in Columns 10 and 11, we list the speedup of RAG against Sim$_{event}$ for $\tau = 0.005$ and Sim$_{comp.}$, respectively. An average speedup of nearly 20× and 65× were obtained.

Table 5.4: Comparison With Tools on the Same Platform with Large Circuits

Circuit	Avg.Reliability			Runtimes (in seconds)					Speedup	
				Event-driven Sim.			Compiled Sim.	RAG	Event	Compiled
	τ=0.005	τ=0.05	τ=0.10	τ=0.005	τ=0.05	τ=0.10			τ=0.005	
c880	0.959	0.770	0.680	2.68	10.92	11.31	7.84	0.15	18.20	53.37
c7552	0.932	0.762	0.713	15.93	83.78	87.32	72.50	1.01	15.79	71.88
s35932	0.985	0.909	0.858	80.38	393.64	425.30	324.31	4.50	17.87	72.11
s38584	0.959	0.752	0.660	80.42	450.14	508.95	384.95	5.34	15.06	72.10
s38417	0.949	0.716	0.627	90.14	513.55	568.32	439.39	6.10	14.78	72.02
b15_C	0.969	0.790	0.691	51.33	205.84	211.56	168.63	2.35	21.89	71.90
b17_C	0.966	0.768	0.658	152.32	830.31	790.86	619.54	8.48	17.96	73.05
b18_C	0.963	0.758	0.644	557.11	2975.57	3028.27	2258.53	30.45	18.30	74.17
b20_C	0.958	0.759	0.655	146.15	533.69	471.44	397.00	5.40	27.08	73.57
b21_C	0.958	0.759	0.655	147.31	483.42	480.17	416.92	5.49	26.83	75.95
b22_C	0.956	0.757	0.655	209.13	719.29	706.77	613.57	7.99	26.19	76.83
avg									**19.99**	**65.09**

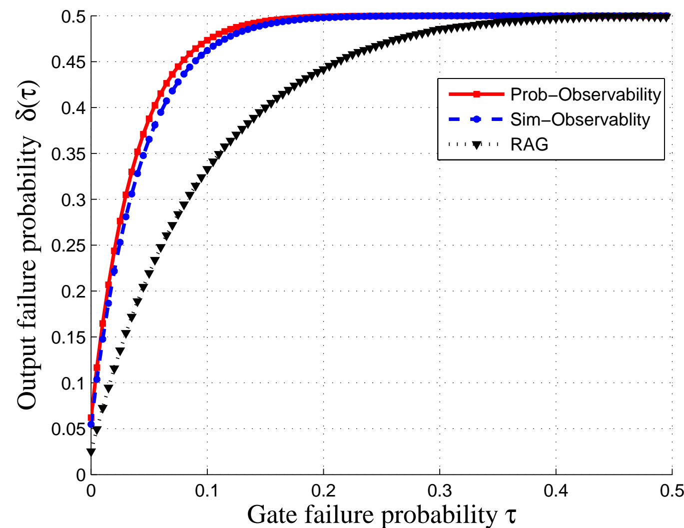

Figure 5.4: Comparison among RAG and two observability-based analysis on benchmark b17.

In Table 5.5, the break down of runtimes for various steps in the simulation is reported in seconds. The stochastic simulation kernel is listed in Column 3 (K_{sim}) which dominates the total runtime in Column 2 (Total). This shows the efficiency of RAG because most of the computation is parallelized and accelerated on the GPU. Column 4 lists another reduction kernel (K_{red}) which is very lightweight. The cost for scheduling of stems and FFRs on the CPU is shown in Column 5 as an initialization of RAG (a one-time cost). Since both scheduling algorithms are linear to the size of the circuits, the overhead is negligible compared with the kernel runtimes. The last column (Misc.) includes the data initialization on the GPU and the transmission overhead between the CPU and the GPU. As illustrated in Section 5.4.1, the communication cost only includes the circuit netlist sent from CPU and the vector of error count from the GPU. Therefore, the overhead is relatively small comparing with the total runtime.

Comparison with testability-based approached

To show the advantage of RAG over approaches based on testability analysis, we compare against the observability-based methods which are introduced in [24]. As illustrated in Figure 5.4, the

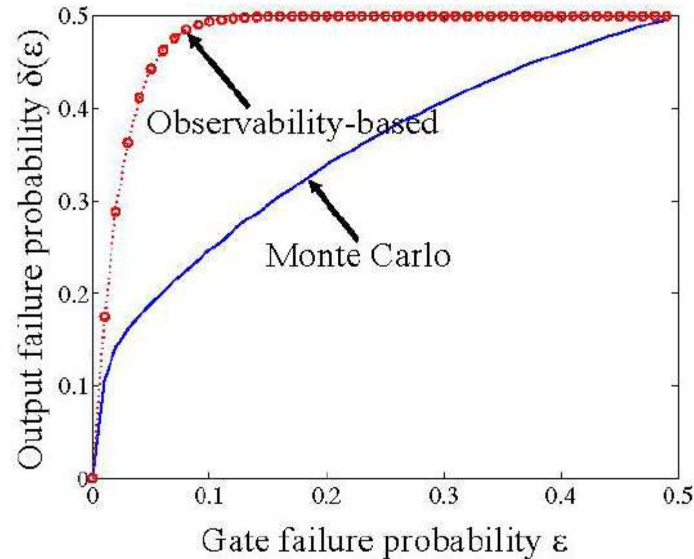

Figure 5.5: Comparison between Monte Carlo and Observability on benchmark b09 from [24].

X-axis is the gate failure probability rate τ ranging from 0 to 0.5 and the Y-axis shows the corresponding failure rate of a specific output which is gate 1206 from circuit b17 in this case. Note that results for other outputs in other large benchmarks show a similar trend as in Figure 5.4. The dotted red line is based on the gates' observability which is calculated analytically while the observability used in the scheme represented with the blue boxed line is obtained through simulation of one million random samples. Although they are close, we do see that the blue line is a bit closer to RAG because its observability is more accurate than the testability-based computation. Furthermore, no matter how accurate the observability, such approaches are fundamentally inaccurate because of the absence of correlation and the assumption of single error only. A detail explanation is given in [24]. Figure 5.5 extracted from [24] also demonstrates the accuracy of our work. Although the experiment was conducted for another circuit b09, we notice that the output failure rate obtained by Monte Carlo based analysis is less than that obtained from the testability-based analysis. This is consistent with what we get from Figure 5.4.

From this discussion, we can observe that in order to obtain accurate reliability estimates, conventional testability metrics are insufficient, especially for those cases where the gate failure proba-

bilities are not near the extremes. In fact, the difference in the reliability measures can be large when the failure rate is near 0.25. Nevertheless, the testability-based methods can serve as a coarse upper-bound.

Table 5.5: Runtime in Steps

Bench	Runtimes (in seconds)				
	Total	K_{sim}	k_{red}	Init.	Misc.
c880	0.147	0.105	2.8e-5	1.5e-4	0.042
c7552	1.006	0.950	5.6e-5	0.002	0.056
s35932	4.468	4.382	5.56e-4	0.030	0.085
s38584	5.316	5.233	4.73e-4	0.024	0.083
s38417	6.076	5.989	4.72e-4	0.025	0.087
b15_C	2.337	2.281	1.65e-4	0.008	0.056
b17_C	8.452	8.370	4.23e-4	0.028	0.082
b18_C	30.266	30.150	8.86e-4	0.183	0.116
b20_C	5.383	5.333	1.64e-4	0.013	0.050
b21_C	5.477	5.427	1.64e-4	0.013	0.050
b22_C	7.969	7.902	2.30e-4	0.017	0.066

5.6 Chapter Summary

In this chapter, we proposed a novel tool, RAG, which is the first GPU based parallel application for reliability analysis of logic circuits. RAG achieves both high accuracy and efficiency by exploiting the power of GPUs with a novel two-stage simulation framework. The proposed greedy algorithms for stems scheduling and post-order tree traverse for non-stem gates arrangement result in an efficient utilization of the available computational resources on GPUs. Experimental results

showed that RAG could achieve an average of 353× and 116× speedup against two state-of-the-art reliability analysis tools (one is an exact approach with sampling and the other is heuristic-based) without compromising accuracy. Moreover, for large benchmarks which are not able to be handled efficiently by previous tools, RAG is also 20× ad 65× faster than another two stochastic simulation based reliability analysis tools implemented on conventional processor architectures.

Chapter 6

Parallel Design Validation with a Modified Ant Colony Optimization

6.1 Chapter Overview

In this chapter, we propose a novel parallel state justification tool, GACO, utilizing Ant Colony Optimization (ACO) on Graphical Processing Units (GPU). With the high degree of parallelism supported by the GPU, GACO is capable of launching a large number of artificial ants to search for the target state. A novel parallel simulation technique, utilizing partitioned navigation tracks as guides during the search, is proposed to achieve extremely high computation efficiency for state justification. We present the results on a GPU platform from NVIDIA (a GeForce GTX 285 graphics card) that demonstrate a speedup of up to 228$\times$ compared to deterministic methods and a speedup of up to 40$\times$ over previous state-of-the-art heuristic based serial tools.

The rest of this chapter is organized as follows. A brief introduction is given in Section 6.2. In Section 6.3, we review the previous works in the area of state justification and introduce the correlation based partition construction. Section 6.4 outlines a high-level process view of the parallel logic simulator, built on the techniques utilized in FSimGP^2[54], with detail description of

the critical approaches. The experimental results are reported in Section 6.5. Finally, Section 6.6 gives the conclusion.

6.2 Introduction

State Justification is an important engine for test and verification. There may be important states and transitions that need to be verified to ensure the correct functionality of the chip which necessitate reaching of corner states. In addition, some design errors and bugs can only be exercised and propagated by reaching specific states. Therefore, finding vectors that can reach these states from known reachable states plays a critical role in design validation. Due to the exponential growth in circuit size predicted by Moore's Law, state justification has become increasingly difficult, as modern circuits have hundreds of thousands to millions of flip-flops. This growth means that deterministically justifying the state will encounter scalability issues. For example, formal methods such as model checking potentially requires traversing large portions of the state space to find a solution. Dynamic, or simulation based approaches, on the other hand, can handle large circuits but may not yield solutions for hard validation instances. A hybrid formal and dynamic methods, also known as semi-formal methods, offer promise. In semi-formal methods, formal techniques are used on an abstraction of the design and simulation on the concrete design. However, simulation is now also becoming a burden as circuits are becoming extremely large.

In order to help make design validation both efficient and scalable, we propose a semi-formal technique that utilizes Ant Colony Optimization (ACO) [31] based search on Graphic Processing Units (GPUs). The abstraction is created by mining highly related state variables from logic simulation and partitioning them into groups. These groups are then analyzed deterministically to find their distances from the target state. To further improve the performance and reduce simulation overhead, graphic processing units are used to simulate the colony of artificial ants in parallel. Using these distance metrics, we implemented a modified ant colony optimization algorithm on the GPUs to guide the search towards the target state.

We have developed a novel ACO based State Justification Tool accelerated on GPUs, called GACO. GACO harnesses the computational power of both swarm intelligence and modern day GPUs to justify the state information for large circuits. Our method exploits pattern-parallelism with an efficient logic simulation tool that is capable of effectively utilizing memory bandwidth and massive data parallelism on the GPU. The overhead of data communication between the host (CPU) and the device (GPU) is minimized by utilizing as much of the individual device's memory as possible. GACO also takes advantage of the inherent bit-parallelism of logic operations on computer words. Additionally, due to the nature of GPUs, we are able to launch many more ants than previous methods and still achieve significant speedups. More ants allow us to explore a larger search space, while parallel simulation on GPUs allows us to reduce execution costs. The technique is implemented on the NVIDIA GeForce GTX 285 with 30 cores and 8 SIMT execution pipelines per core [59]. Our experimental results demonstrate that the proposed GACO can achieve between one and two orders of magnitude speedup in comparison with the state-of-the-art sequential ACO based state justification algorithm [53] implemented on conventional processor architecture.

6.3 Background

6.3.1 Previous Work

Formal verification provides the complete proof at the cost of both space and time in complex designs. On the other hand, conventional simulation-based techniques are incapable of reaching some hard-to-reach states. In order to mitigate the weaknesses of these two approaches, several hybrid techniques have been proposed to combine and complement the strengths of formal techniques and simulation. Among these, the early pioneers in [99] proposed a direct random simulator under an enlarged set of targets by computing preimages of the initial goal. Thus, the state is reachable if any candidates in the enlarged set is hit. However, because of the design complexity, it is often infeasible to compute the complete set with the original circuit. To overcome the memory explosion for computing the exact reachability of the target state(s), researchers proposed the abstraction-guided

simulation, in which formal methods are applied to an abstract model of the original circuit. An abstract model is simply a reduced circuit model that retains a portion of the original (concrete) circuit's characteristics. A popular abstraction approach is to convert some flip-flops in the original circuit to primary inputs, thereby reducing the state space of the abstract model. Note that by such an abstraction, the state space results in an superset of the original reachable space. That is, any state reachable in the original design is also reachable in the abstract model, but not vice versa. For example, suppose the original circuit has four flip-flops, and the abstract model has only the first two of the four flip-flops. Then, among the original state space of $2^4 = 16$ states, suppose the state 1100 is the only unreachable state in the original concrete model, then in the abstract circuit, since the latter 2 flip-flops are now fully controllable, 1100 would be considered reachable in this abstract model. Although inaccuracies are introduced, the simplified abstract model makes formal analysis feasible. And the resulting abstract state transition model, including the distances among abstract states, is used to guide the search towards a target state of interest [90, 68, 34, 78].

The authors in [90] proposed a high-level abstraction model that closely interacts with the property to be verified. The reachability of the target property is computed on this abstract circuit, and the distance information is used to guide a simulator towards the target in a greedy manner. However, due to the inaccuracy of the abstract model, the search can be stuck in a local optimal point. Although a SAT engine is employed to bridge gaps between the current and the next closest abstract state, the cost of using such tools may become expensive. To overcome the inaccuracy of the approximate distance metric, an abstraction refinement strategy was introduce in [68]. During the process of state justification, some of the abstracted state variables are refined (restored back) to the abstract circuit to make the abstract model more closely resemble the concrete circuit. One drawback of this approach is that the cost of formal analysis increases exponentially for each refinement of the circuit. Similar with the previous works, a BMC is applied in [78] to guide the search process through narrow paths towards the target states for corner cases. Although the authors employed a GA-based search engine, it is still hard to get out of the local optimal space without using a BMC. Thus, such a method takes more time to reach the target states. Different from the techniques that resort to full formal techniques as a back-up tactic to resolve the local

optimal problem during simulation-based search, the authors of [34] introduced a "buckets" selection scheme based on a preimage abstraction (onion ring). The states in different onion rings denotes for different distance from the abstract target state. Thus, the states in the same onion ring that have been traversed will be put in a "buckets". Every time the program will flip a fair coin to choose whether to continue simulation or backtrack to the states in the "buckets". While this approach attempts to avoid some local optimal points, those hard-to-reach states remain difficult to reach.

6.3.2 Ant colony optimization

The ACO algorithm [30, 31] is a biologically inspired algorithm: the aim is to convert the problem into a search problem between an ant colony, or nest, and food source(s). Using local pheromone trails for information exchange, the process of ants' reinforcement learning can be formulated as a meta-heuristic algorithm to solve NP-hard search problems.

The basic idea of the ACO algorithm in solving the problem is formulated via a graph $G(N, E)$ and is described as follows. Initially, from the starting node, a fixed number of "ants" randomly walk around through the edges of graph G. They make their transition decisions between vertices in G based on two parameters: *pheromone* (ϕ) and *visibility* (ψ). Pheromone is a metric to evaluate the preference of an edge, while visibility is a metric to measure how promising a transition between two vertices appears to the ant. After an ant finds a solution, based on its attractiveness (*cost*), the ant will lay down an appropriate amount of pheromone along the trails (edges) it has traveled. This process is called *reinforcement*. Conversely, a process of *evaporation* happens at each time unit, which globally reduces the pheromone on each edge by a certain factor. After this process of reinforced/evaporated pheromone levels, the future ants are more likely to followed a better path to reach the target state.

As shown in Figure 6.1, ants indiscriminately follow four possible routes toward the food source. Once an ant discovers the food source, it returns and leaves in the traversed path a trail of pheromone

(denoted as the solid line on the trail), reinforcing its trail. The pheromone laid by the previous ant is attractive to the nearby ants which will be inclined to follow. Let short routes be favored over long routes, then the shorter one will be traveled by more ants. Gradually, the ants aggregate to the shortest route with most pheromone. Since pheromones are volatile and periodically evaporate, the longer routes will eventually disappear.

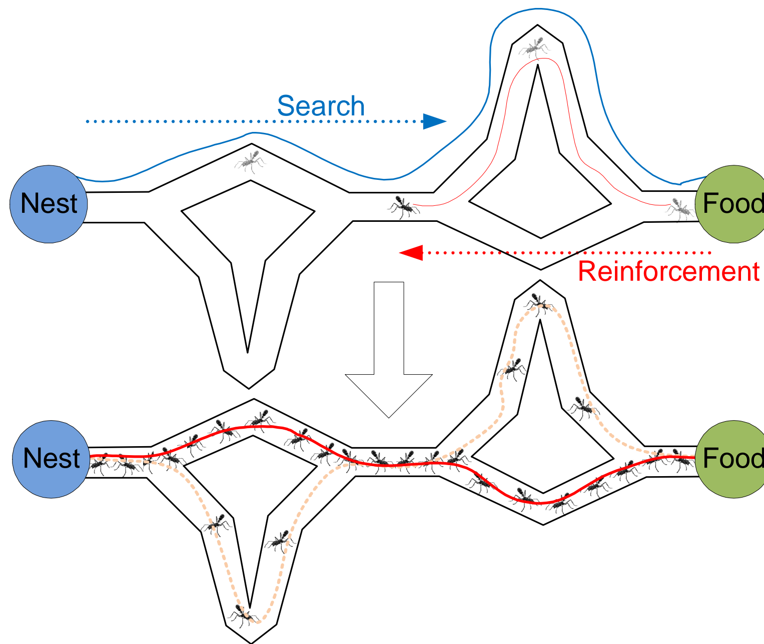

Figure 6.1: Ant Colony Optimization Branches

Most recently, because of its computation efficiency, the ACO algorithm has been widely used to solve various intractable problems, such as the traveling salesman problem [32, 91], graph coloring problem [26], scheduling problem [61], *etc*. In this work, we formulate the process of state justification as an ACO problem.

6.3.3 Random Synchronization Avoidance

Circuits often exhibit the property that certain input cubes synchronize subsets of the state variables [83]. Using random inputs during the search can have the consequence of repeatedly taking the circuit to some synchronized state, thereby continuously leading the algorithm into a local minima.

In order to avoid the effects of random synchronization, we have implemented an input biasing scheme to avoid certain input cubes that potentially synchronize the state space. To check this we simulate each primary input, w_k, such that n_v is the number of flip flops initialized by assigning a value v to w_k and simulating with otherwise unconstrained remaining input and state variables. For each input w_k we get two values, namely n_0 and n_1. Additionally, a scaling factor C is applied to control how quickly we bias against the value. The bias against high values of n is characterized by the function:

$$P_0(k) = 0.5 \times 0.5^{\frac{n_0 - n_1}{\#FFs \times C}}$$

$$P_1(k) = 1.0 - P_0(k)$$

This provides a method under which the probability of a given input value on a PI decays based on the difference in the number of state variables set by the given value and its complement. For use in our experiments, we use a scaling factor of $C = 0.05$ to generate bias. For example, if a PI w_j sets two FFs to 0 and one to 1, then $P_0(j) = 0.5 \times 0.5^{\frac{1}{\#FFs/20}}$. If the number of FFs is large, $P_0(j)$ would be close to 0.5. On the other hand, suppose there exists a PI w_k that can reset all FFs. Then, $P_0(k) = 0.5 \times 0.5^{20} = 0.5^{21}$, a very small value.

6.4 Proposed Method

The high level flow of our algorithm is as follows: Initially, 10,000 random vectors are simulated for the construction of the partition navigation tracks. Then, random synchronization avoidance is calculated, whose result is used to set the input bias of the GPU random input generator. Next, the search for a vector sequence that can bring the circuit from the initial state to the target state begins and the details will be discussed in Sections 6.4.1 and 6.4.2. If GACO finds the target state, the Algorithm is terminated; otherwise, if GACO fails to find the target state, the BMC described in Section 6.4.3, is run to try to bridge the final steps to the target.

6.4.1 Modified Ant Colony Optimization

A simplified Ant Colony Optimization (ACO) is used for this work. Instead of using pheromones to guide the input values, we provide gates or guideposts for the iterative simulation. These guideposts work by selecting the closest states to the target based on our heuristic and launching a new wave of ants from these guideposts. Each ant walks randomly from the guidepost, using logic simulation with random input, attempting to reach a closer state. This process is shown below in Figure 6.2.

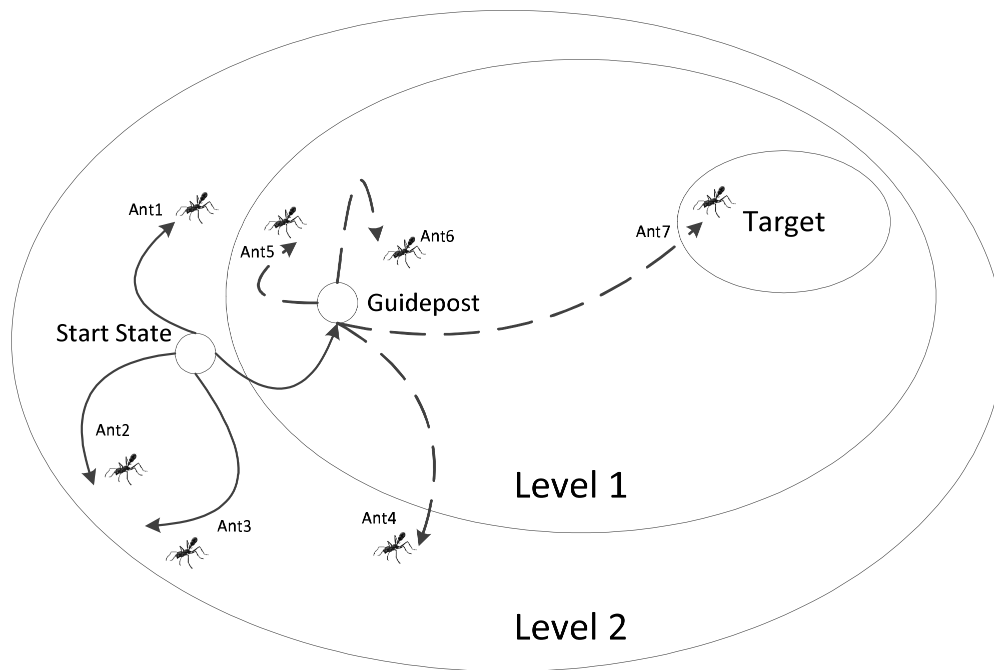

Figure 6.2: Modified Ant Colony Optimization

This method is effective due to the large number of ants we are able to launch from the parallelism offered by the GPU. For any given GPU we can launch the number of blocks in the GPU times the number of threads per blocks. However, the total number of simulations being run simultaneously is determined by the GPU hardware. For example, on the GTX 285 there are 240 CUDA cores or 30 Streaming Multiprocessors(SM), with a maximum of 32 warps in each SM. Since each warp contains 32 threads, this yields a maximum of 24,576 threads (ants) scheduled at any given time.

Generally, we cannot keep this many threads in flight throughout the entire execution due to limits transferring data to the GPU. This inefficiency is seen in our implementation between each round, when the stored data is transferred between the GPU and the CPU, then the fitness operation is performed and the data is transferred back to the GPU. The pseudo-code for the algorithm is shown in Algorithm 6. Lines marked with$*$ are executed on the CPU, others on the GPU.

Algorithm 6 Modified Ant Colony Optimization

```
1: Initialize Start_state, Best_fit *
2: Initialize trace *
3: for all N_rounds rounds * do
4:    for all N_stride strides do
5:       for all N_ants ants do
6:          W = Gen_PI(Seed) { randomly generate PI}
7:          V_tmp = Simulate(Start_state, W)
8:          Fit_tmp = Calc_Fitness(V_tmp)
9:          Add V_tmp to Trace_tmp
10:         if Fit_tmp > best_fit then
11:            Update(Fit_best, V_best)
12:         end if
13:      end for
14:   end for
15:   Start_State = V_best * { set guidepost for next round}
16: end for
```

6.4.2 GPGPU Ants

Implementing logic simulation as ants translates well to the GPU. Since many gates must be simulated and we are simulating many vectors together, the GPU can be efficiently utilized as it is a single instruction path per gate with multiple pieces of data. Similar with what we've shown in 3.1, the execution process of a block where t threads (ants) indexed from Ant_0 to Ant_t are launched. All the threads evaluate the same gates in the circuit concurrently (Right part Figure3.1) followed by a synchronization barrier. Therefore, each gate is then simulated in turn for all different ants and its value is saved for the next level, once all gates have been evaluated then the primary outputs are fed back to the pseudo-primary inputs for the next vector simulation.

After a set number of strides, each ant stops and is evaluated for its fitness. Given a set of n partitions $P_{ant_k} = \{p_1, p_2, ...p_n\}$, the fitness is calculated by the function:

$$Fit = \sum_{i=1}^{n} Cost(p_i)$$

The ant with the best fitness among the entire population is chosen to set the guidepost. This currently leads to the possibility of ants getting stuck in local minima, since there is no mechanism to allow the ants to backtrack in the case of an inaccurate abstraction. However, this is alleviated by the large number of ants being simulated simultaneously.

At the same time, we applied several optimizations which have been propoed in previous chapters to increase performance of the GPU logic simulation. For example, as implemented in Chapter 5, in order to reduce memory usage the fan-out free regions are calculated and all simulation values prior to the fan-out free stem are discarded to save memory. The stem values are kept to propagate through to the rest of the circuit during simulation. This memory optimization allows us to process much larger circuits than without this optimization. Also, we are employing bit level parallelism such that each instance of the simulation is using all 32 bits of an integer to do bit level logic simulation. This means that each ant launched is actually doing 32 random walks per step to further increase the reach of the state space search.

6.4.3 BMC to traverse narrow paths

In the case that the target state cannot be reached by the ACO, or in the case that the ACO fails to progress towards the target according to the heuristic a BMC is employed to attempt to find the final state from the stopping state of the ACO. The BMC provides a method to alleviate the consequences of a inaccurate abstraction. The BMC is implemented using the zChaff[65] SAT solver. The circuit is unrolled to a certain number of time-frames that satisfy $\min(Cost(CS), MAX_TM)$, where CS is the current state and MAX_TM is a constant related to the size of the design. The initial state of the unrolled circuit is constrained to CS while the PPOs of each time-frame is set to all the states whose cost is less than CS. Thus, if the solver returns *true*, a solution from CS to a

new state with low cost is obtained.

6.5 Experimental Results

We evaluated GACO on a set of ISCAS89 [15] and ITC99 [27] benchmark designs. Our platform consists of a workstation with Intel 8-core i7 3.33 GHz CPU, 2 GB memory and one NVIDIA GeForce GTX 285 graphic card as introduced in Section 2.1.1.

Table 6.1 compares our GPU-based ACO algorithm with the BMC implemented on the CPU as well as the sequential method proposed in [53]. For each circuit, we choose hardest-to-justify states taken from [4]. In Table 6.1, Column 1 lists the name of the benchmark. The number of Primary Inputs ($\#PIs$), the number of Flip-Flops ($\#FFs$) and the number of gates ($\#Gates$) are listed in columns 2, 3 and 4, respectively. Column 5 lists the index of hard to justify properties. The execution time for CPU-based BMC and heuristics in [53] are reported in Columns 6 and 7, respectively. Column 8 and 9 reports our GACO's runtime, for different numbers of blocks of ants, 30 and 60 blocks. These runtimes include all the GPU computation time, the communication overhead between the host and the device and the GPU data initialization run on the CPU. Since both block sizes usually complete the search in a similar number of rounds, the 30-block GACO typically outperforms the 60-block run due to fewer computations being executed; however, the benefits of more ants can be seen in a few instances where the larger number of ants enabled the ACO to complete with fewer iterations, particularly s382. This is reflected in the reduced run time. On the other hand, for most of the cases, even when both 30 and 60 block runs would both complete the search, the 30 block would be faster since the 60 block would require us to spread the ants beyond what can be accommodated by the GPU, resulting in higher GPU execution time. The speedups obtained by GACO against the sequential implementation and [53] are listed under Columns 10 and 11, respectively. These speedups are calculated from the 30 ant block run. The average speedups are reported for each benchmarks as well. For example, consider property 9 for circuit b12, which has approximately 1.2K gates. BMC took 143 seconds, while the approach

in [53] took 16.99 seconds. Next, our GACO took only 0.63 seconds. This is a 228× speedup over BMC and a 40× speedup over the heuristic in [53].

In a couple of cases, we see a degradation of performance compared to the CPU based ACO, notably b05 and s1423 property 138. The b05 performance hit is due to the overhead of communication with the GPU, the circuit is small enough that the latency to communicate with the GPU overtakes the actual time to simulate the circuit. In the other smaller circuits, the speedups achieved were also relatively small. This behavior can also be seen in circuit b11 in which there is a significant level of performance variance due to communication latency. In this case however, we see overall performance gains from harder to reach states whose complexity overcome the latency penalty. Secondly, the inability to reach s1423 property 138 stems from a limitation in the algorithms ability to traverse narrow paths. This limitation stems from the fact that we do not interrupt the GPU operation in order to utilize a BMC to help advance to a lower cost state in the case of an inaccurate heuristic or a local minima. However, the overall performance of GACO, particularly in circuits such as b12, is significantly improved over previous deterministic and hybrid tools.

6.6 Chapter Summary

In this chapter, we have proposed a novel Ant-Colony-Optimization based state justification algorithm adapted for the GPU. We have shown that the GPU is an effective tool through the use of several levels of parallelism in circuit simulation to enable the deployment of thousands of ants, increasing the scale of our search compared to previous methods. This increase of scale is shown through our experimental results to lead to performance increases compared to previous state justification attempts as well as compared to deterministic techniques. Though there were some limitations shown to the current algorithm, such as the ability to avoid local minima, in several cases these limitations were overcome by the increase in search scale from the GPU. Up to 228× speedup was achieved when compared with bounded model checking and up to 40× speedup over sequential version of the approach. On average, we achieved an 11x speedup over bounded

Table 6.1: Comparison with other state justification methods

Bench	#Pis	#FFs	#Gate	Property	Runtimes (in seconds)				Speedup, nb=30	
					BMC	[53]	GACO, nb=30	GACO, nb=60	BMC	[53]
s382	3	21	188	7	0.641	1.28	0.29	0.16	2.21	4.42
				15	0.64	1.59	0.23	0.16	2.77	6.89
				23	0.60	1.79	0.26	0.17	2.30	6.86
				85	1.17	2.35	0.53	0.24	2.20	4.42
				106	1.26	1.45	0.53	0.44	2.36	2.73
				Avg					**2.37**	**5.06**
s444	3	21	211	5	0.82	1.28	0.27	0.18	3.01	4.73
				6	0.84	1.36	0.15	0.17	5.61	9.09
				7	0.19	1.69	0.17	0.20	1.12	9.92
				8	0.25	1.78	0.29	0.21	0.86	6.09
				10	0.25	1.13	0.17	0.20	1.48	6.61
				Avg					**2.42**	**7.29**
s1423	17	74	753	2	10.28	0.49	0.49	0.46	20.76	1.00
				10	1.2	66.298	2.28	2.26	0.53	29.08
				21	13.05	0.79	0.93	0.57	14.03	0.85
				24	0.501	0.62	0.488	0.46	1.03	1.27
				138	TO	92.31	TO	TO	N/A	N/A
				Avg					**9.09***	**8.04***
s35932	35	1728	18148	4	4.155	31.43	6.53	7.16	0.63	4.40
				24	43.45	47.13	6.54	7.17	6.64	7.21
				28	12.033	1.66	6.53	7.16	1.84	0.25
				31	36.45	59.85	6.54	7.18	5.57	9.15
				32	178.89	12.83	6.52	7.15	27.43	1.96
				Avg					**8.42**	**4.59**
s38584	12	1452	22601	3998	23.36	13.59	7.45	8.28	3.13	1.82
				4443	23.69	18.39	7.39	8.2	3.21	2.49
				4483	7.77	7.41	7.43	8.24	1.04	0.99
				4653	77.24	28.58	7.40	8.22	10.43	3.86
				4727	45.80	29.57	7.25	8.03	6.32	4.07
				Avg					**4.83**	**2.65**
b05	1	34	1032	371	1.83	0.01	0.34	0.391	5.39	0.06
				373	2.29	0.03	0.4	0.455	5.73	0.08
				735	1.84	0.03	0.34	0.39	5.41	0.09
				1502	0.507	0.03	0.35	0.39	1.44	0.09
				2156	1.722	0.04	0.57	0.65	3.02	0.07
				Avg					**4.20**	**0.07**
b07	1	49	490	27	2.62	0.23	0.19	0.21	14.07	1.24
				224	2.84	0.54	0.29	0.34	9.72	1.84
				551	1.91	0.08	0.19	0.21	10.27	0.43
				580	3.18	0.39	0.29	0.34	10.88	1.33
				835	1.72	0.28	0.29	0.35	9.11	0.96
				Avg					**10.81**	**1.16**
b11	7	31	801	4	0.8	1.38	0.27	0.34	2.96	5.11
				126	0.9	0.11	0.49	0.62	1.83	0.22
				137	11.26	33.53	5.7	5.28	1.97	5.89
				230	1.95	10.28	3.28	3.92	0.59	3.13
				273	1.2	0.11	0.27	0.33	4.44	0.41
				Avg					**2.36**	**2.95**
b12	5	121	1197	9	143.93	16.99	0.63	0.73	228.46	26.95
				520	20.77	16.56	0.64	0.73	32.45	25.87
				1231	4.54	17.08	0.64	0.74	7.09	26.68
				1359	21.13	25.67	0.64	0.73	33.02	40.11
				2586	4.05	23.69	0.64	0.73	6.325	37.01
				Avg					**61.47**	**31.33**
				Overall Avg					**11.77**	**7.02**

TO: 1800 SECONDS   *: TO VALUES NOT INCLUDED IN AVERAGE

model checking and a 7x speedup compared to the sequential approach.

Chapter 7

Conclusion

In this dissertation, we addressed several GPU based applications within two topics: digital systems testing and validation. For testing area, we proposed efficient logic fault simulation, fault-diagnostic simulation and reliability analysis on GPUs. To tackle state justification which is one of the most difficult design validation problems, we introduced a parallel abstraction-guided search scheme using ant colony optimization. All the proposed GPU-based applications aim at accelerating the EDA tools and hence improving the design flow of digital systems.

In Chapter 3, we presented an efficient parallel fault simulator with GPGPU, called FSimGP^2. We proposed a three dimensional parallelism, namely *Pattern-parallelism*, *cf-parallelism* and *Block-parallelism* to achieve a high algorithmic efficiency on GPUs. A large number of gate evaluations can be performed in parallel by employing the large number of threads on a GPU. Fault injection is preformed in a novel compact-fault style which helps to achieve a speedup of 3$\times$. The CUDA running hierarchy is also exploited as block-parallelism which utilizes the high computational power of the many-core system. Experimental results showed that FSimGP^2 could achieve an average of 25.576$\times$ and 3.606$\times$ speedup when compared with two previous GPU-based fault simulators. Moreover, FSimGP^2 is also 35.168$\times$ faster, on average, than a state-of-the-art sequential fault simulator, with a maximal speedup of more than 95$\times$.

We proposed a high-performance parallel fault diagnostic simulator in chapter 4. A novel idea of multi-fault-signature (MFS) is designed for parallelism on GPUs where a number of fault signatures are recorded during parallel fault simulation without introducing much overhead. Fault-pair based diagnostic simulation is also parallelized on GPU. The proposed dynamic load balancing approach results in an efficient utilization of the available computational resources. Experimental results showed that GDSim could achieve an average of 38× speedup when compared with a state-of-the-art sequential fault diagnostic simulator. Moreover, GDSim is also 95× faster than its sequential implementation based on conventional processor architectures.

In Chapter 5, we implemented RAG, which is the first GPU-based reliability analysis tool for logic circuits. The initial barrier to achieve high degree of parallelism is that some large benchmarks cannot be fitted into the global memory of GPUs because all the fault-free and faulty logic values are necessary to store on-board. Novel algorithms including stems scheduling and post-order tree traversal for non-stem gates arrangement are proposed which allow for an efficient utilization of the available computational resources on the GPU. Experimental results showed that RAG could achieve an average of 353× and 116× speedup against two state-of-the-art reliability analysis tools.

In the area of design validation, our ACO-based approach formulates state justification as a path search problem, where artificial ants, starting from their nest (the initial state), attempt to find the paths to food (the target state). We exploited the swarm intelligence to efficiently guide the search which takes advantage of the collective behavior from a colony of ants and can effectively avoid some critical local optimal points during the search. Furthermore, the simulation-based nature of the approach avoids memory explosion often faced by formal techniques. Also, we used our existed GPU framework to achieve several levels of parallelism in circuit simulation and is enable the deployment of thousands of ants, increasing the scale of our search compared to previous methods.

In sum, we chose several applications for which there is a strong motivation to accelerate, since they are extensively used in the VLSI design flow. We implemented varied degrees of inherent

parallelism in them and achieved more than one magnitude speed-up against other tools on the conventional CPU architectures and the GPU systems as well. We believe that the approaches and ideas we proposed for acceleration on GPUs could also be applied to other applications in not only EDA area but also other fields.

Chapter 8

Bibliography

[1] A. Abdollahi. Probabilistic decision diagrams for exact probabilistic analysis. In *Proc. Int. Conf. Computer-Aided Design*, pages 266–272, 2007.

[2] M. Abramovici, M. Breuer, A. Friedman, I. of Electrical, and E. Engineers. *Digital systems testing and testable design*. IEEE press New York, 1990.

[3] M. Abramovici, Y. H. Levendel, and P. R. Menon. A logic simulation machine. In *Proc. Int. Symp. Computer Architecture*, pages 148–157, 1982.

[4] State justification benchmarks. `http://filebox.vt.edu/users/minli/Web/state_just.html`.

[5] P. Agrawal, W. J. Dally, and W. C. F. *et al.* MARS: A multiprocessor-based programmable accelerator. *IEEE Des. Test Comput.*, pages 28–36, 1987.

[6] M. B. Amin and B. Vinnakota. Data parallel fault simulation. In *Proc. Int. Conf. Computer Design*, pages 610–615, 1995.

[7] M. B. Amin and B. Vinnakota. Workload distribution in fault simulation. *J. Electronic Testing: Theory and Applicat.*, 10(3):277–282, 1997.

[8] R. I. Bahar, J. Mundy, and J. Chen. A probabilistic-based design methodology for nanoscale computation. In *Proc. Int. Conf. Computer-Aided Design*, 2003.

[9] S. Bai and D. Nicol. Gpu coprocessing for wireless network simulation. Technical report, Technical Report, University of Illinois at Urbana-Champaign, 2008.

[10] D. K. Beece, G. Deiberg, G. Papp, and F. Villante. The IBM engineering verification engine. In *Proc. Design Automation Conf.*, pages 218–224, 1988.

[11] G. E. Blelloch. *Vector models for data-parallel computing*. MIT Press, Cambridge, MA, USA, 1990.

[12] V. Boppana, S. Rajan, K. Takayama, and M. Fujita. Model checking based on sequential ATPG. In *Proc. Int. Conf. Computer-Aided Verification*, pages 418–430, 1999.

[13] G. Bourianoff. The future of nanocomputing. *Computer*, pages 44–53, 2003.

[14] M. A. Breuer, S. K. Gupta, and T. Mak. Defect and error tolerance in the presence of massive numbers of defects. *IEEE Des. Test Comput.*, 21(3):216–227, 2004.

[15] F. Brglez, D. Bryan, and K. Kozminski. Combinational profiles of sequential benchmark circuits. In *Proc. Int. Symp. Circuits & Systems*, pages 1929–1934, 1989.

[16] J. Burch, E. Clarke, K. McMillan, D. Dill, and L. Hwang. Symbolic model checking: 10^{20} states and beyond. In *Logic in Computer Science, 1990. LICS '90, Proceedings., Fifth Annual IEEE Symposium*, pages 428–439, jun 1990.

[17] P. Camurati, D. Medina, P. Prinetto, and M. R. Sonza. A diagnostic test pattern generation algorithm. In *Proc. Int. Test Conf.*, pages 52–58, 1990.

[18] G. R. Case. Analysis of actual fault mechanisms in cmos logic gates. In *Proceedings of the 13th Design Automation Conference*, DAC '76, pages 265–270, New York, NY, USA, 1976. ACM.

[19] S. Chakravarty, Y. Gong, and S. Venkataraman. Diagnostic simulation of stuck-at faults in combinational circuits. *J. Electronic Testing: Theory and Applicat.*, 8(1):87–97, 1996.

[20] D. Chatterjee, A. DeOrio, and V. Bertacco. Event-driven gate-level simulation with gp-gpus. In *Proc. Design Automation Conf.*, pages 557–562, 2009.

[21] D. Chatterjee, A. DeOrio, and V. Bertacco. GCS: High-performance gate-level simulation with gpgpus. In *Proc. Design Automation & Test Europe Conf.*, pages 1332–1337, 2009.

[22] H. Chen and J. Han. Stochastic computational models for accurate reliability evaluation of logic circuits. In *Proc. Great Lake Symp. VLSI*, pages 61–66, 2010.

[23] S. C. Chen and J. M. Jou. Diagnostic fault simulation for synchronous sequential circuits. *IEEE Trans. Comput.-Aided Des. Integr. Circuits Syst.*, 16(3):299–308, 1997.

[24] M. R. Choudhury and K. Mohanram. Reliability analysis of logic circuits. *IEEE Trans. Comput.-Aided Des. Integr. Circuits Syst.*, 28(3):392–405, 2009.

[25] E. Clarke, O. Grumberg, and D. Peled. Model checking, 2000.

[26] D. Costa and A. Hertz. Ants can colour graphs. *J. Operational Research Society*, 48(3):295–305, 1997.

[27] S. Davidson. ITC99 benchmark circuits - preliminary results. In *Proc. Int. Symp. Circuits & Systems*, page 1125, 1999.

[28] F. De Paula and A. Hu. An effective guidance strategy for abstraction-guided simulation. In *Proc. Design Automation Conf.*, pages 63–68, june 2007.

[29] Y. Deng, B. Wang, and S. Mu. Taming irregular eda applications on gpus. In *Proc. Design Automation Conf.*, pages 539–546, Nov. 2009.

[30] M. Dorigo. *Optimization, learning and natural algorithms*. PhD thesis, Politecnico di Milano, 1995.

[31] M. Dorigo, M. Birattari, and T. Stutzle. Ant colony optimization artificial ants as a computational intelligence technique. *IEEE Computer Intelligence Magazine*, 1(4):28–39, 2006.

[32] M. Dorigo, V. Maniezzo, and A. Colorni. Ant system: Optimization by a colony of cooperating agents. *IEEE Tran. Systems, Man, and Cybernetics*, 26(1):29–41, Feb 1996.

[33] Z. Fan, F. Qiu, A. Kaufman, and S. Yoakum-Stover. Gpu cluster for high performance computing. In *Proceedings of the 2004 ACM/IEEE conference on Supercomputing*, SC '04, pages 47–, Washington, DC, USA, 2004. IEEE Computer Society.

[34] G. D. P. Flavio and A. J. Hu. An effective guidance strategy for abstraction-guided simulation. In *Proc. Design Automation Conf.*, pages 63–68, 2007.

[35] M. K. Ganai, A. Aziz, and A. Kuehlmann. Enhancing simulation with BDDs and ATPG. In *Proc. Design Automation Conf.*, pages 385–390, 1999.

[36] T. Godjoska, S. Filiposka, and D. Trajanov. Parallel execution of the ns-2 sequential simulator on a gpu. In *18th Telecommunications forum TELFOR 2010*, pages 159–162, Nov. 2010.

[37] N. K. Govindaraju, N. Raghuvanshi, and D. Manocha. Fast and approximate stream mining of quantiles and frequencies using graphics processors. In *Proceedings of the 2005 ACM SIGMOD international conference on Management of data*, SIGMOD '05, pages 611–622, New York, NY, USA, 2005.

[38] K. Gulati and S. Khatri. Towards acceleration of fault simulation using graphics processing units. In *Proc. Design Automation Conf.*, pages 822–827, 2008.

[39] K. Gulati and S. P. Khatri. Fault Table Computation on GPUs. *J. Electronic Testing: Theory and Applicat.*, 26(2):195–209, 2010.

[40] I. Hamzaoglu and J. H. Patel. New techniques for deterministic test pattern generation. In *J. Electronic Testing: Theory and Applicat.*, pages 446–452, 1999.

[41] J. Han, E. Taylor, J. Gao, and J. Fortes. Faults, Error Bounds and Reliability of Nanoelectronic Circuits. In *Proc. Int. Conf. Appl.-Specific Sys., Arch. and Proc.*, pages 247–253, 2005.

[42] S. Han, K. Jang, K. Park, and S. Moon. Packetshader: a gpu-accelerated software router. *SIGCOMM Comput. Commun. Rev.*, 41:195–206, Aug. 2010.

[43] N. Ishiura, M. Ito, and S. Yajima. Dynamic two-dimensional parallel simulation technique for high-speed fault simulation on a vector processor. *IEEE Trans. Comput.-Aided Des. Integr. Circuits Syst.*, 9(8):868–875, aug 1990.

[44] IWLS 2005 benchmarks. `http://www.iwls.org/iwls2005/benchmarks.html`.

[45] R. W. Keyes. Fundamental limits of silicon technology. *Proceedings of the IEEE*, 89(3):227–239, 2001.

[46] Y. Kitamura. Exact critical path tracing fault simulation on massively parallel processor AAP2. In *Proc. Int. Conf. Computer-Aided Design*, pages 474–477, 1989.

[47] M. A. Kochte, M. Schaal, H. J. Wunderlich, and C. G. Zoellin. Efficient fault simulation on many-core processors. In *Proc. Design Automation Conf.*, pages 380–385, 2010.

[48] S. Krishnaswamy, G. Viamontes, I. Markov, and J. Hayes. Accurate reliability evaluation and enhancement via probabilistic transfer matrices. In *Proc. Design Automation & Test Europe Conf.*, pages 282–287, 2005.

[49] S. Krishnaswamy, G. F. Viamontes, I. L. Markov, and J. P. Hayes. Probabilistic transfer matrices in symbolic reliability analysis of logic circuits. *ACM Trans. Design Automation Electronic Systems*, 13(1):1–35, 2008.

[50] K. Kubiak, S. Parkes, W. K. Fuchs, and R. Saleh. Exact evaluation of diagnostic test resolution. In *Proc. Design Automation Conf.*, pages 347–352, 1992.

[51] K. Lee and D. Ha. An efficient, forward fault simulation algorithm based on the parallel pattern single fault propagation. In *Proc. Int. Test Conf.*, pages 946–955, 1991.

[52] M. Li, K. Gent, and M. S. Hsiao. Utilizing gpgpus for design validation with a modified ant colony optimization. In *Proceedings of the High-Level Design Validation and Test Workshop*, pages 128–135. IEEE Computer Society, 2011.

[53] M. Li and M. S. Hsiao. An ant colony optimization technique for abstraction-guided state justification. In *Proc. Int. Test Conf.*, pages 1–10, 2009.

[54] M. Li and M. S. Hsiao. FsimGP^2: An efficient fault simulator with GPGPU. In *Proc. Asian Test Symp.*, pages 15–20, 2010.

[55] M. Li and M. S. Hsiao. 3-d parallel fault simulation with gpgpu. *IEEE Trans. Comput.-Aided Des. Integr. Circuits Syst.*, 30(10):1545–1555, Oct. 2011.

[56] M. Li and M. S. Hsiao. High-performance diagnostic fault simulation on gpus. In *Proc. European Test Symp.*, page 210, May 2011.

[57] M. Li and M. S. Hsiao. RAG: an efficient reliability analysis of logic circuits on graphics processing units. In *Proc. Design Automation & Test Europe Conf.*, pages 316–319, 2012.

[58] M. Li, Y. Zheng, M. S. Hsiao, and C. Huang. Reversible logic synthesis through ant colony optimization. In *Proc. Design Automation & Test Europe Conf.*, pages 307–310, 2010.

[59] E. Lindholm, J. Nickolls, and J. M. S. Oberman. NVIDIA Tesla: A unified graphics and computing architecture. *IEEE Micro*, 28(2):39–55, 2008.

[60] D. Luebke, M. Harris, J. Krüger, T. Purcell, N. Govindaraju, I. Buck, C. Woolley, and A. Lefohn. Gpgpu: general purpose computation on graphics hardware. In *ACM SIGGRAPH 2004 Course Notes*, SIGGRAPH ’04, New York, NY, USA, 2004. ACM.

[61] S. Luo, C. Wang, and J. Wang. Ant colony optimization for resource-constrained project scheduling with generalized precedence relations. In *IEEE Proc. Tools with Artificial Intelligence*, pages 284–289, Nov. 2003.

[62] S. Manavski. Cuda compatible gpu as an efficient hardware accelerator for aes cryptography. In *IEEE International Conference on Signal Processing and Communications*, pages 65–68, Nov. 2007.

[63] J. D. Meindl, Q. Chen, and J. A. Davis. Limits on silicon nanoelectronics for terascale integration. *Science*, 293(5537):2044, 2001.

[64] G. Moore. Cramming more components onto integrated circuits. *Proceedings of the IEEE*, 86(1):82–85, 1998.

[65] M. Moskewicz, C. Madigan, Y. Zhao, L. Zhang, and S. Malik. Chaff: engineering an efficient sat solver. In *Proc. Design Automation Conf.*, pages 530–535, 2001.

[66] R. B. Mueller-Thuns, D. G. Saab, and R. F. D. J. A. Abraham. VLSI logic and fault simulation on general-purpose parallel computers. *IEEE Trans. Comput.-Aided Des. Integr. Circuits Syst.*, 12(3):446–460, 1993.

[67] M. Nanjundappa, H. Patel, B. Jose, and S. Shukla. Scgpsim: A fast systemc simulator on gpus. In *Proc. Asia South Pacific Design Automation Conf.*, pages 149–154, Jan. 2010.

[68] K. Nanshi and F. Somenzi. Guiding simulation with increasingly refined abstract traces. In *Proc. Design Automation Conf.*, pages 737–742, 2006.

[69] V. Narayanan and V. Pitchumani. Fault simulation on massively parallel SIMD machines algorithms, implementations and results. *J. Electronic Testing: Theory and Applicat.*, 3(1):79–92, 1992.

[70] T. Niermann and J. H. Patel. HITEC: a test generation package for sequential circuits. In *Proc. Design Automation & Test Europe Conf.*, pages 214–218, 1991.

[71] T. M. Niermann, W. T. Cheng, and J. H. Patel. PROOFS: A fast, memory-efficient sequential circuit fault simulator. *IEEE Trans. Comput.-Aided Des. Integr. Circuits Syst.*, 11(2):198–207, 1992.

[72] NVIDIA CUDA homepage. `http://www.nvidia.com/object/cuda_home.html`.

[73] NVIDIA Tesla Data Center Solutions. `http://www.nvidia.com/object/preconfigured-clusters.html`.

[74] J. Owens, M. Houston, D. Luebke, S. Green, J. Stone, and J. Phillips. Gpu computing. *Proceedings of the IEEE*, 96(5):879–899, May 2008.

[75] J. Owens, D. Luebke, N. Govindaraju, M. Harris, J. Krüger, A. Lefohn, and T. Purcell. A survey of general-purpose computation on graphics hardware. *Computer graphics forum*, 26(1):80–113, 2007.

[76] F. Ozguner, C. Aykanat, and O. Khalid. Logic fault simulation on a vector hypercube multiprocessor. In *Proc. Conf. Hypercube Concurrent Computer and Applications*, pages 1108–1116, 1988.

[77] F. Ozguner and R. Daoud. Vectorized fault simulation on the Cray X-MP supercomputer. In *Proc. Int. Conf. Computer-Aided Design*, pages 198–201, 1988.

[78] A. Parikh, W. Wu, and M. Hsiao. Mining-guided state justification with partitioned navigation tracks. In *Test Conference, 2007. ITC 2007. IEEE International*, pages 1–10, oct. 2007.

[79] S. Parkes, P. Banerjee, and J. Patel. A parallel algorithm for fault simulation based on PROOFS. In *Proc. Int. Conf. Computer Design*, pages 616–621, 1995.

[80] S. Patil and P. Banerjee. Performance trade-offs in a parallel test generation/fault simulation environment. *IEEE Trans. Comput.-Aided Des. Integr. Circuits Syst.*, 10(12):1542–1558, 1991.

[81] M. Pharr and R. Fernando. *GPU Gems 2: Programming Techniques for High-performance Graphics and General-Purpose Computation*. Addison-Wesley Professional, 2005.

[82] I. Pomeranz. On pass/fail dictionaries for scan circuits. In *Proc. Asian Test Symp.*, pages 51–56, 2001.

[83] I. Pomeranz and S. Reddy. Primary input vectors to avoid in random test sequences for synchronous sequential circuits. *Proc. Int. Conf. Computer-Aided Design*, 27(1):193–197, Jan. 2008.

[84] R. Raghavan, J. P. Hayes, and W. R. Martin. Logic simulation on vector processors. In *Proc. Int. Conf. Computer-Aided Design*, pages 268–271, 1988.

[85] P. Rashinkar, P. Paterson, and L. Singh. *System-on-a-chip verification: methodology and techniques*. Springer Netherlands, 2000.

[86] T. Rejimon and S. Bhanja. Scalable probabilistic computing models using Bayesian networks. In *Proc. Int. Symp. Circuits & Systems*, pages 712–715, 2005.

[87] E. M. Rudnick, T. M. Niermann, and J. H. Patel. Methods for reducing events in sequential circuit fault simulation. In *Proc. Int. Conf. Computer-Aided Design*, pages 546–549, 1991.

[88] A. Santone. Heuristic search + local model checking in selective mu-calculus. *Software Engineering, IEEE Transactions on*, 29(6):510–523, June 2003.

[89] J. Shen, W. Maly, and F. Ferguson. Inductive fault analysis of mos integrated circuits. *Design Test of Computers, IEEE*, 2(6):13–26, Dec. 1985.

[90] S. Shyam and V. Bertacco. Distance-guided hybrid verification with GUIDO. In *Proc. Design Automation Conf.*, volume 1, pages 1–6, march 2006.

[91] T. Stutzle and H. Hoos. Max-min ant system and local search for the traveling salesman problem. In *IEEE Int. Conf. Evolutionary Computation*, pages 309–314, Apr 1997.

[92] R. Szerwinski and T. Gneysu. Exploiting the power of gpus for asymmetric cryptography. In *Cryptographic Hardware and Embedded Systems CHES 2008*, volume 5154, pages 79–99. Springer Berlin / Heidelberg, 2008.

[93] S. Tai and D. Bhattacharya. Pipelined fault simulation on parallel machines using the circuit flow graph. In *Proc. Int. Conf. Computer Design*, pages 564–567, 1993.

[94] E. Taylor, J. Han, and J. Fortes. Towards accurate and efficient reliability modeling of nanoelectronic circuits. In *Proc. IEEE Conf. Nanotechnology*, volume 1, pages 395–398, 2006.

[95] C. Timoc, M. Buehler, T. Griswold, C. Pina, F. Stott, and L. Hess. Logical models of physical failures. In *Proc. Int. Test Conf.*, pages 546–553. IEEE Computer Society, 1983.

[96] J. A. Van Meel, A. Arnold, and D. Frenkel. Harvesting graphics power for MD simulations. *Molecular Simulation*, 34(3):259–266, 2008.

[97] J. Waicukauski and E. Lindbloom. Failure diagnosis of structured vlsi. *IEEE Design and Test of Computers*, pages 49–60, 1989.

[98] Q. W. Wu and M. S. Hsiao. State variable extraction to reduce problem complexity for atpg and design validation. In *Proc. Int. Test Conf.*, pages 820–899, 2004.

[99] C. Yang and D. Dill. Validation with guided search of the state space. In *Proc. Design Automation Conf.*, pages 599–604, June 1998.

[100] V. V. Zhirnov, R. K. Cavin III, J. A. Hutchby, and G. I. Bourianoff. Limits to binary logic switch scaling-a gedanken model. *Proceedings of the IEEE*, 91(11):1934–1939, 2003.